Frame transformation relations and multipole transitions in symmetric polyatomic molecules

William G. Harter

Joint Institute for Laboratory Astrophysics, University of Colorado and National Bureau of Standards, Boulder, Colorado 80309

Chris W. Patterson*

Theoretical Division, Los Alamos Scientific Laboratory, University of California, Los Alamos, New Mexico 87545

Fernando J. da Paixao

Instituto de Fisica, UNICAMP, Campinas, S. P., Brazil

The theory of transformation relations between states of Born Oppenheimer and weak coupling approximations is developed for polyatomic molecules. The relations are a generalization of frame transformation relations used by Chang and Fano for symmetric-top molecules, and they lead to a more convenient symmetry labeling system than was previously available. A key internal symmetry label (named "soul") is defined so that it remains a constant label for frame transformation relations, and is conserved during vibronic transitions, ionization, and even dissociation provided the nuclear spin–rotation interaction is relatively small. Various nomograms, graphs, and tableaus associated with the soul label make it easy to predict and visualize the form of many types of complex high-resolution spectra. Simplified procedures are given for obtaining selection rules, statistical weights, and matrix elements of multipole operators for common molecules having various point symmetries. Simplifications of computational theory using the new level cluster bases for high J are discussed.

CONTENTS

GLOSSARY

$\{\alpha\beta\gamma\}$ or $\{\phi\theta\chi\}$ Euler Angles (Sec. II.A)

A or $\binom{A}{a}$ Activity label for vibronic wave functions used in BOA bases. Usually finite symmetry IR label (viz.

$$A=B_2\text{, or } \binom{A}{a}=\binom{T_{1u}}{(x)},\ldots)$$

$[A]$ Dimension of IR(A) (viz: $[B_2]=1,[T_{1u}]=3,\ldots$)

A_v Rotational constant $1/I_{\bar{z}}$

B or $\binom{B}{b}$ Bare rotor label for finite symmetry rotational wave functions. May be accompanied by correlated Young Tableau:

$$\left(\binom{B}{b},\{u\}\right).$$

$[B]$ Dimension of IR(B)

B_v Rotation constant $1/I_{\bar{xy}}$

C or $\binom{C}{c}$ Constricted rotor label for finite symmetry rotational wave function of a rotor carrying a BOA vibronic state. C must be contained in the Clebsch-Gordan series of $A\times B$.

*Work performed under the auspices of the United States Department of Energy, and the Instituto de Fisica, UNICAMP, S. P., Brazil.

$[C]$	Dimension of IR(C)
$C^{kJJ'}_{sMM'}$	R_3 Clebsch-Gordan coefficient
$C^{k^qJ^pJ'^{p'}}_{s\ M\ M'}$	O_3 Clebsch-Gordan coefficient
$C^{ABC}_{a\,b\,c}$	Finite symmetry coupling coefficient
C_n	Cyclic group of order n
C_i	Inversion group $\{1, \mathbf{I}\}$
D or (^D_d)	Label for finite symmetry IR tensor operator, usually dipole operator
D_n	Dihedral or polygonal symmetry group
$\mathfrak{D}^N_{mn}(\alpha\beta\gamma)$	Irreducible representation of R_3 symmetry (Also rigid rotor wave function)
$\mathfrak{D}^{N^p}_{mn}(O(\alpha\beta\gamma))$	Irreducible representation of O_3 symmetry
$\mathfrak{D}^A_{a',a}(R)$	Irreducible representation of finite ($\mathcal{G}$) symmetry
$\epsilon_\Sigma, \epsilon_\Pi$	Energy of Σ and Π electronic waves in the absence of rotation
$f_B^{[\mu_s]}$	Correlation frequency between bare rotor label B and Young tableau $[\mu_s]$ (See for example Appendix D)
$^{\circ}\mathcal{G}$	Order of, or number of, elements in finite group $\mathcal{G}$
$\mathbf{H}(\langle\mathbf{H}\rangle)$	Hamiltonian operator (matrix)
$\mathbf{I}=\bar{\mathbf{I}}$	Inversion which reflects all particles effected by it through the origin. May be defined to effect only select particles or activity: $\mathbf{I}_N$ inverts nuclei, $\mathbf{I}_{ev}$ inverts vibronic activity
I	Nuclear spin
$I_{\bar{z}}, I_{\bar{x}\bar{y}}, I_{\bar{x}\bar{y}\bar{z}}$	Rotational inertia constants for rotors
$\mathbf{J}_x\mathbf{J}_y\mathbf{J}_z$	Lab components of total angular momentum operators. Usually $\mathbf{J}=\mathbf{L}+\mathbf{N}$
$\mathbf{J}_{\bar{x}}\mathbf{J}_{\bar{y}}\mathbf{J}_{\bar{z}}$	Body components of $\mathbf{J}$
J	Total momentum label of R_3 IR
J^p	Total momentum-parity label of O_3 IR
$[J]$	$=2J+1$
K	Body or $\bar{z}$ component of total angular momentum, usually $K=\Lambda+n$
k	Multipolarity of R_3 tensor operator
k^q	Multipolarity–parity of O_3 tensor operator (1^- = electric dipole, 1^+ = magnetic dipole, 2^+ = electric quadrupole etc.)
$\mathbf{L}_x\mathbf{L}_y\mathbf{L}_z$	Lab components of vibronic angular momentum operators
$\mathbf{L}_{\bar{x}}\mathbf{L}_{\bar{y}}\mathbf{L}_{\bar{z}}$	Body components of $\mathbf{L}$
l	Total electronic or vibronic angular momentum quantum number
$l^{[\mu_s]}$	Spin degeneracy of Young tableau state (see Fig. 28)
Λ	Body component of electronic or vibronic angular momentum in BOA state
M	Lab or z component of total angular momentum
m	Lab component of rotor angular momentum
$\{\mu\}$	$=\{\mu_1\mu_2\ldots\mu_r\}$ Young tableau with μ_j boxes in jth row (see Fig. 26)
$\{\mu_s\}$	Young tableau associated with nuclear spin states (see Fig. 26)
N (or N^q)	Nuclear orbital or rotor angular momentum (and parity q) numbers
$[N]$	$=2N+1$
n	Body component of rotor angular momentum
$\bar{\mathbf{O}}(\alpha\beta\gamma)$	Body operator in O_3
$\mathbf{O}(\alpha\beta\gamma)$	Lab operator in O_3
O_2	Orthogonal group of two dimensions
O_{2i}	Infinite dihedral group $D_{\infty h}$
O_3	Orthogonal group in three dimensions $R_3 \times C_i$
O	Octahedral group
O_h	$=O\times C_i$
$\mathbf{P}^N_{mn}$	R_3 projection operator
$\mathbf{P}^{J^p}_{mn}$	O_3 projection operator
p	Parity index (even: $p=+1$; odd: $p=-1$)
$r^{NB}_{mb}(\alpha\beta\gamma)$	Rotor wave function adjusted for finite symmetry and centrifugal distortion [see Eq. 2.33]
$\mathbf{R}(\alpha\beta\gamma)$	Lab rotation operator in R_3
$\bar{\mathbf{R}}(\alpha\beta\gamma)$	Body rotation operator in R_3
$\bar{\mathbf{R}}_{ev}, \bar{\mathbf{R}}_N, \bar{\mathbf{R}}_J$	Finite rotation operators defined in body frame. $\bar{\mathbf{R}}_{ev}$ effects vibronic activity, $\bar{\mathbf{R}}_N$ effects rotor, $\bar{\mathbf{R}}_J$ effects the whole molecule (see Fig. 23)
R_2	Rotation group in two dimensions
R_3	Rotation group in three dimensions
S_n	Symmetric group or permutation group for n particles
$\bar{\sigma}_{ev}, \bar{\sigma}_N, \bar{\sigma}_J$	Reflection operators defined in the same way as $\bar{\mathbf{R}}_{ev}$ etc. (see Fig. 24)
S	Nearest-neighbor tunneling amplitude
$\mathbf{T}^k_r$	(r)th component of irreducible 2^k-pole tensor operator (T^1_0 is z-component of dipole operator)
$\mathcal{T}^D_d$	(d)th component of irreducible D-tensor operator defined by finite symmetry
U_m	Unitary group in m dimensions
V_Λ	Vibronic wave function (BOA)
$\mathbf{V}^k_r$	Irreducible tensors like $\mathbf{T}^k_r$
W_B	Statistical weight of bare rotor state B [see Eq. 3.33]
xyz	Lab coordinates
$\bar{x}\bar{y}\bar{z}$	Body coordinates
Y^l_m	(l)th spherical harmonic with axial momentum m
$\mathcal{Y}^A_a$	Finite symmetry harmonic belonging to IR(A)
ξ	Coriolis or effective angular momentum constant
$(l^p_m \mid ^A_a)$	Transformation coefficients between angular momentum (and parity) eigenstates defined by $R_3(O_3)$ symmetry, and finite symmetry states
↓	See *Correlation* in Synopsis.
↑	See *Induced Representation* in Synopsis.

I. INTRODUCTION

The invention and development of lasers has led to a tremendous increase in the number of applications and analyses of molecular spectra. The spectral properties of one type of molecule are used to design a laser which is then used to study some other molecular structures. This knowledge in turn is used to study more nonlinear optical devices, and so on. When added to the new developments for isotope separation, plasma diagnostics, molecular collisions, chemical lasers, frequency standards, electron scattering, or astrophysics, it begins to look like the beginning of a revolution in molecular spectroscopy.

In short, quite a number of physicists and chemists, who are not specialists in any area of spectroscopy, are having to study certain molecular structures. Very often they do it with more detail and precision than was ever possible before. Most of the workers who are getting involved in spectroscopy now have not had the years of experience it requires to become "old friends" with every line in an interesting spectrum. Therefore, it is imperative that a comprehensive theoretical framework be assembled that is as simple as possible and unprejudiced by any specialized area of molecular physics or any single type of molecule.

It is hoped that the present work will be another step

in this direction for a large number of molecular systems which have some sort of geometrical symmetry in their structure. This work is meant to expose the simplest and most powerful symmetry analysis methods which are now available. Some of the methods reviewed are quite standard, or slight variations of standard ones, while some others are brand new. (In this respect it is hoped our referencing is ample enough, but we apologize for not being able to make it encyclopedic.) In fact, one of the advantages of a "new" labeling scheme which is introduced is that it allows one to more easily use the "standard" Appendices I–IV of Herzberg's text III (Herzberg, 1966; see also Steinfeld, 1974). One may now more easily understand rovibronic structure of symmetric molecules of complexity ranging from that of H_2 to that of NH_3, CH_4, or SF_6. A simpler and more powerful basis for deriving molecular levels, transitions, statistical weights, perturbations and so forth, can be made using only standard symmetry representations.

The new scheme arises from a generalization of Chang–Fano frame transformation relations (Fano, 1970; Chang and Fano, 1972) from diatomic molecules to polyatomic molecules. These relations smoothly transform from weakly coupled electron-rotor scattering or Rydberg states to tightly bound states of the Born–Oppenheimer approximation. To accomplish this, one must make physically clear how symmetry operations, particularly inversions, relate to the space or "lab" coordinates as well as the molecular or "body" coordinates. The new scheme makes those transformations quite simple; to begin with, Fano's original H_2 transformations for multichannel quantum defect theory (Herzberg and Jungen 1972) are perhaps easier to understand.

Previously, inversion and reflection symmetry transformations have not been presented clearly even in regard to simple diatomic molecules. In a modern, otherwise lucid text (Steinfeld 1974) we still read the following: "1. The operation of (axial plane reflection) in the molecule fixed system is equivalent to inversion of coordinates in the space fixed system. 2. The operation of co-ordinate inversion in the molecule-fixed system is equivalent to interchange of nuclei in the space fixed system." (See also Hougen, 1963.) The new scheme will define one inversion operator **I** which obeys much simpler rules. Using **I** and other standard symmetry operations, it will be shown how diatomic selection rules, statistical weights, and so forth can be derived *clearly* in a minute or two. Furthermore, the same rules are then used for polyatomic molecules.

The key to the labeling scheme is to divide molecular quantum labels into "external" or "lab" labels and "internal" or "body" labels. For the free molecule the external labels $(J^p, M, m, k^q, \ldots)$ are angular momenta which are treated more or less according to standard rules of atomic spectroscopy. The internal labels $(A_2, B_1, {}^{T}_{x}{}_1, \Sigma^-_g, \ldots)$ are finite symmetry irreducible representation labels which are treated according to standard rules of group theory. The prerequisite for using the labeling is some acquaintance with atomic rules (viz: The k^q multipole transition of $J'^{p'} \to J^p$ is forbidden unless J' is contained in $k \otimes J$ and the parities satisfy $p' = qp$) and finite symmetry rules (viz: The $A' \to A$ transition due to perturbation D is forbidden unless $A \otimes D$ contains A'.) The prerequisite for understanding the derivation of the labeling will be some acquaintance with coupling coefficients and the Wigner Eckart theories of the orthogonal spatial symmetry (viz:

$$\langle {}^{J'^{p'}}_{m'} \,|\, \mathbf{T}^{k^q}_{s} \,|\, {}^{J^p}_{m} \rangle = C^{k^q J^p J'^{p'}}_{s\ m\ m'} \langle J' \| k \| J \rangle)$$

and some finite symmetries

(viz: $\langle {}^{A'}_{a'} \,|\, \mathcal{T}^{D}_{d} \,|\, {}^{A}_{a} \rangle = C^{DAA'}_{d\,a\,a'} (A' \| D \| A)$.

Many texts discuss these two problems separately (Heine, 1960; Tinkham, 1967).

Upon assembling these two parts, we will find external and internal quantum labels which are variously "good" ones or "bad" ones depending upon the closeness to a weak coupling approximation on one hand or a Born–Oppenheimer Approximation (BOA) on the other. However, the key to the labeling scheme involves finding one external and one internal label which are "best" for either approximation. The best external label will be an overall or total angular momentum and parity label (J^p), while the best internal label will be an "underall" or "bare rotor" finite symmetry label (B) which might well be called the "soul" of the molecule. The (B) is a generalization of what is commonly known as the rovibronic species label, but is probably simpler than any previous definition.

We shall try to keep to a minimum the number of mathematical concepts introduced. Indeed all symmetry transformations will be made from a rotation $\mathbf{R}(\alpha\beta\gamma)$ and inversion **I**, i.e., the orthogonal group (O_3). More rigorous mathematical treatments of rotations and molecular frames are contained in a recent review (Louck and Galbraith, 1976) and text (Judd, 1975) both of which describe lab and body based rotation operations. We shall be content to give heuristic physical arguments for the properties of the lab and body operators in Sec. II as well as the symmetry analysis of the bare rigid and semi-rigid rotor which is to be surrounded with electronic or vibronic excitations in Sec. III.

However, in the process of including excitations, care will be taken to distinguish between the standard coupling of products of independent wave functions of the form

$$\psi_{\mu_1}(x_1)\psi_{\mu_2}(x_2)\psi_{\mu_3}(x_3) = \langle x_1 \,|\, \mu_1 \rangle \langle x_2 \,|\, \mu_2 \rangle \langle x_3 \,|\, \mu_3 \rangle$$

and product wave functions such as

$$\langle x_e q_v \theta_r \,|\, \mathrm{BOA} \rangle = \psi_\epsilon^{\mathrm{electronic}}(x_e q_v, \theta_r) \times \phi^{\mathrm{vibration}}_{\nu_\epsilon}(q_v \theta_r) \rho^{\mathrm{rotation}}_{\lambda\nu_\epsilon}(\theta_r)$$

which are used in BOA bases. In the latter the *co-ordinates* of each factor may depend upon those contained in the factors to its right, while the *quantum labels* of each factor may depend upon those held by factors on the left. The dependence of the coordinates in the BOA wave functions is a result of the assumption that the electron and vibrational wave functions are fixed to a body co-ordinate system which rotates relatively slowly so that the vibronic waves ride around with the rotor. The vibrational motions are in turn much slower than those of the electrons so one imagines adjusting for a new manifold of electron eigenstates with each change of nuclear co-

ordinates. The quantum number dependence occurs because the vibronic activity tightly embraces the rotor and so the internal vibronic momentum must be included in the quantum numbers of the rotor in the third factor ρ. Also, it is well known that the vibrational ν depends on the electronic excitation ϵ through the molecular potential.

Products $\psi_a^A(x_1)\psi_b^B(x_2)$ of independent wave functions are convenient bases for describing weakly coupled systems. For small A–B interactions the coupled wave functions

$$\Psi_c^C = \sum_{ab} C_{abc}^{ABC}\, \psi_a^A\, \psi_b^B$$

made using appropriate Clebsch-Gordan coefficients C_{abc}^{ABC} are approximate eigenfunctions. However, something more than ordinary coupling will be needed if the two systems interact strongly, particularly if one part is constricting the coordinate axes used by the other as in a BOA state. In Sec. III various polyatomic BOA states are given in terms of a stronger version of coupling, which is named BOA-constriction, and BOA bases are related to weakly coupled bases through a generalization of Chang–Fano theory. The key to this relation is the (B) label which is valid for either set of bases.

The (B) label is correlated with Young tableau labels $\{\mu\}$ of nuclear permutation symmetry in a way which has several advantages over previous labeling systems (Longuet Higgins, 1963; Hougen, 1963; Bunker, 1975; Louck and Galbraith, 1976) for common symmetric molecules. First, (B) labels are the standard representation labels of the common point groups. Second, one is able to use the powerful tableau algorithms which have recently been discovered (Robinson, 1964; Harter, 1971; Harter and Patterson, 1976) to derive statistical weights and properties of hyperfine structure. Third, selection rules for multipole transitions are simpler partly because (B) is conserved as shown in Sec. IV–V. Finally, since the labeling scheme is based upon Chang–Fano frame transformation theory it is probably a more natural one for treating ionization, scattering, and possibly dissociation or molecular collisions as discussed in Sec. VI.

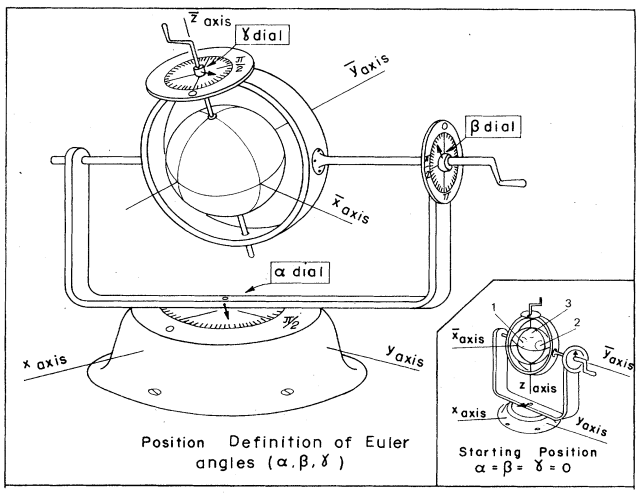

FIG. 1. Definition of Euler angles as coordinates of rotational position state $|\alpha\beta\gamma\rangle$. α = "Azimuth," β = "Polar angle," and γ = "Twist."

Exceptional molecules or transitions such as the "Berry rotating" PF_5 (Dalton, 1971) or other "floppy" molecules are not discussed. (The most "floppy" molecule to be discussed here is NH_3.) The exceptional molecules require internal group operations outside of the ordinary O_3 orthogonal group for their symmetry analysis (Higgins, 1963; Hougen, 1964; Bunker, 1975). The present work is intended to provide the simplest possible framework for discussing most of the spectra of common symmetric molecules which is showing up in modern high resolution experiments.

Since there are many more lines involving high angular momentum (J = 10–100) it is important to emphasize simplifications which are possible in these cases. These include a new theory of rotor level clusters which is derived in Sec. II following a review of the basic theory of symmetric rotors.

II. REVIEW OF QUANTUM ROTOR THEORY

A. Analysis of pure rotations (R_3)

In the description of the quantum rotor, we use Euler angles $(\alpha\beta\gamma)$ as rotor coordinates ($\alpha=\phi$, $\beta=\theta$, $\gamma=\chi$) and as parameters in rotation operators $\mathbf{R}(\alpha\beta\gamma)$.

Figure 1 shows a machine which clearly defines the rotational position of a rotor for body frame $(\bar{x}\bar{y}\bar{z})$ relative to a laboratory (xyz) frame, for a given setting of the Euler angle dials. The original position (see insert) $\alpha=\beta=\gamma=0$ is where $\bar{x}$ points along x, $\bar{y}$ along y, and $\bar{z}$ along z.

We shall define a molecular frame position state using these angles. Here $|\phi\theta\chi\rangle$ shall be that state in which the molecule is tipped in the lab like the machine with the setting $\alpha=\phi$, $\beta=\theta$, and $\gamma=\chi$.

Figure 2(a) shows a machine which can be used to define rotation operators. Operator $\mathbf{R}(\alpha\beta\gamma)$ is defined so that it gives position state $|\alpha\beta\gamma\rangle$ when applied to $|000\rangle$

$$\mathbf{R}(\alpha\beta\gamma)|000\rangle = |\alpha\beta\gamma\rangle \ . \tag{2.1}$$

The y and z cranks in Fig. 2(a) may be used to perform the operations $\mathbf{R}(0\beta0)$ and $\mathbf{R}(\alpha00)=\mathbf{R}(00\alpha)$, respectively. Done consecutively and in the right order, they will give the general rotation

$$\mathbf{R}(\alpha\beta\gamma)=\mathbf{R}(\alpha00)\mathbf{R}(0\beta0)\mathbf{R}(\gamma00) \ , \tag{2.2}$$

where we mean the rightmost factor to act *first*. One can visualize this equation as follows: first $\mathbf{R}(\gamma00)$ sets the twist dial (γ), then $\mathbf{R}(0\beta0)$ sets the polar angle dial (β), and finally $\mathbf{R}(\alpha00)$ sets the azimuthal dial (α).

Figure 2(b) shows a machine which would perform operations $\bar{\mathbf{R}}(\alpha\beta\gamma)$ defined with respect to body coordinates. One may imagine that $\bar{\mathbf{R}}(\alpha\beta\gamma)$ operators rotate the whole universe. In other words, for each $\mathbf{R}(\alpha\beta\gamma)$ that makes a particular tipping of the $\bar{x}\bar{y}\bar{z}$ frame in the lab, let $\bar{\mathbf{R}}(\alpha\beta\gamma)$ make the same tipping of xyz in the body frame. Then the multiplication rules, i.e., R_3 group structure of the two kinds of operators are identical. Furthermore, the lab operators commute with the body operators since they are operationally independent:

$$\mathbf{R}(\alpha\beta\gamma)\bar{\mathbf{R}}(\alpha'\beta'\gamma')=\bar{\mathbf{R}}(\alpha'\beta'\gamma')\mathbf{R}(\alpha\beta\gamma) \ . \tag{2.3}$$

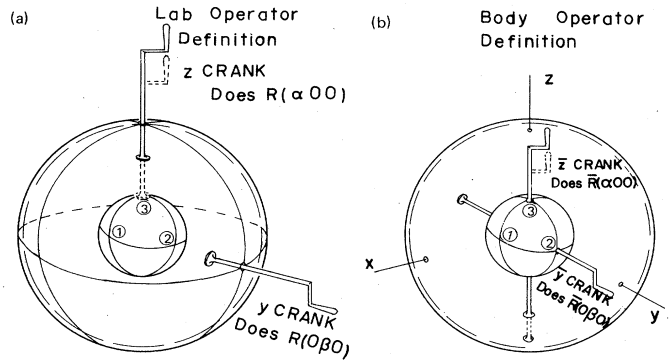

FIG. 2. Definition of Euler angles as parameters of rotational operator $\mathbf{R}(\alpha\beta\gamma)$. (a) Lab based rotation operators like "rotation by χ around z" ($\mathbf{R}(\chi 00)$ or $\mathbf{R}(00\chi)$) or "rotation by β around y" ($\mathbf{R}(0\beta 0)$) are represented by cranks with suction cups which can slide along z or y axes respectively and perform the rotation. The operator $\mathbf{R}(\alpha\beta\gamma)$ which converts starting position (000) in Fig. 1 (see inset) to the $(\alpha\beta\gamma)$ position is the product $(\mathbf{R}(\alpha\beta\gamma)=\mathbf{R}(\alpha 00)\mathbf{R}(0\beta 0)\mathbf{R}(00\gamma))$. (b) Body based rotation operators $\bar{\mathbf{R}}(\alpha\beta\gamma)$ are defined similarly by body based cranks. The difference is that the *inverse* $(\bar{\mathbf{R}}^{-1}(\alpha\beta\gamma)=\bar{\mathbf{R}}(-\gamma-\beta-\alpha))$ converts position (000) to $(\alpha\beta\gamma)$.

However, moving the universe is fictitious, and the only thing that matters is the relative rotational position of the lab and the body (this reminds one of Mach's Principle). Therefore we shall demand that

$$|\alpha\beta\gamma\rangle=\mathbf{R}(\alpha\beta\gamma)|000\rangle=\bar{\mathbf{R}}^{-1}(\alpha\beta\gamma)|000\rangle \\ \bar{\mathbf{R}}(-\gamma-\beta-\alpha)|000\rangle \tag{2.4}$$

for any Euler angles. [This does *not* mean $\mathbf{R}(\alpha\beta\gamma)=\bar{\mathbf{R}}^{-1}(\alpha\beta\gamma)$. Only the original state $\phi=\theta=\chi=0$ which lines up body cranks with lab cranks is affected in the same way by $\mathbf{R}(\alpha\beta\gamma)$ or $\bar{\mathbf{R}}^{-1}(\alpha\beta\gamma)$.]

A more widely known set of rotation operator parameters are the axis angles ($\mathbf{R}[\phi\theta\omega]$) which are schematized by the machine in Fig. 3. Generally, one knows the polar angles ϕ and θ of a given n-fold symmetry axis, and the angle $\omega=2\pi/n$ of the allowed rotation instead of Euler angles. However, $[\phi\theta\omega]$ do not make convenient coordinates for rotational position. [Fortunately, there is a slide rule which allows one to conveniently convert $[\phi\theta\omega]$ to $(\alpha\beta\gamma)$ (Harter and de Santos, 1978).]

Rotation operators $\mathbf{R}(\alpha\beta\gamma)$ and orthogonal transformations in general can aid in the task of finding energy eigenvectors. For the rotor problem one needs combinations of position states $|000\rangle,\ldots|\alpha\beta\gamma\rangle=\mathbf{R}(\alpha\beta\gamma)|000\rangle$,

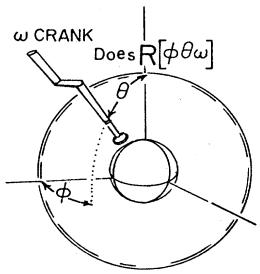

FIG. 3. Definition of axis angles as parameters of rotational operator $\mathbf{R}[\phi\theta\omega]$. A single crank turn by ω around $[\phi\theta]$ axis may be used to define an arbitrary rotation.

which are eigenvectors of various rotor Hamiltonians $\mathbf{H}$. If $\mathbf{H}$ has high enough symmetry, i.e., if enough operators $\mathbf{R}(\alpha\beta\gamma)$ and $\bar{\mathbf{R}}(\alpha\beta\gamma)$ commute with $\mathbf{H}$, then it may be convenient to find eigenvectors in terms of *symmetry projection operators* $\mathbf{P}^A_{mn}$ defined as follows:

Discrete symmetry group $\mathcal{G}$:
$$\mathbf{P}^A_{mn}=([A]/{}^\circ\mathcal{G})\sum_{\mathbf{R}\text{ in }\mathcal{G}}\mathfrak{D}^{A*}_{mn}(\mathbf{R})\mathbf{R} \tag{2.5a}$$

Continuous rotation group R_3:
$$\mathbf{P}^N_{mn}=([N]/8\pi^2)\times\int d(\alpha\beta\gamma)\mathfrak{D}^{N*}_{mn}(\alpha\beta\gamma)\mathbf{R}(\alpha\beta\gamma)\ . \tag{2.5b}$$

Here, $[A]$ and $[N]$ are dimensions of irreducible representations $\mathfrak{D}^A$ and $\mathfrak{D}^N$ of groups $\mathcal{G}$ and R_3 respectively ($[N]=2N+1$ for R_3), ${}^\circ\mathcal{G}$ is the order or number of operators R in group $\mathcal{G}$, and the Euler integral is given by

$$\int d(\alpha\beta\gamma)=\int_0^{2\pi}d\gamma\int_0^{2\pi}d\alpha\int_0^{\pi}\sin\beta d\beta\ . \tag{2.5c}$$

Most of the theory of symmetry projection operators can be found in standard texts (Hamermesh, 1960), and in Lowdin's review article (Lowdin, 1967). Nevertheless, the convenience of P operators for calculation and for theoretical analysis is still not appreciated as much as it could be. For one thing the inverse of Eqs. (2.5), the so-called symmetry "completeness" relations:

$$\mathbf{1}=\sum_A\sum_{m=1}^{[A]}\mathbf{P}^A_{mm} \tag{2.6a}$$

$$\mathbf{R}=\sum_A\sum_{m=1}^{[A]}\sum_{n=1}^{[A]}\mathfrak{D}^A_{mn}(\mathbf{R})\mathbf{P}^A_{mn} \tag{2.6b}$$

are not as widely known as the "orthogonality" relations

$$\mathbf{P}^A_{mn}\mathbf{P}^{A'}_{m'n'}=\delta^{AA'}\delta_{nm'}\mathbf{P}^A_{mn'}\ . \tag{2.7}$$

Both are helpful toward understanding and applying symmetry analysis. For example, we obtain the left and right transformation properties of P operators by substituting Eq. (2.6b) for $\mathbf{R}$ and using Eq. (2.7)

$$\mathbf{R}\mathbf{P}^A_{mn}=\sum_{m'}\mathfrak{D}^A_{m'm}(\mathbf{R})\mathbf{P}^A_{m'n}\ , \tag{2.8a}$$

or

$$\mathbf{P}^A_{mn}\mathbf{R}=\sum_{n'}\mathfrak{D}^A_{nn'}(\mathbf{R})\mathbf{P}^A_{mn'}\ . \tag{2.8b}$$

These, in turn, will give the "laboratory" and "body" transformation rules as we will see shortly.

While it is inappropriate to give a complete derivation of the P operator properties here, we can at least give some elementary examples for which the relations are more or less obvious. The simplest examples are the bilateral symmetry groups of order two (C_2, C_i, C_v, S_2, etc.) each consisting only of the identity $\mathbf{1}$ and a "reflection" operation $\mathbf{R}$ where $\mathbf{R}^2=\mathbf{1}$. There are two irreducible representations $\mathfrak{D}^A$: one "even" ($A=A_1, A_g, A'$; s, etc.), and one "odd" ($A=A_2, A_u, A''$, a, etc.) as given by Table I. It is easy to see that the $\mathbf{P}$ operators [Eq. (2.5a)]

TABLE I. Irreducible representations $D^A(g)$ of various bilateral symmetries (various notations are shown).

C_2 180° rotation	C_i inversion	C_v mirror reflection	S_2 permutation	g = (1	R)
$A = A_1$ or (0_2)	A_g or (+)	A'	s or {2}	1	1
A_2 or (1_2)	A_u or (−)	A''	a or {11}	1	−1

$$\mathbf{P}^{A_1} = \tfrac{1}{2}(\mathbf{1} + \mathbf{R}) , \tag{2.9a}$$

$$\mathbf{P}^{A_2} = \tfrac{1}{2}(\mathbf{1} - \mathbf{R}) , \tag{2.9b}$$

satisfy Eq. (2.6)

$$\mathbf{1} = \mathbf{P}^{A_1} + \mathbf{P}^{A_2} ,$$
$$\mathbf{R} = \mathbf{P}^{A_1} - \mathbf{P}^{A_2} , \tag{2.10}$$

as well as Eqs. (2.7) and (2.8). Furthermore, any bistable or two-level quantum system with basis $\{|1\rangle, |2\rangle \equiv \mathbf{R}|1\rangle\}$ must have eigenstates given by P projection, i.e.,

$$|A_1\rangle = \mathbf{P}^{A_1}|1\rangle\sqrt{2} = (|1\rangle + |2\rangle)/\sqrt{2} ,$$
$$|A_2\rangle = \mathbf{P}^{A_2}|1\rangle\sqrt{2} = (|1\rangle - |2\rangle)/\sqrt{2} , \tag{2.11}$$

if its Hamiltonian commutes with R. This is because off-diagonal (A_1, A_2) matrix elements of a bisymmetric $\mathbf{H}$ must vanish

$$\langle A'|\mathbf{H}|A\rangle \sim \langle 1|\mathbf{P}^{A'}\mathbf{H}\mathbf{P}^{A}|1\rangle = \langle 1|\mathbf{H}\mathbf{P}^{A'}\mathbf{P}^{A}|1\rangle$$
$$= 0 \quad \text{if } A' \neq A . \tag{2.12}$$

Another simple example of P operator application involves any cyclic n-stable quantum system with a basis $\{|1\rangle, |2\rangle = \mathbf{r}|1\rangle, |3\rangle = \mathbf{r}^2|1\rangle, \ldots |n\rangle = \mathbf{r}^{n-1}|1\rangle\}$ for which the Hamiltonian has symmetry $C_n = \{\mathbf{1}\ \mathbf{r}\ \mathbf{r}^2 \ldots \mathbf{r}^{n-1}\}$ where $\mathbf{r}^n = \mathbf{1}$. The irreducible representations of C_n are the nth roots of unity

$$D^{k_m}(\mathbf{r}^p) = e^{ik_m p} , \tag{2.13a}$$

where k_m is an integral multiple (m) of $2\pi/n$

$$k_m = m(2\pi/n) . \tag{2.13b}$$

The energy eigenstates will be the P-projected states

$$|k_m\rangle = \mathbf{P}^{k_m}|1\rangle\sqrt{n}$$
$$= (|1\rangle + e^{-ik_m}|2\rangle + e^{-i2k_m}|3\rangle + \ldots)/\sqrt{n} \tag{2.14}$$

which are just the Bloch or Fourier-analyzed wave states.

The main idea of symmetry analysis, or "group theory" as it is usually called, is to extend Fourier analysis to problems in which the symmetry operators do not necessarily commute with each other. Most R_3 rotational operators $\mathbf{R}(\alpha\beta\gamma)$ are of this type, i.e., generally

$$\mathbf{R}(\alpha\beta\gamma)\mathbf{R}(\alpha'\beta'\gamma') \neq \mathbf{R}(\alpha'\beta'\gamma')\mathbf{R}(\alpha\beta\gamma) .$$

The irreducible representations $\mathfrak{D}^N$ are $[N]\times[N]$ matrices and more complicated than the simple 1×1 Fourier coefficients in Eq. (2.13) or Table I. We shall use R_3 IR defined by the standard formula

$$\mathfrak{D}^N_{mn}(\alpha\beta\gamma) = \sum_{k=0} (-1)^k \frac{[(N+m)!(N-m)!(N+n)!(N-n)!]^{1/2}}{(N+m-k)!\,k!\,(N-n-k)!(n-m+k)!}$$
$$\times e^{-i(m\alpha+n\gamma)}\left(\cos\frac{\beta}{2}\right)^{2N+m-n-2k}\left(\sin\frac{\beta}{2}\right)^{n-m+2k} . \tag{2.15}$$

The $\mathfrak{D}$ are unitary

$$\mathfrak{D}^{N*}_{nm}(\alpha\beta\gamma) = \mathfrak{D}^{N\dagger}_{mn}(\alpha\beta\gamma) = \mathfrak{D}^{N-1}_{mn}(\alpha\beta\gamma) = \mathfrak{D}^{N}_{mn}(-\gamma-\beta-\alpha) . \tag{2.16}$$

[See Feynman (1963) or Hamermesh (1960) for derivation of $\mathfrak{D}^N$.] Nevertheless, the procedure is quite the same. Applying P operators (Eq. 2.5b) to the first rotor position state $|000\rangle$ gives rotor angular momentum eigenbases

$$\left|\begin{matrix} N \\ mn \end{matrix}\right\rangle \equiv \mathbf{P}^N_{mn}|000\rangle/\sqrt{[N]}$$
$$= \frac{1}{8\pi^2}\int d(\alpha\beta\gamma)\mathfrak{D}^{N*}_{mn}(\alpha\beta\gamma)\sqrt{[N]}\ \mathbf{R}(\alpha\beta\gamma)|000\rangle$$
$$= \frac{1}{8\pi^2}\int d(\alpha\beta\gamma)\mathfrak{D}^{N*}_{mn}(\alpha\beta\gamma)\sqrt{[N]}\ |\alpha\beta\gamma\rangle . \tag{2.17}$$

Note that the rotor wave function, i.e., the amplitude for the rotor in state $|{}^N_{mn}\rangle$ to be found at position $(\alpha\beta\gamma)$ is proportional to the IR matrix element

$$\langle\alpha\beta\gamma\,|{}^N_{mn}\rangle = \mathfrak{D}^{N*}_{mn}(\alpha\beta\gamma)\sqrt{[N]} . \tag{2.18}$$

We now identify the row (m) and column (n) indices with external "laboratory" and internal "body" momenta, respectively. If the rotor Hamiltonian $\mathbf{H}_R$ commutes with all external lab operators $\mathbf{R}(\alpha\beta\gamma)$ then it commutes with all P operators, as well. Using this and the unitarity condition

$$\mathbf{P}^{N\dagger}_{mn} = \mathbf{P}^N_{nm}$$

which follows from Eq. (2.16) we deduce that the $\mathbf{H}_R$ matrix must be reduced to diagonal form with respect to m and N

$$\langle{}^N_{mn}|\mathbf{H}_R|{}^{N'}_{m'n'}\rangle \cong \langle 000|\mathbf{P}^{N\dagger}_{mn}\mathbf{H}_R\mathbf{P}^{N'}_{m'n'}|000\rangle ,$$
$$= \langle 000|\mathbf{P}^N_{nm}\mathbf{H}_R\mathbf{P}^{N'}_{m'n'}|000\rangle ,$$
$$= \langle 000|\mathbf{H}_R\mathbf{P}^N_{nm}\mathbf{P}^{N'}_{m'n'}|000\rangle ,$$
$$= \delta^{NN'}\delta_{mm'}\langle 000|\mathbf{H}_R\mathbf{P}^N_{nn'}|000\rangle . \tag{2.19}$$

Further reduction depends upon which of the body frame or internal symmetry operators $\bar{\mathbf{R}}$ commute with the Hamiltonian. The effect of $\bar{\mathbf{R}}$ on a projected state is as follows

$$\bar{\mathbf{R}}(\alpha\beta\gamma)|{}^N_{mn}\rangle = \bar{\mathbf{R}}(\alpha\beta\gamma)\mathbf{P}^N_{mn}|000\rangle/\sqrt{[N]}$$
$$= \mathbf{P}^N_{mn}\bar{\mathbf{R}}(\alpha\beta\gamma)|000\rangle/\sqrt{[N]} \quad \text{(using 2.3)}$$
$$= \mathbf{P}^N_{mn}\mathbf{R}(-\gamma-\beta-\alpha)|000\rangle/\sqrt{[N]} \quad \text{(using 2.4)}$$
$$= \sum_{n'}\mathbf{P}^N_{mn'}|000\rangle\mathfrak{D}^N_{nn'}(-\gamma-\beta-\alpha)/\sqrt{[N]} \quad \text{(using 2.8b)}$$

$$\bar{\mathbf{R}}(\alpha\beta\gamma)\left|\begin{matrix} N \\ mn \end{matrix}\right\rangle = \sum_{n'}\left|\begin{matrix} N \\ mn' \end{matrix}\right\rangle\mathfrak{D}^{N*}_{n'n}(\alpha\beta\gamma) . \tag{2.20}$$

The unitarity of $\mathfrak{D}$ [Eq. (2.16)] was used in the last step. This should be compared with the similarly derived laboratory transformation

$$\mathbf{R}(\alpha\beta\gamma)\left|\begin{matrix}N\\mn\end{matrix}\right\rangle=\sum_{m'}\left|\begin{matrix}N\\m'n\end{matrix}\right\rangle\mathfrak{D}^{N}_{m',m}(\alpha\beta\gamma)\ . \tag{2.21}$$

To relate this last equation to more standard relations involving spherical harmonics $\langle\mathbf{r}|{}^{N}_{n}\rangle=Y^{N}_{m}(\mathbf{r})$, let $|\mathbf{r}\rangle$ be a position state for a particle located at $\mathbf{r}=(x,y,z)$ in the lab system or $\bar{\mathbf{r}}=(\bar{x},\bar{y},\bar{z})$ in the body system. Then Eq. (2.21) reads

$$\left\langle\mathbf{r}\left|\mathbf{R}(\alpha\beta\gamma)\right|\begin{matrix}N\\m\end{matrix}\right\rangle=\sum_{m'}\left\langle\mathbf{r}\left|\begin{matrix}N\\m'\end{matrix}\right\rangle\mathfrak{D}^{N}_{m',m}(\alpha\beta\gamma)\right.$$

which becomes

$$Y^{N}_{m}(\bar{\mathbf{r}})=\sum_{m'}Y^{N}_{m'}(\mathbf{r})\mathfrak{D}^{N}_{m',m}(\alpha\beta\gamma)\ , \tag{2.22a}$$

where we use the definitions

$$|\bar{\mathbf{r}}\rangle=\mathbf{R}^{-1}(\alpha\beta\gamma)|\mathbf{r}\rangle=\mathbf{R}^{\dagger}(\alpha\beta\gamma)|\mathbf{r}\rangle$$
$$\langle\bar{\mathbf{r}}|=\langle\mathbf{r}|\mathbf{R}(\alpha\beta\gamma)\ .$$

The inverse

$$Y^{N}_{m}(\mathbf{r})=\sum_{m'}Y^{N}_{m'}(\bar{\mathbf{r}})\mathfrak{D}^{N*}_{mm'}(\alpha\beta\gamma) \tag{2.22b}$$

will be required later.

If the usual definition of angular momentum generators $\mathbf{N}_a$ and $\bar{\mathbf{N}}_a$ are combined with Eq. (2.2), then we have

$$\mathbf{R}(\alpha\beta\gamma)=e^{\alpha\mathbf{N}_z/i}e^{\beta\mathbf{N}_y/i}e^{\gamma\mathbf{N}_z/i}\ . \tag{2.23a}$$

$$\bar{\mathbf{R}}(\alpha\beta\gamma)=e^{\alpha\bar{\mathbf{N}}_{\bar{z}}/i}e^{\beta\bar{\mathbf{N}}_{\bar{y}}/i}e^{\gamma\bar{\mathbf{N}}_{\bar{z}}/i}\ . \tag{2.23b}$$

The matrices of the generators follow from the rotation matrices or vice versa. For example, we have

$$\mathbf{N}_z\left|\begin{matrix}N\\mn\end{matrix}\right\rangle=m\left|\begin{matrix}N\\mn\end{matrix}\right\rangle\ , \tag{2.24a}$$

$$\mathbf{N}_{\bar{z}}\left|\begin{matrix}N\\mn\end{matrix}\right\rangle=n\left|\begin{matrix}N\\mn\end{matrix}\right\rangle\ , \tag{2.24b}$$

where we shall define (Van Vleck, 1951)

$$\mathbf{N}_{\bar{x}}\equiv-\bar{\mathbf{N}}_{\bar{x}}\ ,\ \mathbf{N}_{\bar{y}}\equiv-\bar{\mathbf{N}}_{\bar{y}},\ \mathbf{N}_{\bar{z}}\equiv-\bar{\mathbf{N}}_{\bar{z}}\ . \tag{2.25}$$

Here $\mathbf{N}_{\bar{\mu}}$ are the body components of angular momentum. (The sign change is necessary if we want a molecule spinning counter clockwise around its $\bar{z}$ axis to give positive $\langle N_{\bar{z}}\rangle$.) Other relations are the following:

$$\mathbf{N}_y\left|\begin{matrix}N\\mn\end{matrix}\right\rangle=-\frac{i}{2}[(N-m)(N+m+1)]^{1/2}\left|\begin{matrix}N\\m+1\ n\end{matrix}\right\rangle+\frac{i}{2}[(N+m)(N-m+1)]^{1/2}\left|\begin{matrix}N\\m-1\ n\end{matrix}\right\rangle, \tag{2.26a}$$

$$\mathbf{N}_{\bar{y}}\left|\begin{matrix}N\\mn\end{matrix}\right\rangle=\frac{i}{2}[(N-n)(N+n+1)]^{1/2}\left|\begin{matrix}N\\m\ n+1\end{matrix}\right\rangle-\frac{i}{2}[(N+n)(N-n+1)]^{1/2}\left|\begin{matrix}N\\m\ n-1\end{matrix}\right\rangle, \tag{2.26b}$$

$$\mathbf{N}_x\left|\begin{matrix}N\\mn\end{matrix}\right\rangle=\frac{1}{2}[(N-m)(N+m+1)]^{1/2}\left|\begin{matrix}N\\m+1\ n\end{matrix}\right\rangle+\frac{1}{2}[(N+m)(N-m+1)]^{1/2}\left|\begin{matrix}N\\m-1\ n\end{matrix}\right\rangle, \tag{2.27a}$$

$$\mathbf{N}_{\bar{x}}\left|\begin{matrix}N\\mn\end{matrix}\right\rangle=\frac{1}{2}[(N-n)(N+n+1)]^{1/2}\left|\begin{matrix}N\\m\ n+1\end{matrix}\right\rangle+\frac{1}{2}[(N+n)(N-n+1)]^{1/2}\left|\begin{matrix}N\\m\ n-1\end{matrix}\right\rangle. \tag{2.27b}$$

For a rigid spherical rotor Hamiltonian

$$\mathbf{H}^{\text{sphere}}_{R}=(\mathbf{N}^2_{\bar{x}}+\mathbf{N}^2_{\bar{y}}+\mathbf{N}^2_{\bar{z}})/2I_{\bar{x}\bar{y}\bar{z}} \tag{2.28}$$

which commutes with all internal $\bar{\mathbf{R}}$, it is clear that the energy spectrum consists of $(2N+1)(2N+1)$ degenerate N levels (see center of Fig. 4) of energy

$$\left\langle\begin{matrix}N\\mn\end{matrix}\right|\mathbf{H}^{\text{sphere}}_{R}\left|\begin{matrix}N'\\m'n'\end{matrix}\right\rangle=\delta^{NN'}\delta_{mm'}\delta_{nn'}N(N+1)/2I_{\bar{x}\bar{y}\bar{z}}\ . \tag{2.29}$$

The symmetric rigid rotor Hamiltonian

$$\begin{aligned}\mathbf{H}^{\text{sym}}_{R}&=(\mathbf{N}^2_{\bar{x}}+\mathbf{N}^2_{\bar{y}})/2I_{\bar{x}\bar{y}}+\mathbf{N}^2_{\bar{z}}/2I_{\bar{z}}\\&=(\mathbf{N}^2_{\bar{x}}+\mathbf{N}^2_{\bar{y}}+\mathbf{N}^2_{\bar{z}})/2I_{\bar{x}\bar{y}}+\mathbf{N}^2_{\bar{z}}(1/2I_{\bar{z}}-1/2I_{\bar{x}\bar{y}})\end{aligned} \tag{2.30}$$

commutes with internal $\bar{z}$ axis rotations $\bar{\mathbf{R}}(\gamma 00)$, and its energy levels are given by

$$\left\langle\begin{matrix}N\\mn\end{matrix}\right|\mathbf{H}^{\text{sym}}_{R}\left|\begin{matrix}N'\\m'n\end{matrix}\right\rangle=\delta^{N'N}\delta_{mm'}\delta_{nn'}[N(N+1)/2I_{\bar{x}\bar{y}}+n^2(1/2I_{\bar{z}}-1/2I_{\bar{x}\bar{y}})]\ , \tag{2.31}$$

i.e., $(2N+1)$-fold degenerate levels with $n=0$, and (if $I_{\bar{z}}>0$) $2(2N+1)$-fold degenerate levels for each $0<|n|\leq N$ (see Fig. 4).

The symmetry of any rotor can be written $\mathfrak{IC}$(external) $\times\bar{\mathcal{G}}$ (internal). If the rotor is free then $\mathfrak{IC}$ is R_3 (or O_3 as explained in the following section) since all external operations $\mathbf{R}(\alpha\beta\gamma)$ are symmetry operators. If the rotor is in a crystal matrix then $\mathfrak{IC}$ is the site group of the lattice. If the rotor is in a homogeneous electric (or magnetic) field then $\mathfrak{IC}$ is O_2 (or R_2). $\mathfrak{IC}$ is the "applied" symmetry.

Meanwhile, $\bar{\mathcal{G}}$ is the internal or basic symmetry of the rotor structure. However, rotors are made of nuclear points so the real internal symmetry is finite, usually some molecular point group.

It is well known how externally applied fields split l orbitals into various finite symmetry A orbitals. Since the invention of "crystal field theory" (Bethe, 1929) many methods have been given for finding the crystal field transformation coefficients $\left(\begin{matrix}l\\m\end{matrix}\middle|\begin{matrix}A\\a\end{matrix}\right)$ in expansions of the form

$$\mathcal{Y}^{A}_{a}=\sum_{m}\left(\begin{matrix}l\\m\end{matrix}\middle|\begin{matrix}A\\a\end{matrix}\right)Y^{l}_{m}\ . \tag{2.32}$$

The relations convert spherical harmonics Y^{l}_{m} of a given l into "cubic" or "trigonal" harmonics $\mathcal{Y}^{A}_{a}$ belonging to some IR $\mathfrak{D}^{A}$ of a point group.

Now we may use the same theory for the internal sym-

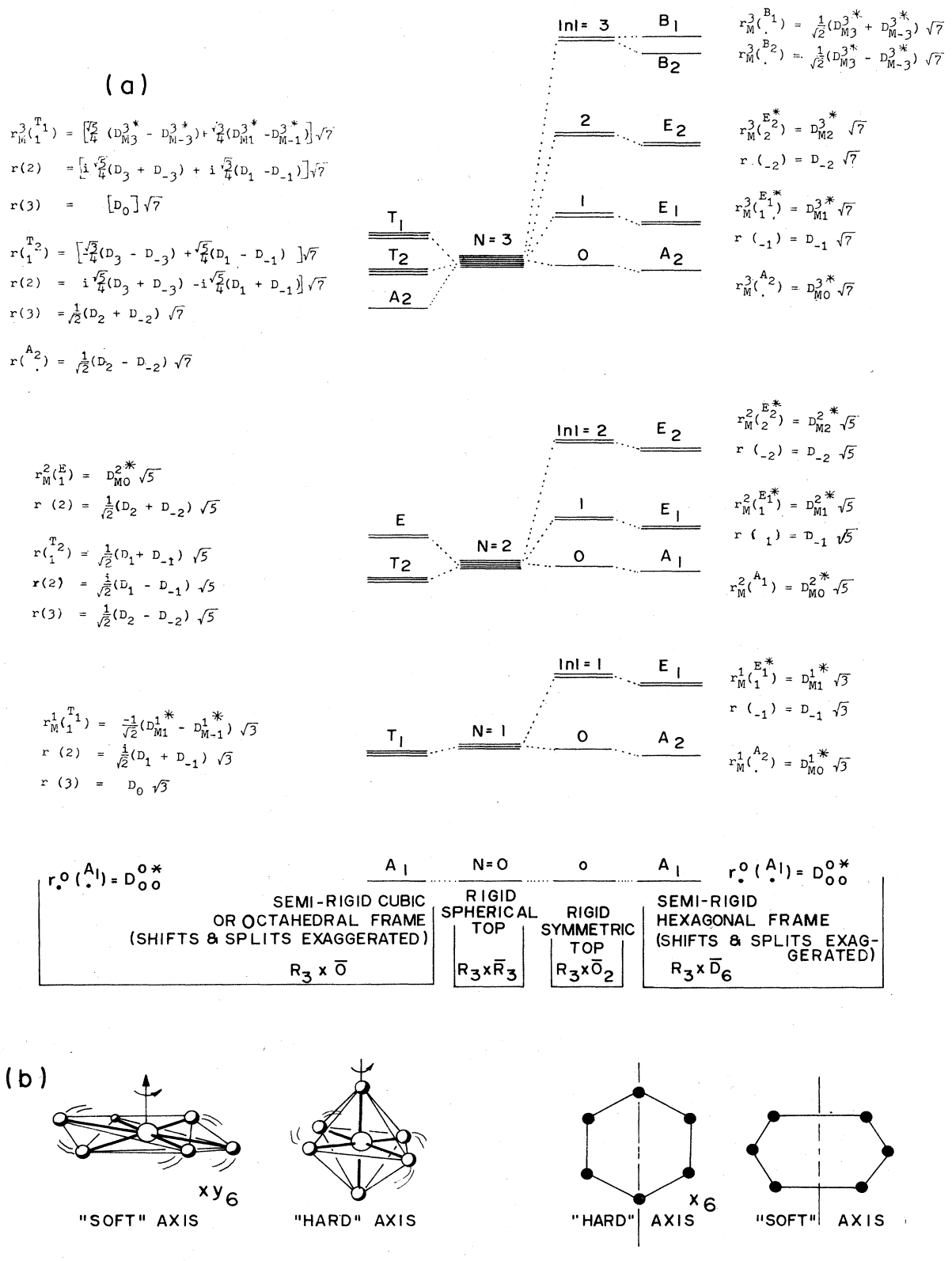

FIG. 4. (a) Correlation of lowest levels of rigid spherical and symmetric rotors with semirigid rotors. (b) Centrifugal distortion of semirigid rotors. Amount of distortion depends on direction of rotation axis. Some directions are softer than others. This directional anisotropy must have the symmetry of the rotor. Hence the levels and wave functions must be defined by representations of that symmetry as shown in the figure and explained in Secs. II.A.1–4.

metry. According to (2.11), the internal transformation differs only by a complex conjugate from the external one. So we may take our finite rotor functions to be

$$\left\langle \begin{vmatrix} N & B^* \\ m & b \end{vmatrix} \right\rangle \equiv r^{N\ B^*}_{m\ b} = \sum_n \begin{pmatrix} N \\ n \end{pmatrix} \begin{vmatrix} B \\ b \end{vmatrix}^* \mathfrak{D}^{N*}_{mn}(\phi\theta\chi)\sqrt{[N]} \ , \qquad (2.33)$$

where $[N] = 2N+1$.

We insert the normalization factor $\sqrt{[N]}$ so that

$$\frac{1}{8\pi^2}\int_0^{2\pi} d\phi \int_0^{\pi} \sin\theta\, d\theta \int_0^{2\pi} d\chi (r^{N'A'}_{m'a'})^* r^{NA}_{ma} = \delta^{N'N}\delta_{m'm}\delta^{A'A}\delta_{a'a} \qquad (2.34)$$

follows from the standard R_3 orthogonality relation

$$\frac{1}{8\pi^2}\int_0^{2\pi} d\phi \int_0^{\pi} \sin\theta\, d\theta \int_0^{2\pi} d\chi\, \mathfrak{D}^{N'*}_{m'n'}(\phi\theta\chi)\mathfrak{D}^{N}_{mn}(\phi\theta\chi) = \delta^{N'N}\delta_{m'm}\delta_{n'n}/([N]) \ , \qquad (2.35)$$

and the assumption that each crystal field transformation is orthonormal and complete

$$\sum_{A,a} \begin{pmatrix} N \\ n \end{pmatrix} \begin{vmatrix} A \\ a \end{vmatrix}^* \begin{pmatrix} N \\ n' \end{pmatrix} \begin{vmatrix} A \\ a \end{vmatrix} = \delta_{nn'} \ , \qquad (2.36a)$$

$$\sum_{n} \begin{pmatrix} N \\ n \end{pmatrix} \begin{vmatrix} A' \\ a' \end{vmatrix}^* \begin{pmatrix} N \\ n \end{pmatrix} \begin{vmatrix} A \\ a \end{vmatrix} = \delta^{A'A}\delta_{a'a} \ . \qquad (2.36b)$$

For low N the finite symmetry projection operators [Eq. (2.5a)] may be used to derive the coefficients $\binom{N}{n}\begin{vmatrix} A \\ a \end{vmatrix}$ to make finite symmetry rotor functions. Results for cubic-octahedral (O) symmetric XY_6 rotors, and hexagonal (C_6 or D_6) symmetric X_6 rotors are shown in Fig. 4 for momentum $N = 0-3$. Tables of functions for $N \leq 20$ are given by Jahn (1938), Hecht (1960), and Moret-Bailly (1965).

However, for larger N the standard approaches to symmetry projection become mathematically more complicated and more tedious. For one thing, two or more independent states with the same symmetry label will appear, and it is difficult to distinguish them. (In $N = 30$ there are seven independent T_1 levels, for example.)

The following sections (1–4) discuss a way out of this difficulty. A new approximate scheme for finding finite-symmetry bases from angular momentum states is discussed. The scheme becomes easier to apply as the angular momentum increases, and is perhaps easier to understand physically than other schemes.

1. Semirigid symmetric rotors: Reducing $\bar{R}_2$ to polygonal symmetry ($\bar{C}_n$, $\bar{D}_n$)

It is very useful to draw analogies between rotor Hamiltonians with anisotropic centrifugal perturbations and the Hamiltonians of an orbiting electron with anisotropic crystal field perturbations. Consider an electron orbiting in a cylindrical geometry, i.e., R_2 symmetry. The eigenfunctions are the elementary Bohr waves

$$\psi_n(\text{Bohr}) \sim e^{in\phi} (n = 0, \pm 1, \pm 2, \ldots),$$

where ϕ is the azimuthal coordinate, and quantum number $|n|$ gives the number of wave crests in the range $0 \leq \phi < 2\pi$, while $n\hbar$ is the angular momentum in (energy) (time) units. The Bohr energy spectrum is given by

$$E = an^2 + b \ ,$$

where a and b are constant. Its energy levels are doubly degenerate for $|n| > 0$. The spectrum looks like that of the rigid symmetric rotor for each N provided n is restricted by $|n| \leq N$. [See the Rigid Symmetric Top column of Fig. 4(a).]

TABLE II. IR and characters of C_6 ($\epsilon = e^{\pi i/3}$; $\delta = e^{2\pi i/3}$).

Operation = Rotation angle α =	1 0°	r 60°	r^2 120°	r^3 180°	r^4 240°	r^5 300°
$A = 0_6$	1	1	1	1	1	1
$\epsilon_1 = 1_6$	1	ϵ	δ	−1	δ^*	ϵ^*
$\epsilon_2 = 2_6$	1	δ	ϵ	−1	ϵ^*	δ^*
$B = 3_6$	1	−1	1	−1	1	−1
$\epsilon_2^* = 4_6$	1	δ^*	ϵ^*	−1	ϵ	δ
$\epsilon_1^* = 5_6$	1	ϵ^*	δ^*	−1	δ	ϵ

Now suppose we introduce p equivalent point charges or potential wells each centered on the vertices of a regular p-gon. This reduces the symmetry from R_2 to C_p and perturbs the Bohr levels in a systematic fashion. Let us discuss the hexagonal ($p = 6$) case since that is complex enough to contain all the relevant structure. The six potential wells will be analogous to a hexagonally anisotropic centrifugal perturbation for the X_6 rotor. Well bottoms and tops correspond to "soft" and "hard" rotation axes, respectively, in the plane of the rotor as shown on the right side of Fig. 4(b).

Now each Bohr state $|n\rangle$ belongs to one of the C_6 IR (a_6) shown in Table II where $n = a$ mod 6. (Note the correspondence between our notation and the usual alphabetical one.) The lowest Bohr level which is split by a hexagonal perturbation is the $|n| = 3$ level. Since both the right- and left-handed moving wave states ($|n = 3\rangle$ and $|n = -3\rangle$) belong to the $B = (3_6)$ IR of C_6 they can be mixed and split by the perturbation. Physically, these ($|n| = 3$, $B = (3_6)$) waves have exactly one half-wavelength per well spacing and are called Brillouin zone boundary or band boundary states in crystal physics. (The coincidence of B's here is probably just that.) If each well is bilaterally symmetric, then the moving waves will mix to form the two standing waves labeled B_1 and B_2 in Fig. 4(a). The antisymmetric wave state

$$|B_2\rangle = (|3\rangle - |-3\rangle)/\sqrt{2} \sim \sin 3\phi$$

has higher energy since it hovers over the hills and has nodes at well centers. The symmetric wave state

$$|B_1\rangle = (|3\rangle + |-3\rangle)/\sqrt{2} \sim \cos 3\phi$$

is lower in energy since it sits in the wells (see Fig. 5a).

B_1 and B_2 are standard labels for IR of D_6 symmetry which includes subgroup C_6 plus two-fold rotation operations around axes through well centers and well tops. Table III gives the IR characters of D_6. Comparing Tables II and III gives the correlation table between D_6 and C_6 [Table IV(A)]. We say that B_1 and B_2 are both *correlated* with $B = (3_6)$ since they both have the same

TABLE III. D_6 characters.

	1	120°($\bar{z}$) rotations	180°($\bar{y}$..) rotations	180°($\bar{z}$) rotations	60°($\bar{z}$) rotations	180°($\bar{x}$..) rotations
A_1	1	1	1	1	1	1
A_2	1	1	−1	1	1	−1
E_2	2	−1	0	2	−1	0
B_1	1	1	1	−1	−1	−1
B_2	1	1	−1	−1	−1	1
E_1	2	−1	0	−2	1	0

numbers as (3_6) under C_6 operations in Table III. Note also the degenerate IR E_1 and E_2 are correlated with moving waves of angular momentum ±1 and ±2 respectively, i.e., with pairs $[(1_6),(5_6)]$ and $[(2_6),(4_6)]$.

The D_6 symmetry properties of the wave functions do not change as the potential increases provided its symmetry is maintained. However, the wave functions will be squeezed out of the regions of high potential as shown in Fig. 5(b). Furthermore, the lowest bands will shrink into nearly degenerate level configurations $(A_1E_1E_2B_1)$ and $(B_2E_2E_1A_2)$ which we will call the (0)th and (1)st *clusters*. In the limit of infinitely deep wells, tunneling between wells becomes "unfeasible" and the cluster degeneracy is exact. Then the only symmetry that matters is the local symmetry of each well, i.e., the group C_2 involving the two-fold axis that goes through each potential well center. The waves in a given well will be classified as *symmetric* which is labeled (0_2) in our notation, or else antisymmetric which is labeled (1_2).

There is a simple way to tell which IR of the bigger group D_6 belong in a cluster made of (0_2) or (1_2) waves. One simply correlates (0_2) and (1_2) IR of the appropriate subgroup C_2 with IR of "super" group D_6. The (0_2) column of Table IV(B) contains the IR $(A_1E_1E_2B_1)$ which are just the ones in the (0)th cluster, and the (1_2) column contains $(A_2E_1E_2B_2)$. In the same way we found that the C_6 axis clusters (A_1A_2), (E_1), (E_2), and (B_1B_2) showed up

TABLE IV A. Correlation table between representations of hexagonal symmetry (D_6) and C_6.

D_6 \ C_6	(0_6)	(1_6)	(2_6)	(3_6)	(4_6)	(5_6)
A_1	1	···	···	···	···	···
A_2	1	···	···	···	···	···
B_1	···	···	···	1	···	···
B_2	···	···	···	1	···	···
E_1	···	1	···	···	···	1
E_2	···	···	1	···	1	···

TABLE IV B. Correlation table between representations of hexagonal symmetry (D_6) and $C_2(\bar{y}$ axis).

D \ C_2	(0_2)	(1_2)
A_1	1	···
A_2	···	1
B_1	1	···
B_2	···	1
E_1	1	1
E_2	1	1

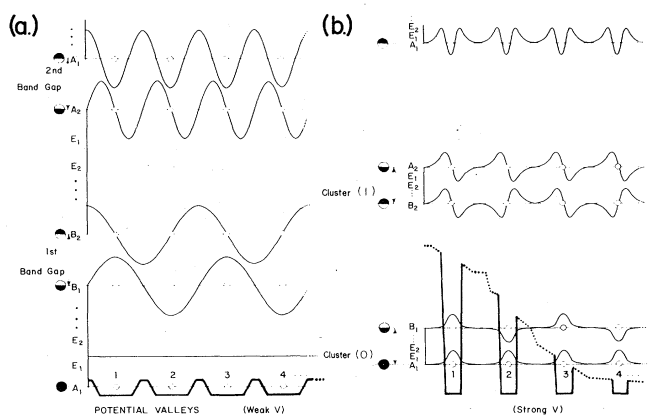

FIG. 5. (A) and (B) Type standing wave eigenfunctions in D_n symmetric potential. ((E) Type moving waves are not drawn.) (a) *Weak Potential*. Energy differences are determined by potential energy only in this limit. Waves which hover over potential hills belong to higher energy levels. (b) *Strong Potential*. Energy differences are determined by the number of nodes in the wave. Waves with more nodes must have more total energy even if it means having less potential energy. For a given band or "cluster" the wave form within the wells are identical for all levels $AE_1E_2\ldots$ except for phase. Nodes within the wells tell to which cluster the wave belongs.

in the (0_6), (1_6), (2_6), and (3_6) columns of Table IV(A) and represented degenerate or nearly degenerate levels when the six fold potential was weak [Fig. 5(a)].

The contents of a cluster like $(A_2E_1E_2B_2)$ make up what is called an *induced representation* $(1_2)\uparrow D_6$ of the "super" group. The theory of induced representation is turning out to be very important for quantum mechanics (Mackey, 1968). It is the basis of the "correlation method" (Fately *et al.*, 1972) used for deriving space group selection rules. It underlies the theory of the important Young tableau labeling of unitary and permutation group representations, (Coleman, 1966; Harter and Patterson, 1976b) whose applications will be introduced in Sec. III.D–E. It is probably the key to convenient analyses of internal rotations (Watson, 1965) or of "Berry rotations" (Berry, 1960; Dalton, 1971). In a very elementary way, we will use correlation methods to analyze rotation and inversion spectra in the second half of this paper. Now we use them to derive cluster properties.

Series of $(a_2)\uparrow D_6$ or $(b_6)\uparrow D_6$ level clusters may appear in the spectrum of any D_6-symmetric rotor Hamiltonians evaluated in an angular momentum (N) manifold. Since an N-manifold has only $[N]=2N+1$ states (we are counting only internal, or else only external quantum states now), its series of levels may begin or else end in the middle of some cluster. Nevertheless, simple circular monograms or "cluster wheels" (Fig. 6) can be made to show which D_6 levels and clusters are correlated with any given orbital $(J=N)$ level. For example, for $J=3$ we read the D_6 IR between the $(J=1,\underline{3},5,\ldots)$ arrow on the outside of the odd-J wheel and the $(J=\underline{3},9,\ldots)$ arrow in the inside. The IR may be grouped into either $(a_2\uparrow D_6)$ clusters:

$$(J=3)\uparrow D_6=(A_2\oplus E_1\oplus E_2\oplus B_2)_{1_2}\oplus(B_1\cdots)_{0_2},$$

or $(a_6)\uparrow D_6$ clusters:

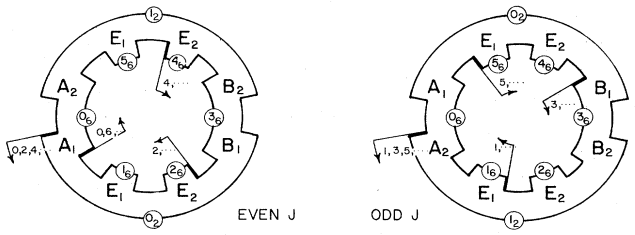

FIG. 6. Cycles of D_6 IR contained in a level of total angular momentum J.

$$(J=3)\uparrow D_6=(\ldots A_2)_{0_6}\oplus(E_1)_{1_6}\oplus(E_2)_{2_6}\oplus(B_2\oplus B_1)_{3_6},$$

using the "teeth" on the inside and outside of the wheels. [The latter corresponds to the spectrum on the upper right hand side of Fig. 4(a).]

The wheels always give the correct contents for any J regardless of ordering. For $J=6+j, 12+j, 18+j, \ldots (j<6)$ it will be necessary to read around a wheel $1, 2, 3, \ldots$ times plus a fraction of a turn for j. For certain Hamiltonians the wheels give the levels in the right order (Harter and Patterson, 1977c).

So far, the spectroscopy of D_n symmetric molecules has not shown anything like the "giant" (0_2) or (1_2) clusters. Instead one usually finds the standard $\bar{z}$ angular momentum levels associated with $(0_n)(1_n)(2_n), \ldots$ clusters. Even the splitting of clusters like $(0_6)\uparrow D_6=(A_1\oplus A_2)$ and the $(3_6)\uparrow D_6$ is generally unresolved. However, it is conceivable that for high enough J in the right polygonal molecule the centrifugal distortion anisotropy might dominate to the extent that a rotor could become "stuck" rotating on a twofold axis. Then the "giant" clusters would appear if the spectral resolution and analysis permitted.

We turn now to cases where analogous types of "giant" clusters have already been observed. Then in Secs. II.A.3 and 4 we give a more quantitative discussion of what it takes to get a rotor "stuck" on a particular axis and how the clusters split when the "unsticking" becomes feasible.

2. Semirigid spherical rotors: Reducing $\bar{R}_3$ to cubic or tetrahedral symmetry ($\bar{O}$, $\bar{T}_d$)

Using laser diode techniques (Hinkley *et al.*, 1968; Hinkley and Freed, 1969; Hinkley and Kelley, 1971) and computer analysis, the Los Alamos group resolved and labeled many bands in the 947 cm^{-1} vibration of SF_6 (Aldridge *et al.*, 1975; McDowell, *et al.* 1976; Fox *et al.*, 1976). They noticed many nearly degenerate clusters of lines in the diode spectrum and in the level structure predicted by the computer. Their observations were independent of those made in earlier computer calculations which had shown clusters, too. Lea, Leask, and Wolf (1962) modeled rare earth crystal field splitting of $J=2$–8 levels in cubic symmetry and noticed interesting clustering. Calculations of tetrahedral splitting in CH_4 fine structure for $J=2$–20 (Dorney and Watson, 1972) showed clusters. Dorney and Watson were the first to explain the sixfold and eightfold near-degeneracies in terms of rotation on six fourfold and eight threefold symmetry axes of a tetrahedron. However, the most extensive computer calculations ($J=2$–100) were done at Los Alamos (Krohn, 1976). These were used to deduce and develop approximate quantum models and analytic formulas for cluster structure (Harter and Patterson, 1977 a, b, and c; Patterson and Harter, 1977). We review some of these results here and in the following sections.

Fig. 7(a) shows examples of clusters of lines belonging to octahedral IR in the spectra of the molecule SF_6 (Table V lists the IR characters of octahedral group O.) Spectral lines represent *differences* between select rotational levels in the ground and vibrationally excited states. However, for reasons discussed in Sec. V it turns out that each spectral $P(N)$ pattern is a scale model of the centrifugally split *N-level* pattern in the ground state. So for the time being let us pretend that Fig. 7(a) is a rotor level diagram.

The mathematical problems of cubic crystal-field splitting and SF_6 rotor levels are similar. Wolf and Leask computed the effect of the anisotropic potential

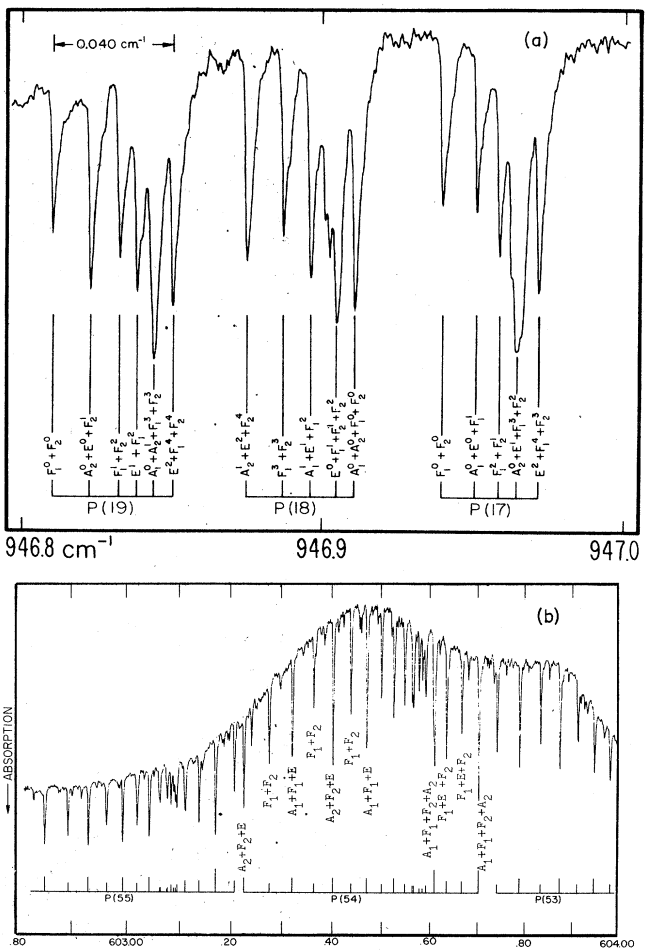

FIG. 7. (a) Tunable laser diode absorption spectra of SF_6 [J. P. Aldridge, H. Filip, H. Flicker, R. F. Holland, R. S. McDowell, and N. G. Nerson, J. Mol. Spectrosc. 58, 167 (1975)]. (b) CF_4 absorption spectra. Laser diode spectra taken at 296 °K 1m path, and 2.1 torr. (R. S. McDowell, H. W. Galbraith, M. J. Reisfeld, and J. P. Aldridge; unpublished; 1977).

TABLE V. O characters.

	1	120° rotations $\bar{r}=\bar{R}[2\pi/3]$	180° ($\bar{x}\bar{y}\bar{z}$) rotations $\bar{R}(\pi 00)$	90° ($\bar{x}\bar{y}\bar{z}$) rotations $\bar{R}=\bar{R}\left(\frac{\pi}{2}00\right)$	180° (diagonal) rotations $\bar{R}\left(\frac{\pi}{2}\frac{\pi}{2}\frac{\pi}{2}\right)$
A_1	1	1	1	1	1
A_2	1	1	1	−1	−1
E	2	−1	2	0	0
T_1	3	0	−1	1	−1
T_2	3	0	−1	−1	1

$$V^4(x)=a(x^4+y^4+z^4)+b \text{ (isotropic)}$$

on electronic orbitals. For positive (a) and fixed radius the electron finds the highest energy on the fourfold x, y, or z axes $[(x,y,z)=r(\pm 100)$, $r(0\pm 10)$, or $r(00\pm 1)]$, and the lowest on the threefold axes. $[(x,y,z)=r(\pm 1,\pm 1,\pm 1)/\sqrt{3}.]$ The analogous octahedral centrifugal operator

$$\bar{V}^4(\mathbf{N})=a(\mathbf{N}_{\bar{x}}^4+\mathbf{N}_{\bar{y}}^4+\mathbf{N}_{\bar{z}}^4)+b \text{ (isotropic)} \qquad (2.37)$$

has similar properties. For fixed total momentum N ($\mathbf{N}^2=\mathbf{N}_{\bar{x}}^2+\mathbf{N}_{\bar{y}}^2+\mathbf{N}_{\bar{z}}^2$) we find that rotation around the fourfold axes requires the most energy while rotation around threefold axes needs the least. This rotational anisotropy is consistent with one's intuition about the bonding of octahedral SF_6. The radial "stretch" bonds are much stronger than the "bending" ones. Therefore we expect to have the most centrifugal distortion during rotation around the "soft" threefold axes, and hence the least rotation energy. [See left-hand side of Fig. 4(b).] By the same arguments we expect that the sign of (a) should be negative for tetrahedral CH_4-like molecules for which the "hard" rotational directions should be the three-fold axes.

While it is true that tetrahedral (T or T_d) symmetry does allow one lower order anisotropic operator of the form

$$\bar{\mathbf{V}}^3=\mathbf{N}_{\bar{x}}\mathbf{N}_{\bar{y}}\mathbf{N}_{\bar{z}} ,$$

this is ruled out by time reversal symmetry, i.e., rotational distortion should be the same for rotation around axis ω as it is for axis $-\omega$. Hence, the mathematical problem of CH_4 distortion is the same as that of SF_6. The same type of clusters show up in SF_6 spectra, CH_4 spectra (Pine, 1976), and CF_4 spectra [See Fig. 7(b)].

In order to understand the cluster levels, we think of the molecule more or less "stuck" rotating on one of its "soft" axes or else on one of its "hard" axes. In this situation it will be centrifugally distorted so that it no longer has spherical or even its cubic or tetrahedral shape. [It is interesting to note that a tetrahedral XY_4 molecule distorted by threefold axis rotation could have a "permanent" dipole moment which would otherwise be forbidden in T_d symmetry. In fact "forbidden" rotational transitions have been observed (Oka, 1976).] An octahedral rotor stuck on one of its threefold or fourfold axes may behave as though it has only C_3 or C_4 symmetry, respectively. However, if it is at all feasible for it to become unstuck and change internal axes, then it will "remember" its full cubic symmetry, and clusters of levels belonging to cubic IR will appear.

TABLE VIA. C_3 characters ($\epsilon=e^{2\pi i/3}$).

	1	$\bar{r}$	$\bar{r}^2$
$0_3=A$	1	1	1
$1_3=E_{x+iy}$	1	ϵ	ϵ^*
$2_3=E_{x-iy}$	1	ϵ^*	ϵ

TABLE VIB. C_4 characters ($i=e^{2\pi i/4}$).

	1	$\bar{R}$	$\bar{R}^2$	$\bar{R}^3$
$0_4=A$	1	1	1	1
$1_4=E_{x+iy}$	1	i	−1	$-i$
$2_4=B$	1	−1	1	−1
$3_4=E_{x-iy}$	1	$-i$	−1	i

To see which cubic IR show up in a given level cluster, we may use the correlation procedure introduced in the preceding Sec. II.A.1. First we use the standard character tables of O (Table V), C_3 (Table VIA), and C_4 (Table VIB) to derive the reduction or splitting of O IR into C_3 and C_4 IR. The reduction ($A\downarrow C_3$) or ($A\downarrow C_4$) of IR(A) of group O is given in the (A)th row of Table VII A or Table VII B, respectively. (Physically, the rows of Tables VII A and VII B label the Zeeman splitting of cubic levels which would occur if a magnetic field were put along a three- or fourfold axis, respectively, of a cubic crystal.) Now we find the observed clusters in the *columns* of correlation Tables VII.

Finally, it is possible to predict the relative location of various clusters in an N pattern using the correlation tables. Suppose the rotor is stuck on a threefold axis with angular momentum K_3, i.e., in a state $|^N_{m\ n=K_3}\rangle$. The internal transformation relations [Eqs. (2.20), (2.23b), and (2.14b)] for a rotation $\bar{r}$ by $2\pi/3$ gives

$$\bar{r}\left|\begin{matrix}N\\ mn=K_3\end{matrix}\right\rangle = e^{2\pi i n/3}\left|\begin{matrix}N\\ mn=K_3\end{matrix}\right\rangle .$$

Comparing this with Table VI A we see that the state $|^N_{mn=K_3}\rangle$ belongs to C_3 IR (a_3), where

TABLE VIIA. Correlation table for $O\downarrow C_3$.

O \ C_3	0_3	1_3	2_3
A_1	1	⋯	⋯
A_2	1	⋯	⋯
E	⋯	1	1
T_1	1	1	1
T_2	1	1	1

TABLE VIIB. Correlation table for $O\downarrow C_4$.

O \ C_4	0_4	1_4	2_4	3_4
A_1	1	⋯	⋯	⋯
A_2	⋯	⋯	1	⋯
E	1	⋯	1	⋯
T_1	1	1	⋯	1
T_2	⋯	1	1	1

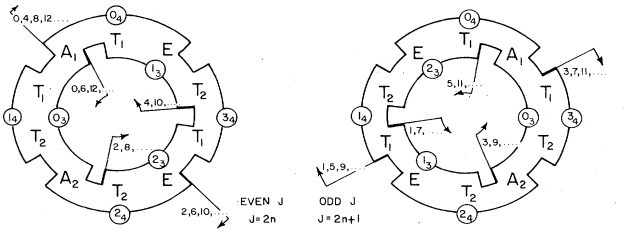

FIG. 8. Cycles of O IR contained in a level of total angular momentum J.

$$K_3 = a \bmod 3 , \tag{2.38}$$

and to the (a_3) cluster given by the (a_3)th column of Table VII A. Excluding higher order effects, the extreme octahedral cluster in an N level will be the one spinning the most, i.e., $K_3 = N$. Indeed, we observe the $K_3 = 18$ level in the form of a (O_3) cluster $(A_1 T_1 T_2 A_2)$ on the extreme right-hand side of $P(18)$ for SF_6 in Fig. 7(a).

The other octahedral clusters in an N level will involve states of the form $|^{N}_{mn=K_4}\rangle$ internally quantized with respect to a fourfold axis. They will be associated with C_4 IR (a_4) for which

$$K_4 = a \bmod 4 . \tag{2.39}$$

The highest one will have $K_4 = N$, the next highest will have $K_4 = N-1$, and so on until they split and fade into threefold clusters on the low side of the N pattern. Approximate formulas for the cluster positions are given in Sec. II.A.4.

Cubic IR cycle wheels (Fig. 8) can be constructed for cubic splitting of J or N levels. These wheels are analogous to the D_6 wheels given in Fig. 6. As in the D_6 case the cubic wheels work for all J, even if J is too small to clearly manifest clusters. For example, from the even-J wheel we read $(J=2) \uparrow 0 = T_2 \oplus E$ between the $J=2$ arrows. From the odd-J wheel we find $(J=3) \uparrow 0 = A_2 \oplus T_2 \oplus T_1$ reading counterclockwise from the inside $(J=3)$ arrow to the outside $(J=3)$-arrow. The wheels give in this way the correct order of the split levels which are sketched on the left-hand side of Fig. 4. For larger J the "teeth" indicate favored clusters: (a_4)-clusters within outside teeth, and (a_3)-clusters within inside teeth.

3. Rotational feasibility and cluster splitting

If it becomes feasible for a rotor to move from one internal rotation axis to another, then the energy level clusters belonging to the axis may split up. However, for "low feasibility" the clusters will split according to simple formulas involving interaxis tunneling amplitudes.

Consider for example the D_n cluster wave functions sketched on the right-hand side of Fig. 5. Let us define the n base states of the first cluster (O_2) to be $\{|1\rangle, |2\rangle = \mathbf{r}|1\rangle, |3\rangle = \mathbf{r}^2|1\rangle, \ldots, |n\rangle = \mathbf{r}^{n-1}|1\rangle\}$ where the wave function $\psi_1(\chi) = \langle \chi | 1 \rangle$ of state $|1\rangle$ is a single Gaussian-like "lump" sitting in well #1, while the wave functions of states $|2\rangle, |3\rangle, \ldots,$ and $|n\rangle$ are each the same lump moved over to wells #2, #3, . . . , and n by C_n symmetry operators $\mathbf{r}, \mathbf{r}^2, \ldots, \mathbf{r}^{n-1}$, respectively. Furthermore, let the Hamiltonian matrix $\langle \mathbf{H} \rangle$ be given in this basis by

$$\langle \mathbf{H} \rangle = \begin{bmatrix} H & -S & 0 & 0 & & 0 & -S \\ -S & H & -S & 0 & 0 & & 0 \\ 0 & -S & H & -S & 0 & 0 & \\ 0 & & & & H & -S & \\ -S & 0 & & & -S & H & \end{bmatrix} ,$$

where H is the local energy of each well, and $-S$ is the tunneling amplitude between adjacent wells. (Tunneling between next-nearest, next-next-nearest, etc. wells is assumed zero.)

The eigenvectors of $\langle \mathbf{H} \rangle$ are the $|k_m\rangle$ states given by C_n symmetry analysis or Fourier analysis in Eqs. (2.14). Acting on these with $\langle \mathbf{H} \rangle$ gives the eigenvalues

$$\langle k_m | \mathbf{H} | k_m \rangle = H - 2S \cos k_m ,$$

where $k_m = m(2\pi/n)$ $(m = 0, 1, 2, \ldots, n-1)$. This is the well-known dispersion relation for tightly bound electronic Bloch waves in a one-dimensional lattice. [See Feynman (1963).] The same formula can be used to describe the second cluster (1_2) of anti-symmetric "lumps" in Fig. 5(b) using different (presumably larger) numerical values for the H and $|S|$ parameters (S changes sign) and so on for each succeeding cluster. Eventually, though, this model must break down when we cannot correctly assume that next-nearest neighbor tunneling is zero. Note, however, that all one-dimensional periodic lattice potentials must preserve the order within each cluster since more nodes require more total energy. If somehow we arrange to make next-nearest neighbor tunneling larger than $|S|$ (this requires access to two or three dimensions), then the ordering is changed (Harter and Patterson, 1977c).

Similar splitting and ordering rules can be made for the cubic-octahedral or tetrahedral clusters. Consider $(O_4) \uparrow O$ cluster states $\{|1\rangle, |2\rangle = \bar{\mathbf{R}}(2)|1\rangle, |3\rangle = \bar{\mathbf{R}}(3)|1\rangle, |4\rangle = \bar{\mathbf{R}}(4)|1\rangle, |5\rangle = \bar{\mathbf{R}}(5)|1\rangle, |6\rangle = \bar{\mathbf{R}}(6)|1\rangle\}$, where $|1\rangle$ is an angular momentum state

$$|1\rangle = \left| {}^{N}_{mn=K_4} \right\rangle \tag{2.40}$$

with component $K_4 = 0 \bmod 4$ [Eq. (2.39)] on the first fourfold axis (say $\bar{z}$), and $R(2), \ldots R(6)$ are each appropriate group operators which set up the equivalent states on the other octahedral axes numbered 2–6 in Fig. 9(a). Let the Hamiltonian in this cluster basis be

$$\langle \mathbf{H} \rangle = \begin{bmatrix} H & 0 & -S & -S & -S & -S \\ 0 & H & -S & -S & -S & -S \\ -S & -S & H & 0 & -S & -S \\ -S & -S & 0 & H & -S & -S \\ -S & -S & -S & -S & H & 0 \\ -S & -S & -S & -S & 0 & H \end{bmatrix} ,$$

where $(-S)$ is the nearest neighbor tunneling amplitude. (Next-nearest or opposite neighbor tunneling is assumed zero here.)

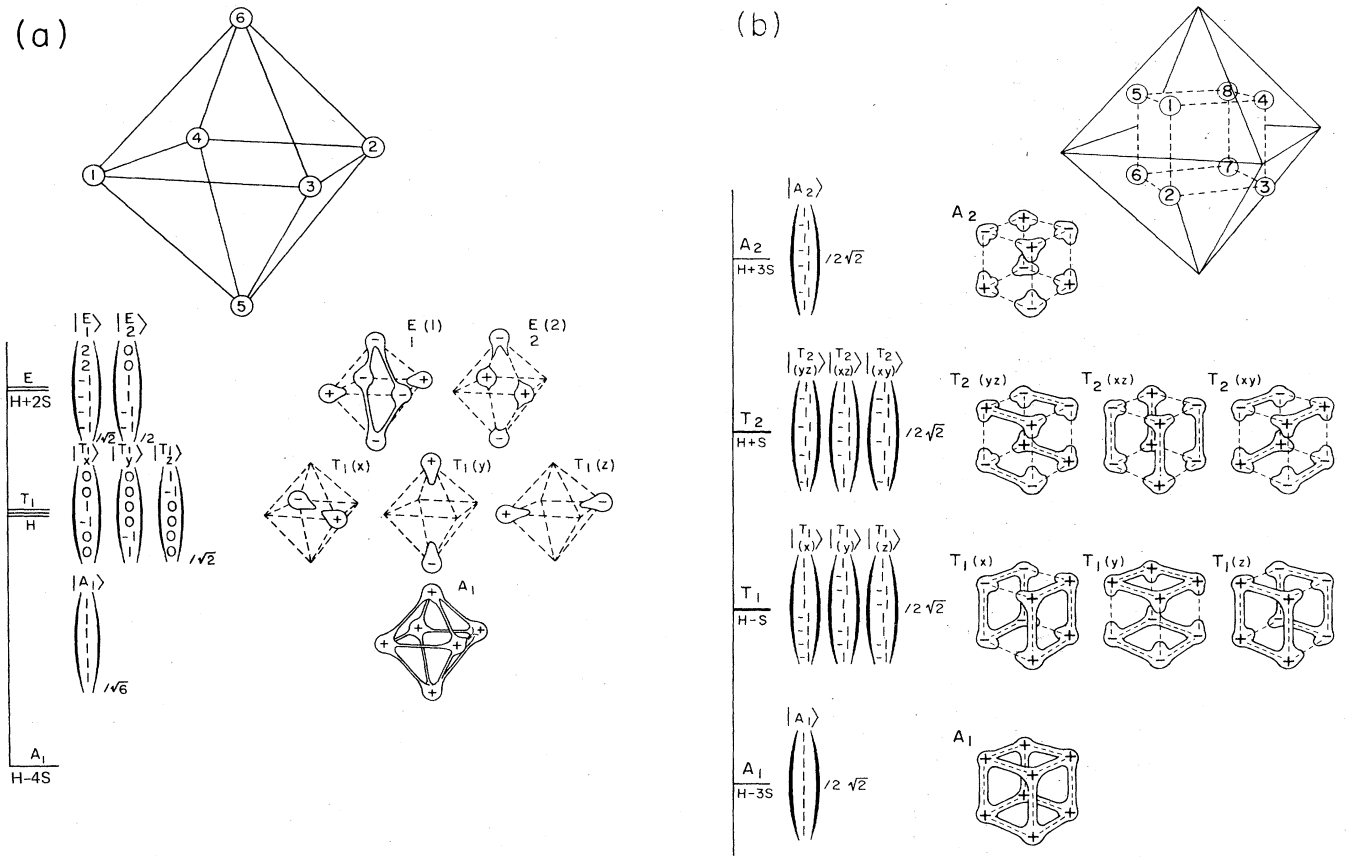

FIG. 9. (a) Eigenstates of octahedral cluster $(O_4)\downarrow O = E \oplus T_1 \oplus A_1$. Eigenvalues obtained by assuming only nearest $(1 \leftrightarrow 3, 3 \leftrightarrow 2, \ldots)$ neighbor tunneling amplitude $(-S)$. (b) Eigenstates of octahedral cluster $(O_3)\downarrow O = A_1 \oplus T_1 \oplus T_2 \oplus A_2$. Eigenvalues obtained by assuming only nearest $(1 \leftrightarrow 2, 2 \leftrightarrow 3, \ldots)$ neighbor tunneling amplitude $(-S)$.

The eigenvectors of $\langle \mathrm{H} \rangle$ may be obtained by using P^A operators [Eq. (2.5a)] in which standard cubic IR (Dimmock *et al.*, 1962) are substituted for $\mathfrak{D}^A(R)$. The resulting cluster eigenvectors

$$\left|\begin{matrix} A \\ i \end{matrix}\right\rangle = \mathrm{P}^A_{ij} |1\rangle / \text{norm}$$

and corresponding "wave functions" are sketched in Fig. 9(a). The eigenvalues are obtained by acting on the vectors with the $\langle \mathrm{H} \rangle$ matrix. Note that a 2 : 1 ratio is predicted for the $(A_1 - T_1) : (T_1 - E)$ splitting.

For another example, consider $(O_3)\downarrow O$ cluster states $\{|1\rangle, |2\rangle = \bar{\mathbf{R}}(2)|1\rangle, \ldots, |8\rangle = \bar{\mathbf{R}}(8)|1\rangle\}$ where $|1\rangle$ is an angular momentum state

$$|1\rangle = \left|\begin{matrix} N \\ mn = K_3 \end{matrix}\right\rangle \tag{2.41}$$

with component $K_3 = 0$ mod3 on the first threefold axis (111), and $|2\rangle$ through $|8\rangle$ are equivalent states on the other cubic axes numbered 2–8 in Fig. 9(b). Again, we assume only nearest-neighbor tunneling $(-S)$ in the Hamiltonian matrix

$$\langle \mathrm{H} \rangle = \begin{bmatrix} H & -S & 0 & -S & -S & 0 & 0 & 0 \\ -S & H & -S & 0 & 0 & -S & 0 & 0 \\ 0 & -S & H & -S & 0 & 0 & -S & 0 \\ -S & 0 & -S & H & 0 & 0 & 0 & -S \\ -S & 0 & 0 & 0 & H & -S & 0 & -S \\ 0 & -S & 0 & 0 & -S & H & -S & 0 \\ 0 & 0 & -S & 0 & 0 & -S & H & -S \\ 0 & 0 & 0 & -S & -S & 0 & -S & H \end{bmatrix}$$

and derive the eigenvectors and eigenvalues sketched in Fig. 9(b).

These examples show the procedures for deriving the splitting structure of clusters when it is small compared to the energy spacing between different clusters. The latter is determined by H, and we discuss approximate formulas for H as well as S in the following section.

4. Approximate angular momentum states and cluster parameters

One may predict the onset of clustering by appealing to elementary angular momentum theory. Consider

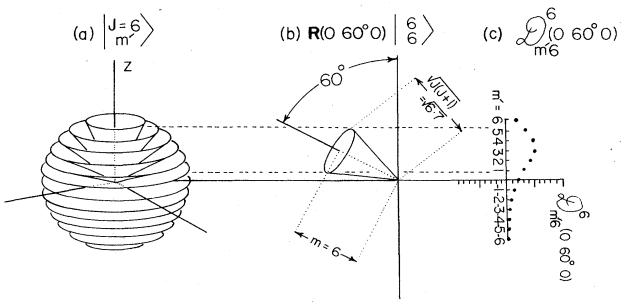

FIG. 10. Estimating semiclassical behavior of rotation matrix amplitudes $\langle^{J}_{m'}|\mathbf{R}(0\beta 0)|^{J}_{m}\rangle = \mathcal{D}^{J}_{m',m}(0\beta 0)$. (a) $(J=6)$ states $|^{J}_{m}\rangle$ are represented by cones of altitude m and slant height $\sqrt{J(J+1)} = \sqrt{42}$. (b) Rotated state $\mathbf{R}(0\,60°\,0|^{6}_{6}\rangle$. (c) Amplitudes $\mathcal{D}^{6}_{m'6}(0\,60°\,0)$ are largest within the limits defined by the rotated cone base.

standard angular momentum states $|^{J}_{m}\rangle$ defined by the eigenequations:

$$\mathbf{J}^2\left|\begin{matrix}J\\m\end{matrix}\right\rangle = J(J+1)\left|\begin{matrix}J\\m\end{matrix}\right\rangle ,$$

$$\mathbf{J}_z\left|\begin{matrix}J\\m\end{matrix}\right\rangle = m\left|\begin{matrix}J\\m\end{matrix}\right\rangle, |m| \leq J .$$

The equations suggest the following picture: the J vector is constrained to lie on a cone of slant height $[J(J+1)]^{1/2}$ and altitude m' as shown in Fig. 10(a) for the states of $J=6$. Then the J vector of a rotated state $\mathbf{R}(0\beta 0)|^{J}_{m}\rangle$ should lie on a $\mathbf{R}(0\beta 0)$-rotated cone as shown in Fig. 10(b) where the values ($\beta = 60°$) and ($m = 6$) are chosen. The projection of the cone base (note the dotted lines in the figure) encloses the components (m') of the states $|^{J}_{m'}\rangle$ which we would expect to have the greatest overlap with the rotated state. A calculation of the overlap amplitudes

$$\left\langle\begin{matrix}J\\m'\end{matrix}\right|\mathbf{R}(0\beta 0)\left|\begin{matrix}J\\m\end{matrix}\right\rangle = \mathcal{D}^{J}_{m',m}(0\beta 0)$$

[recall Eqs. (2.15) and (2.21)] for $J=m=6$ and various m' shows that the amplitudes inside the dotted lines of Fig. 10(c) are indeed the largest. Other values of (m) and (β) are plotted in the same way in Fig. 11. It is seen that the amplitudes seem to form a "lump" which lies under the cone base and "tails off" outside the projection. This is seen much more clearly for higher $J(J=20)$ in Fig. 12. In the upper part of the figure it is clear that the cone base marks the inflection or "classical turning" points of each lump. Inside these points there are $(J-m)$ reversals of amplitudes sign, i.e., $(J-m)$ "nodes."

The behavior of these amplitudes seems to indicate when various cluster states are well defined. For example consider the octahedral fourfold axes which are separated by at least $\beta = 90°$. Figure 12 indicates that the overlap $\langle^{20}_{m}|\mathbf{R}(0\ 90°0)|^{20}_{m}\rangle$ is small for $m > 16$. Therefore, we may expect three or four well defined clusters for $J=20$ and $K_4 = m = 20$, 17, 18, and possibly 16. The splitting of each will be increasing roughly exponentially as m decreases. The three-fold axes are separated by only 70.5° and so there are correspondingly fewer three-fold clusters. Figure 11 shows that $J=6$ cluster bases have appreciable overlap except possibly for $\beta = 90°$ and

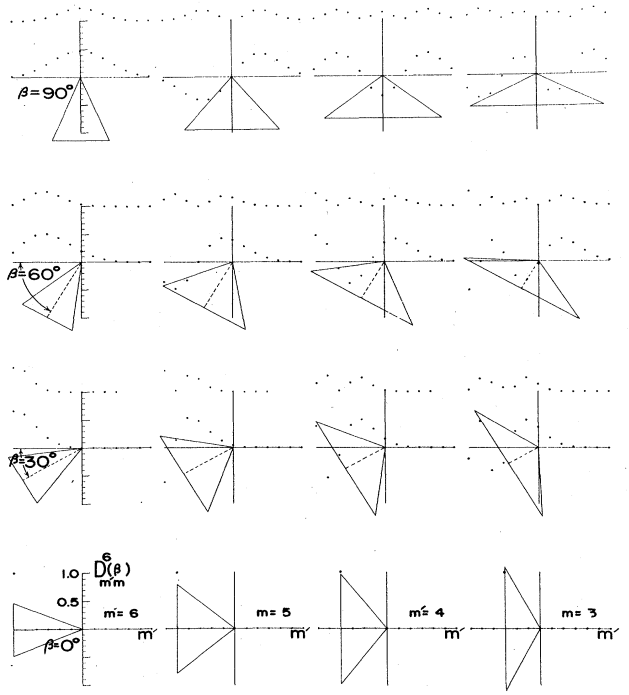

FIG. 11. $\mathcal{D}^{6}_{m',m}(0\beta 0)$ plots similar to Fig. 10(c) for various m and β.

$m = 6$. $J = 6$ seems to be about the lower limit for cluster theory.

To test these qualitative arguments a perturbative calculation of $\mathbf{V}^4$ eigenvalues has been compared to Krohn's diagonalization (Patterson and Harter, 1977). The first step is write $\mathbf{V}^4$ in Racah tensor form

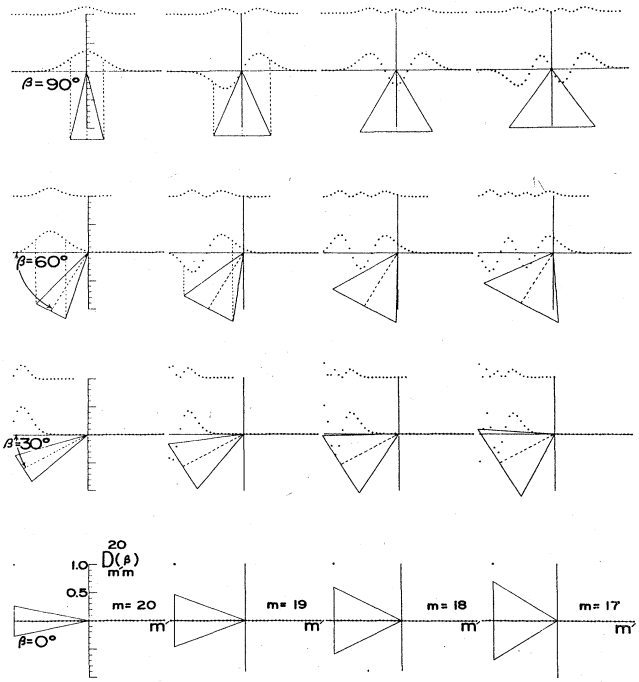

FIG. 12. $\mathcal{D}^{20}_{m'm}(0\beta 0)$ plots.

$$\mathbf{V}^4 = \alpha\,\mathbf{T}^4 + \beta\,\mathbf{T}^0\,, \tag{2.42}$$

where

$$\mathbf{T}^4 = \begin{cases} (7/12)^{1/2}\mathbf{V}_0^4 + (5/24)^{1/2}(\mathbf{V}_{-4}^4 + \mathbf{V}_4^4) \\ \qquad\qquad \text{(on fourfold axes)} \\ -\frac{2}{3}\left[(7/12)^{1/2}\mathbf{V}_0^4 + 2(5/24)^{1/2}(\mathbf{V}_{-3}^4 - \mathbf{V}_3^4)\right] \\ \qquad\qquad \text{(on threefold axes)} \end{cases}$$

The scalar T^0 causes no splitting and will be ignored here. The Wigner-Eckart Theorem gives

$$\left\langle \begin{matrix} N' \\ n' \end{matrix} \middle| \mathbf{T}_r^k \middle| \begin{matrix} N \\ n \end{matrix} \right\rangle = C_{rnn'}^{kNN'} \langle N' \| T^k \| N \rangle$$

$$= (-1)^{N'-n'} \begin{pmatrix} N' & k & N \\ -n' & r & n \end{pmatrix} (N' \| T^k \| N)\,, \tag{2.43}$$

where Clebsch–Gordan and Wigner coefficients are related by (Rotenberg *et al.*, 1959)

$$C_{m_1 m_2 m_3}^{j_1 j_2 j_3} = (-1)^{j_1 - j_2 + m_3} \sqrt{[j_3]} \begin{pmatrix} j_1 & j_2 & j_3 \\ m_1 & m_2 & -m_3 \end{pmatrix}, \tag{2.44}$$

and the reduced matrix element

$$(N' \| T^k \| N) = \sqrt{[N']}\, \langle N' \| T^k \| N \rangle (-1)^k \tag{2.45}$$

is factored out of the following calculation.

In Fig. 13 the arrows labeled K_4 indicate the values of the following perturbation formula for cluster energies:

$$H(N,n) = -\langle T^4 \rangle / (N \| T^4 \| N) = H^1(N,n) + H^2(N,n)\,, \tag{2.46}$$

where for fourfold clusters $n = K_4$

$$H^1(N,n) = (-1)^{N-n+1}(7/12)^{1/2} \begin{pmatrix} N & 4 & N \\ -n & 0 & n \end{pmatrix} \tag{2.47}$$

$$H^2(N,n) = 5/24 \left\{ \frac{\begin{pmatrix} N & 4 & N \\ -(n+4) & 4 & n \end{pmatrix}^2}{H^1(N,n) - H^1(N,n+4)} + \frac{\begin{pmatrix} N & 4 & N \\ -(n-4) & -4 & n \end{pmatrix}^2}{H^1(N,n) - H^1(N,n-4)} \right\}.$$

For larger N and n, the Wigner coefficient

$$\begin{pmatrix} N & 4 & N \\ -n & 0 & n \end{pmatrix} = (-1)^{N-n} \frac{6(N+2)(N+1)N(N-1) - 10n^2(6N^2+6N-5) + 70n^4}{[(2N+5)!/(2N-2)!]^{1/2}} \tag{2.48}$$

in the first term dominates the second perturbative terms containing the coefficients

$$\begin{pmatrix} N & 4 & N \\ -(n+4) & 4 & n \end{pmatrix} = (-1)^{N-n} \left[\frac{70(N-n)!(N+n+4)!(2N-2)!}{(N-n-4)!(N+n)!(2N+5)!} \right]^{1/2}$$

$$\begin{pmatrix} N & 4 & N \\ -(n-4) & -4 & n \end{pmatrix} = (-1)^{N-n} \left[\frac{70(N+n)!(N-n+4)!(2N-2)!}{(N+n-4)!(N-n)!(2N+5)!} \right]^{1/2} \tag{2.49}$$

[Angular momentum cone pictures analogous to Fig. 12 exist for coupling coefficients and Racah coefficients (Ponzano and Regge, 1968; Shulton and Gordon, 1975).]

The levels predicted by the formulas are generally very close to the exact fourfold cluster centers obtained by computer diagonalization, as seen in Fig. 13. The levels in the center of the figure are those computed by Krohn. Notice that errors show up when the clusters are well split. One can expect these errors near the cross-over point where fourfold H values approach those obtained from the threefold formulas. The threefold formulas are

$$H^1(N,n) = (-1)^{N-n}\tfrac{2}{3}(7/12)^{1/2} \begin{pmatrix} N & 4 & N \\ -n & 0 & n \end{pmatrix}$$

$$H^2(N,n) = \frac{16}{9}(5/24) \left\{ \frac{\begin{pmatrix} N & 4 & N \\ -(n+3) & 3 & n \end{pmatrix}^2}{H^1(N,n) - H^1(N,n+3)} + \frac{\begin{pmatrix} N & 4 & N \\ -(n-3) & -3 & n \end{pmatrix}^2}{H^1(N,n) - H^1(N,n-3)} \right\}, \tag{2.50}$$

However, the threefold formulas give accurately the rest of the (threefold) cluster spectrum beyond the cross-over point.

Approximate formulas for the splitting or tunneling amplitudes S can be derived (Patterson and Harter, 1977). However, the ratio of the error $\Delta S : S$ is much greater than the corresponding ratio for the H parameters. One does obtain the right order of magnitude and sign, but it is hoped that alternative perturbation techniques will be found which improve the accuracy of tunneling estimation.

In the results of Lea *et al.*, combinations of the cubic fourth order potential $\mathbf{V}^4$ and a sixth order potential

$$\mathbf{V}^6 = \alpha[\mathbf{V}_0^6 - (7/2)^{1/2}(\mathbf{V}_4^6 + \mathbf{V}_{-4}^6)] + \beta\mathbf{V}^0$$

were treated. Their computer generated graphs show

exactly degenerate four-fold clusters for certain combinations, i.e., the effective tunneling parameters vanish. [Indeed the clusters might have gone unnoticed in the low J ($J \leq 8$) spectra if this had not occurred.] Apparently no precise explanation exists for this behavior.

B. Analysis of proper and improper rotations (O_3)

Most molecular point symmetry groups include improper operators, i.e., operators for which the determinant of the vector representation is (−1). In addition, the usual Hamiltonian for a molecule in free space will include all inversions and reflections as well as the rotational $\mathrm{R}(\alpha\beta\gamma)$ in R_3. All such operations form the full orthogonal group $O_3 = R_3 \times \mathbf{C}_i$ where $\mathbf{C}_i = \{1, \mathrm{I}\}$ contains the identity and inversion I only.

An improper operation converts a right-handed frame into a left-handed one. It is quite clear that no rotation operator will ever do such a thing, so there is no point in trying to find ways to make Euler angle transformations that correspond to inversions. Instead we will extend our fundamental basis to include two sets. The first set will be the one we have been using: namely all rotational position states:

$$\{|000R\rangle \cdots |\alpha\beta\gamma R\rangle = \mathrm{R}(\alpha\beta\gamma)|000R\rangle \ldots\}$$

of the right-handed frame [see Fig. 14(a)]. The second set will be all position states

$$\{|000L\rangle = \mathrm{I}|000R\rangle \ldots |\alpha\beta\gamma L\rangle = \mathrm{IR}(\alpha\beta\gamma)|000R\rangle \ldots\}$$

of the left-handed or inverted rotor and frame [see Fig. 14(b)]. Then we have one state $\mathbf{O}(\alpha\beta\gamma)|000R\rangle$ for each O_3 operator $\mathbf{O}(\alpha\beta\gamma)$. This makes a basis for the "perfect" or "regular" representation of O_3.

We then have the O_3 analyzed states

$$\left|\begin{matrix} N^{\pm} \\ mn \end{matrix}\right\rangle = \mathbf{P}^{N^{\pm}}_{mn}|000R\rangle/\sqrt{[N]} = \int d(\alpha\beta\gamma)\mathfrak{D}^{N*}_{mn}(\alpha\beta\gamma)\sqrt{[N]}\,|\alpha\beta\gamma\pm\rangle\,, \tag{2.51a}$$

where

$$|\alpha\beta\gamma\pm\rangle \equiv (|\alpha\beta\gamma R\rangle \pm |\alpha\beta\gamma L\rangle)/\sqrt{2}\,, \tag{2.51b}$$

with all the same basic properties discussed in the preceding section, except now we have two states for each value of N, m, and n. One has positive parity (+) while the other has negative (−) parity, i.e.,

$$\mathrm{I}\left|\begin{matrix} N^{\pm} \\ mn \end{matrix}\right\rangle = \pm\left|\begin{matrix} N^{\pm} \\ mn \end{matrix}\right\rangle. \tag{2.52}$$

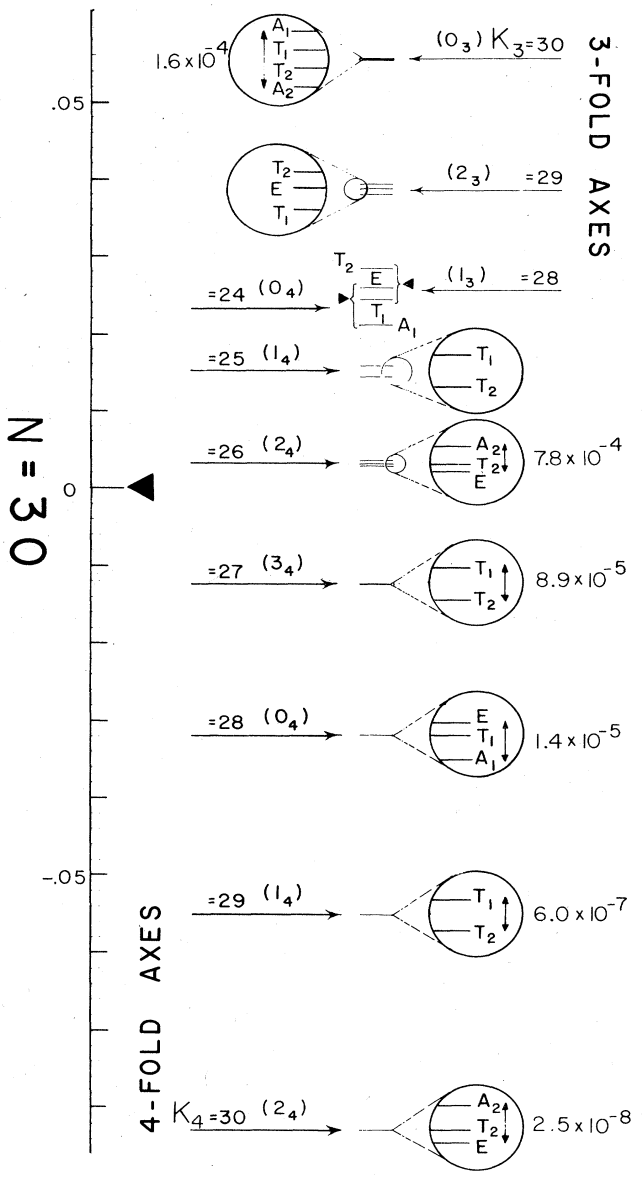

FIG. 13. Eigenvalue spectrum of $(-V^4)$ in the $N=30$ manifold. Center column shows the eigenvalues found by computer diagonalization. Arrows and circles indicate level structure which may be found by Eqs. (2.46)–(2.50). K_n is the approximate component of angular momentum on an n-fold symmetry axis.

Again we may define internal or body frame operator $\bar{\mathbf{O}}$:

$$\begin{aligned} \bar{\mathbf{O}}(\alpha\beta\gamma)|\phi\theta\chi\ \pm\rangle &= \bar{\mathbf{O}}(\alpha\beta\gamma)\mathbf{R}(\phi\theta\chi)|000\pm\rangle \\ &= \mathbf{R}(\phi\theta\chi)\bar{\mathbf{O}}(\alpha\beta\gamma)|000\pm\rangle \\ &= \mathbf{R}(\phi\theta\chi)\mathbf{O}^{-1}(\alpha\beta\gamma)|000\pm\rangle = \begin{cases} \mathbf{R}(\phi\theta\chi)\mathbf{R}(-\gamma-\beta-\alpha)|000\pm\rangle \\ \qquad \text{if } O \text{ is proper } (O=R) \\ \pm\mathbf{R}(\phi\theta\chi)\mathbf{R}(-\gamma-\beta-\alpha)|000\pm\rangle \\ \qquad \text{if } O \text{ is improper } (O=IR)\,. \end{cases} \end{aligned} \tag{2.53}$$

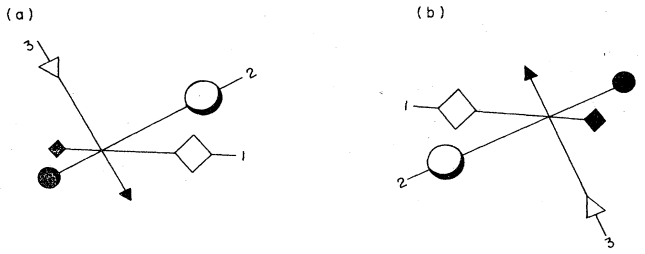

FIG. 14. Rotation-inversion position states for O_3 symmetry analysis. (a) State $|\alpha\beta\gamma R\rangle = \mathbf{R}(\alpha\beta\gamma)|000R\rangle$ (right-handed frames). (b) State $|\alpha\beta\gamma L\rangle = \mathbf{R}(\alpha\beta\gamma)\mathbf{I}|000R\rangle$ (left-handed frames).

Note that there is no need to distinguish between internal and external inversion since it commutes with all operations. I and $\bar{\mathrm{I}}$ do exactly the same thing to the body frame versus lab frame relative position.

It may seem strange to include what are called "unfeasible" operations. Indeed, Hougen (1963) defines inversions for electrons but makes the frame immune to them. This might seem reasonable since the amplitude for most molecules (NH_3 excluded) to change handedness is negligible. However, we find that allowing inversions in some cases but not others leads to more complicated selection rules than are really necessary.

In any case we will not lose anything. If it turns out that the universe contains nothing but right-handed versions of our molecule, that simply means that they are all in states

$$|\alpha\beta\gamma R\rangle = (|\alpha\beta\gamma +\rangle + |\alpha\beta\gamma -\rangle)/\sqrt{2}\,.$$

We may use group theory to give the correct finite (molecular) symmetry rotor functions

$$\left\langle \left| \begin{matrix} N^p & B \\ m & b \end{matrix} \right\rangle \equiv r^{N^p B}_{m\ b}[O(\phi\theta\chi)] \tag{2.54}$$

which transform according to IR $\mathfrak{D}^B$ of internal symmetry $\bar{\mathcal{G}} = \{\ldots \bar{\mathrm{O}}_g \ldots\}$

$$\left\langle \left| \bar{\mathrm{O}}_g \right| \begin{matrix} N^p & B \\ m & b \end{matrix} \right\rangle = \sum_{b'} \mathfrak{D}^B_{b'b}(g) \left\langle \left| \begin{matrix} N^p & B \\ m & b' \end{matrix} \right\rangle \right. \tag{2.55a}$$

and IR $\mathfrak{D}^{N^p}$ $(p = \pm 1)$ of external symmetry $O_3 = \{\ldots \mathrm{O}(\alpha\beta\gamma) \ldots\}$

$$\left\langle \left| \mathrm{O}(\alpha\beta\gamma) \right| \begin{matrix} N^p & B \\ m & b \end{matrix} \right\rangle = \sum_{m'} \mathfrak{D}^{N^p}_{m'm}[O(\alpha\beta\gamma)] \left\langle \left| \begin{matrix} N^p & B \\ m' & b \end{matrix} \right\rangle \right. , \tag{2.55b}$$

where

$$\mathfrak{D}^{N^p}_{m'm}[O(\alpha\beta\gamma)] = \begin{cases} \mathfrak{D}^N_{m'm}(\alpha\beta\gamma) \text{ if O is proper:} \\ \qquad \mathrm{O}(\alpha\beta\gamma) = \mathbf{R}(\alpha\beta\gamma) \\ p\mathfrak{D}^N_{m'm}(\alpha\beta\gamma) \text{ if O is improper:} \\ \qquad \mathrm{O}(\alpha\beta\gamma) = \mathbf{IR}(\alpha\beta\gamma) \end{cases} \qquad (p = \pm 1)\,. \tag{2.56}$$

The conjugated coefficients $\left(\begin{matrix} N^p & B \\ n & b \end{matrix}\right)^*$ apply directly to the O_3 IR $\mathfrak{D}^{0^+}$, $\mathfrak{D}^{1^-}$, $\mathfrak{D}^{2^+}$, $\mathfrak{D}^{3^-}$, . . . with parity $p = (-1)^N$ since spherical harmonics Y^l_m are of parity $(-1)^l$. (Y^l is an lth order polynomial of x/r, y/r and z/r, and inversion gives $x \to -x$, $y \to -y$, $z \to -z$, and $r \to r$.)

$$r^{N^p B}_{m\ b}{}^*(O(\phi\theta\chi)) = \sum_n \left(\begin{matrix} N^p & B \\ n & b \end{matrix}\right)^* \mathfrak{D}^{N^p}_{mn}{}^*[O(\phi\theta\chi)]\sqrt{[N]}$$

$$\text{where: } [p = (-1)^N]\,. \tag{2.57}$$

However, for the pseudoharmonic IR $\mathfrak{D}^{0^-}$, $\mathfrak{D}^{1^+}$, $\mathfrak{D}^{2^-}$, . . . with $p = (-1)^{N+1}$, we will need to first form the product of Eq. (2.57) with the $\bar{\mathcal{G}}$ pseudoscalar IR $\mathfrak{D}^{\mathrm{PS}}$. Here $\mathfrak{D}^{\mathrm{PS}}$ is defined by

$$\mathfrak{D}^{\mathrm{PS}}(\bar{\mathrm{O}}_g) = \begin{cases} 1 \text{ if } \bar{\mathrm{O}}_g \text{ is proper} \\ -1 \text{ if } \bar{\mathrm{O}}_g \text{ is improper}\,. \end{cases}$$

The desired functions are

$$r^{N^p B'}_{m\ b'}{}^*(O(\phi\theta\chi)) = \sum_b \sum_n C^{B\,*PSB'*}_{b\ \cdot\ b'} \left(\begin{matrix} N^{-p} & B \\ n & b \end{matrix}\right) \times {}^*\mathfrak{D}^{N^p}_{m\,n}{}^*(O(\phi\theta\chi))\sqrt{[N]}$$

$$= \sum_n \left(\begin{matrix} N^p & B' \\ n & b' \end{matrix}\right)^* \mathfrak{D}^{N^p}_{mn}[O(\phi\theta\chi)]\sqrt{[N]}$$

$$\text{where: } [p = (-1)^{N+1}] \tag{2.58}$$

where $C^{B\,*PSB'*}_{b\ \cdot\ b'}$ is the pseudoscalar coupling coefficients of $\bar{\mathcal{G}}$. (Note if $\bar{\mathcal{G}}$ contains only proper R, then $\left(\begin{matrix} N^p & B \\ n & b \end{matrix}\right) = \left(\begin{matrix} N^{-p} & B \\ n & b \end{matrix}\right)$.)

For example, consider the internal symmetry $\bar{O}_{2i} \equiv D_{\infty h}$ of the diatomic X_2 rotor, as sketched in Fig. 15. The pseudoscalar IR is clearly $\mathrm{PS} = \Sigma^-_u$. Using the characters shown in the figure we derive the $O_3 \downarrow O_{2i}$ correlation table (Table VIII). The $(1^-, \Pi_u)$ standing wave functions follow from the familiar x and y harmonic relations

$$\begin{aligned} Y^1_1 &\sim -(x + iy) \quad x \sim \mathcal{Y}^{\Pi_u}_x = (-Y^1_1 + Y^1_{-1})/\sqrt{2} \\ Y^1_{-1} &\sim (x - iy) \quad y \sim \mathcal{Y}^{\Pi_u}_y = i(Y^1_1 + Y^1_{-1})/\sqrt{2}\,. \end{aligned} \tag{2.59}$$

Then complex conjugation gives the rotor functions

$$\begin{aligned} r^{1^-\,\pi_u}_{m\ x} &= (-\mathfrak{D}^{1^-*}_{m\,1} + \mathfrak{D}^{1^-*}_{m,-1})\left(\frac{3}{2}\right)^{1/2} \\ r^{1^-\,\pi_u}_{m\ y} &= -i(\mathfrak{D}^{1^-*}_{m1} + \mathfrak{D}^{1^-*}_{m,-1})\left(\frac{3}{2}\right)^{1/2}\,. \end{aligned} \tag{2.60}$$

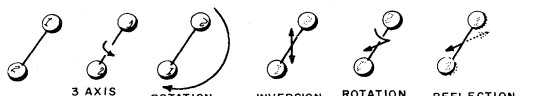

	1	R(α00)	R(-α180°α)	I	I.R(α00)	I.R(-α180°α)
$A_{1g} = \Sigma^+_g$	1	1	1	1	1	1
$A_{1u} = \Sigma^+_u$	1	1	-1	-1	-1	1
$A_{2g} = \Sigma^-_g$	1	1	-1	1	1	-1
$A_{2u} = \Sigma^-_u$	1	1	1	-1	-1	-1
$E_{1g} = \pi_g$	2	2 cos α	0	2	2 cos α	0
$E_{1u} = \pi_u$	2	2 cos α	0	-2	-2 cos α	0
$E_{2g} = \Delta_g$	2	2 cos 2α	0	2	2 cos 2α	0
$E_{2u} = \Delta_u$	2	2 cos 2α	0	-2	-2 cos 2α	0
.	.	.	.	.	.	.
.	.	.	.	.	.	.
.	.	.	.	.	.	.

FIG. 15. Characters of $D_{\infty h} = O_{2i}$ symmetry of X_2 rotor.

TABLE VIII. $O_3\downarrow(O_{2i}=D_{\infty h})$ correlation of representations.

O_3 \ O_{2i}	$B=\Sigma_g^+$	Σ_u^+	Σ_g^-	Σ_u^-	Π_g	Π_u	Δ_g	Δ_u	Φ_g	Φ_u	$\Gamma_g\ldots$
$N^b=0^+$	1	···	···	···	···	···	···	···	···	···	
$=0^-$	···	···	···	1	···	···	···	···	···	···	
$=1^+$	···	···	1	···	1	···	···	···	···	···	
$=1^-$	···	1	···	···	···	1	···	···	···	···	
$=2^+$	1	···	···	···	1	···	1	···	···	···	
$=2^-$	···	···	···	1	···	1	···	1	···	···	
$=3^+$	···	···	1	···	1	···	1	···	1	···	
$=3^-$	···	1	···	···	···	1	···	1	···	1	
$=4^+$	1	···	···	···	1	···	1	···	1	···	1

Now in order to find the Π_g rotor functions, we need the $\bar{O}_{2i}$ pseudo-scalar coupling coefficients:

$$\Pi_u\times\Sigma_u^- = \begin{array}{c|cc} & \Pi_g\,\Pi_g=B' \\ & x \quad y=b' \\ \hline x \quad \cdot & \cdot \quad 1 \\ y \quad \cdot & -1 \quad \cdot \end{array} \quad . \tag{2.61}$$

Combining this with Eq. (2.58) and (2.60) gives

$$\gamma^{1^+\Pi_g}_{mx} = i\left(\mathfrak{D}^{1^+*}_{m1}+\mathfrak{D}^{1^+*}_{m,-1}\right)\left(\frac{3}{2}\right)^{1/2}$$

$$\gamma^{1^+\Pi_g}_{my} = \left(-\mathfrak{D}^{1^+*}_{m1}+\mathfrak{D}^{1^+*}_{m,-1}\right)\left(\frac{3}{2}\right)^{1/2} . \tag{2.62}$$

C. Excluded IR and bare rotors

Before we consider the effect of adding excited vibrations or electrons to a rotor we should note that some representations are forbidden or excluded for certain rotors.

The diatomic rotor is one example. If we do not consider the nuclear structure, then we must agree that rotation $\bar{\mathrm{R}}(00\gamma)$ around the $\bar{z}$ axis containing the two nuclear points has no effect on such a rotor. In other words the third Euler angle χ(or γ) is superfluous.

We may express this fact by writing

$$\bar{\mathrm{R}}(00\gamma)\left|\begin{matrix}N\\mn\end{matrix}\right\rangle = \left|\begin{matrix}N\\mn\end{matrix}\right\rangle \tag{2.63}$$

and derive the consequences of it. Combining Eq. (2.15) and (2.20) we have

$$\left|\begin{matrix}N\\mn\end{matrix}\right\rangle = \bar{\mathrm{R}}(00\gamma)\left|\begin{matrix}N\\mn\end{matrix}\right\rangle = \sum_{n'}\mathfrak{D}^{N*}_{n',n}(00\gamma)\left|\begin{matrix}N\\mn'\end{matrix}\right\rangle = e^{in\gamma}\left|\begin{matrix}N\\mn\end{matrix}\right\rangle$$

or

$$n=0\,.$$

In other words, if the rotor has nothing to "stick out" perpendicular to its axis to mark χ rotational position then it cannot have any momentum around this axis. [Indeed, Eq. (2.30) shows that $n\neq0$ levels go to infinity for $I_{\bar{z}}=0$.]

Furthermore, an X_2 rotor would not notice any of the internal reflections shown on the extreme right of Fig. 15, that is

$$\mathrm{IR}(-\gamma\ 180^\circ\ \gamma)\left|\begin{matrix}N^b\ B\\m\ b\end{matrix}\right\rangle = \left|\begin{matrix}N^b\ B\\m\ b\end{matrix}\right\rangle .$$

Only two B satisfy this, namely,

$$B=\Sigma_g^+,\ \text{or}\ B=\Sigma_u^+ \tag{2.64}$$

This "selection" of allowed bare quantum states is very important for the definition of the "rovibronic species" and the nuclear spin-permutation symmetry, as we shall see.

Detailed discussion of labeling states of linear molecules is given by Bunker and Papousek (1969).

III. COUPLING, BOA CONSTRICTION AND FRAME TRANSFORMATION RELATIONS

A. Symmetric-top and electron

Let us begin with the weak-coupling limit in which an electron is in a large radius l- orbit around a relatively small symmetric-top rotor. Suppose the rotor is in a state described by wave functions

$$\left\langle\alpha\beta\gamma\left|\begin{matrix}N\\mn\end{matrix}\right\rangle\right. \equiv \gamma^N_{mn}(\alpha\beta\gamma) = \mathfrak{D}^{N*}_{mn}(\alpha\beta\gamma)\sqrt{[N]}\,. \tag{3.1}$$

In this limit reasonable approximations for eigenstates are obtained by standard coupling analysis.

$$\left\langle\left|\begin{matrix}l\ NJ\\n\ m\end{matrix}\right\rangle\right. = \sum_m C^{l\ N\ J}_{M-m\ m\ M}\,Y^l_{M-m}(\theta\phi)\mathfrak{D}^{N*}_{mn}(\alpha\beta\gamma)\sqrt{[N]} \tag{3.2}$$

Now Eq. (2.22b) gives the transformation of the harmonics from the lab coordinates [see Fig. 16(a)] to body coordinates [see Fig. 16(b)]:

$$Y^l_m(\theta\phi) = \sum_\Lambda Y^l_\Lambda(\bar{\theta}\bar{\phi})\mathfrak{D}^{l*}_{m\Lambda}(\alpha\beta\gamma)\,. \tag{3.3}$$

Inserting this into (3.2) gives

$$\left\langle\left|\begin{matrix}l\ N\ J\\n\ M\end{matrix}\right\rangle\right. = \sum_m\sum_\Lambda C^{l\ N\ J}_{M-m\ m\ M}\,Y^l_\Lambda(\bar{\theta}\bar{\phi})\mathfrak{D}^{l*}_{M-m\Lambda}(\alpha\beta\gamma) \times\mathfrak{D}^{N*}_{mn}(\alpha\beta\gamma)\sqrt{[N]}\,. \tag{3.4}$$

Finally we use the fundamental definition of coupling:

$$\sum_{m\Lambda n} C^{l\ N\ J}_{M-m\ m\ M}\mathfrak{D}^{l*}_{M-m\Lambda}\mathfrak{D}^{N*}_{mn}C^{l\ N\ J'}_{\Lambda n K} = \delta^{JJ'}\mathfrak{D}^{J*}_{MK}\,, \tag{3.5a}$$

revised slightly by coupling orthonormality as follows:

$$\sum_m C^{l\ N\ J}_{M-m\ m\ M}\,\mathfrak{D}^{l*}_{M-m\Lambda}\mathfrak{D}^{N*}_{mn} = \sum_k C^{l\ N\ J}_{\Lambda n K}\,\mathfrak{D}^{J*}_{MK}\,. \tag{3.5b}$$

Inserting (3.5) into (3.4) gives the weakly coupled states

$$\left|\begin{matrix}l\ N\ J\\n\ M\end{matrix}\right\rangle = \sum_{K,\Lambda}\left(\frac{[N]}{[J]}\right)^{1/2} C^{l\ N\ J}_{\Lambda n K=\Lambda+n}\left|\mathrm{BOA}\ \begin{matrix}l\\\Lambda\end{matrix}\ \begin{matrix}N\\n\end{matrix}\ \begin{matrix}J\\M\end{matrix}\right\rangle, \tag{3.6}$$

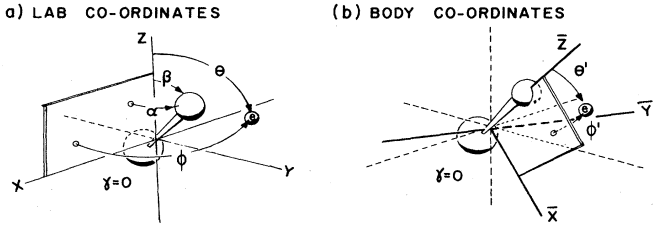

FIG. 16. Coordinates of electron defined in (a) Lab frame and (b) Body frame. With $\gamma=0$ the $\bar{x}\bar{z}$ plane is parallel to the z axis.

in terms of BOA-constricted states, where

$$\left\langle \overline{\theta\phi}\,\alpha\beta\gamma \middle| \mathrm{BOA}\ {}^{l}_{\Lambda}\ n\ {}^{J}_{M} \right\rangle \equiv Y^{l}_{\Lambda}(\overline{\theta\phi})\mathfrak{D}^{J*}_{MK=\Lambda+n}(\alpha\beta\gamma)\sqrt{[J]}\,. \quad (3.7)$$

Eq. (3.7) is a BOA-constricted wave function in which the electronic wave Y^{l}_{Λ} (body) tightly embraces the rotor body and has body momentum component Λ. The effect of the electronic "load" shows up in the rotor wave function which now has a body component $K=\Lambda+n$ generally different from the "bare" rotor n, as well as a total momentum J generally differing from N. One may imagine that Y^{l}_{Λ} represents a flywheel riding with frictionless bearings on an axle represented by $\mathfrak{D}^{J*}_{MK}$.

Eq. (3.6) is the most elementary frame transformation relation. It relates each state on one side of Fig. 17 with those on the opposite side which have the same J, M, and n. For example, for $J=2$, $l=1$, $n=1$ and states of a given M, we have from (3.6) the matrix (3.8).

$$\begin{array}{|ccc|c|}
\left\langle \left| {}^{l=1}_{n=1} \right. {}^{N=1}_{M} \ {}^{J=2}_{} \right\rangle & \left\langle \left| {}^{l=1}_{n=1} \right. {}^{N=2}_{M} \ {}^{J=2}_{} \right\rangle & \left\langle \left| {}^{l=1}_{n=1} \right. {}^{N=3}_{M} \ {}^{J=2}_{} \right\rangle & \\
\hline
(3/5)^{1/2} & (1/3)^{1/2} & (1/15)^{1/2} & Y^{1}_{1}\mathfrak{D}^{2*}_{M2} \\
(3/10)^{1/2} & -(1/6)^{1/2} & -(8/15)^{1/2} & Y^{1}_{0}\mathfrak{D}^{2*}_{M1} \\
(1/10)^{1/2} & -(1/2)^{1/2} & (2/5)^{1/2} & Y^{1}_{-1}\mathfrak{D}^{2*}_{M0}
\end{array} \quad (3.8)$$

Note that orbital Coriolis perturbations can mix only states with the same J, M, and n. For example, the matrix of the Hamiltonian

$$\mathbf{H}=\mathbf{H}_e+\mathbf{H}_N=\mathbf{H}_e+\mathbf{N}^2/2I_{\bar{x}\bar{y}}+\mathbf{N}^2_{\bar{z}}(1/2I_{\bar{z}}-1/2I_{\bar{x}\bar{y}})$$

is easily found in the $(J=2, n=1)$ BOA basis. We let $\mathbf{J}=\mathbf{L}+\mathbf{N}$ be the total momentum so we have

$$\mathbf{H}=\mathbf{H}_e+(\mathbf{J}^2+\mathbf{L}^2-2\mathbf{J}_{\bar{z}}\mathbf{L}_{\bar{z}}-2\mathbf{J}_{\bar{x}}\mathbf{L}_{\bar{x}}-2\mathbf{J}_{\bar{y}}\mathbf{L}_{\bar{y}})/2I_{\bar{x}\bar{y}}+(\mathbf{J}_{\bar{z}}-\mathbf{L}_{\bar{z}})^2(1/2I_{\bar{z}}-1/2I_{\bar{x}\bar{y}}), \quad (3.9)$$

and calculate its matrix elements using Eqs. (2.26) and (2.27). For example the relations

$$\mathbf{J}_{\bar{y}}\mathfrak{D}^{2*}_{M2}=-i\mathfrak{D}^{2*}_{M1},\ \mathbf{J}_{\bar{y}}\mathfrak{D}^{2*}_{M1}=i\mathfrak{D}^{2*}_{M2}-i(3/2)^{1/2}\mathfrak{D}^{2*}_{M0},\ \ldots$$

follow from "body equation" (2.26b), while the relations

$$\mathbf{L}_{\bar{y}}Y^{1}_{1}(\bar{\theta},\bar{\phi})=i/\sqrt{2}\,Y^{1}_{0},\ \mathbf{L}_{\bar{y}}Y^{1}_{0}(\bar{\theta},\bar{\phi})=-i/\sqrt{2}\,Y^{1}_{1}+i/\sqrt{2}\,Y^{1}_{-1},\ \ldots$$

are "standard" angular momentum relations i.e. (2.26a). (Here both the operator and the function are referred to the body system so we use standard "lab" relations). The Hamiltonian matrix is then given.

$$\langle \mathbf{H} \rangle = \begin{vmatrix}
\epsilon_\pi+1/2I_{\bar{z}}+3/2I_{\bar{x}\bar{y}} & -\sqrt{2}/I_{\bar{x}\bar{y}} & 0 \\
-\sqrt{2}/I_{\bar{x}\bar{y}} & \epsilon_\Sigma+1/2I_{\bar{z}}+7/2I_{\bar{x}\bar{y}} & -\sqrt{3}/I_{\bar{x}\bar{y}} \\
0 & -\sqrt{3}/I_{\bar{x}\bar{y}} & \epsilon_\pi+1/2I_{\bar{z}}+7/2I_{\bar{x}\bar{y}}
\end{vmatrix} \begin{matrix} Y^{1}_{1}\mathfrak{D}^{2*}_{M2} \\ Y^{1}_{0}\mathfrak{D}^{2*}_{M1} \\ Y^{1}_{-1}\mathfrak{D}^{2*}_{M0} \end{matrix} \quad (3.10)$$

This example shows clearly when the BOA constricted states are nearly eigenstates, i.e., when electronic parameters are very different, say $|\epsilon_\pi-\epsilon_\Sigma|\gg 1/I_{\bar{x}\bar{y}}$. As ϵ_π approaches ϵ_Σ the electrons start to "slip" from the constriction until finally, when $\epsilon_\pi=\epsilon_\Sigma$, the weakly coupled states given in (3.8) are eigenstates. Note that even in the BOA limit there is still a splitting between the Π states. We give an explanation of this while reviewing the generalized symmetric-top BOA state.

Equation (3.7) may be generalized to

$$\left\langle \left| \mathrm{BOA}\ \ \Lambda n\ {}^{J}_{M} \right\rangle = V_\Lambda(\mathrm{BODY})\mathfrak{D}^{J*}_{MK=\Lambda+n}\sqrt{[J]} \quad (3.11)$$

which is the general BOA wavefunction for a "loaded" symmetric top. The "load" or "flywheel" described by $V_\Lambda(\mathrm{BODY})=V(\bar{r}\bar{\theta})e^{i\Lambda\bar{\phi}}$ may be any electronic, vibrational, or vibronic disturbance with definite body (z-axis) momentum Λ. In an attempt to give a clear picture of model BOA states we show in Fig. 18 schematic representation of the spectrum of symmetric tops carrying $\Sigma(\Lambda=0)$ and $\Pi(\Lambda=\pm1)$ disturbances.

By dropping the nondiagonal terms $\mathbf{J}_{\bar{x}}\mathbf{L}_{\bar{x}}$ and $\mathbf{J}_{\bar{y}}\mathbf{L}_{\bar{y}}$ from Eq. (3.9) we obtain the approximate eigenvalues

$$\langle \mathbf{H} \rangle = \epsilon_v+B_vJ(J+1)+(A_v-B_v)K^2=2A_v\xi\Lambda K, \quad (3.12)$$

where ϵ_v depends on Λ only, $A_v=1/2I_{\bar{z}}(v)$, and $B_v=1/2I_{\bar{x},\bar{y}}(v)$ are rotational constants, and ξ is the effective momentum parameter which is used to describe vibrations that have non-integral angular momentum. The plot of Eq. (3.12) in Fig. 18 uses arbitrarily chosen constant $A_v=1.1$, $B_v=1$, and $\xi=0.3$.

For each value of $J=2, 3$ and $|n|=1, 2, \ldots |J-1|$ of rotor momentum there will be two separate pairs of $\Pi(\Lambda=\pm1)$ states as indicated in Fig. 18. For the lower pair of states the rotor and load rotate together, while for the higher pair the rotor rotates in the opposite direction of the load. One may imagine that the Π load is like a gyrocompass which tends to allign with the earth's spin. The corresponding energy difference is often called Coriolis splitting. The $(n=0, \Pi)$ states may

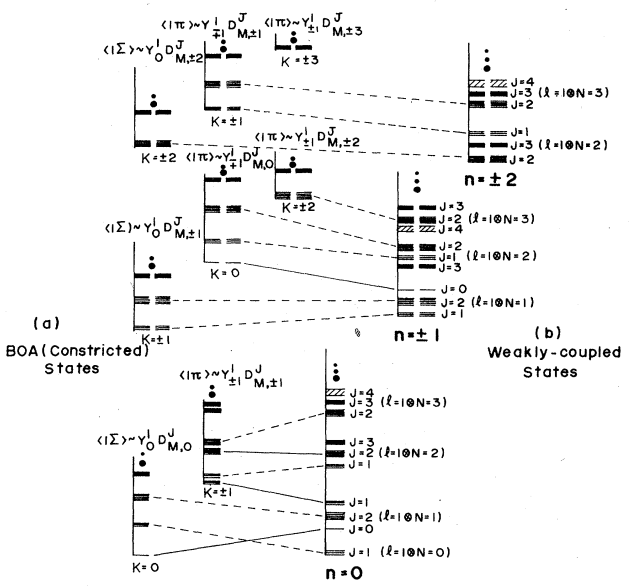

FIG. 17. Correlation diagram for ($l=1$) rotonic levels of a symmetric top. (a) Born–Oppenheimer approximation, and (b) Weak-coupling approximation. On the BOA side (a) the quantum numbers $\Lambda(=\Sigma,\Pi)$ and K are good. On the opposite side (b) total rotor or core momentum N is good. On either side the quantum numbers J and $n=K_c$ are good. The lines across the figure connect states for which (J,n) are the same. Solid lines indicate states which are exactly the same in the "low l-spoiling" approximation for which only $l=1$ electronic momentum is considered. For a physical picture of the BOA states refer ahead to Fig. 18. For a more detailed labeling of just the $n=0$ states see Fig. 19. Quantitative correlation trajectories are shown in Figs. 20 and 21.

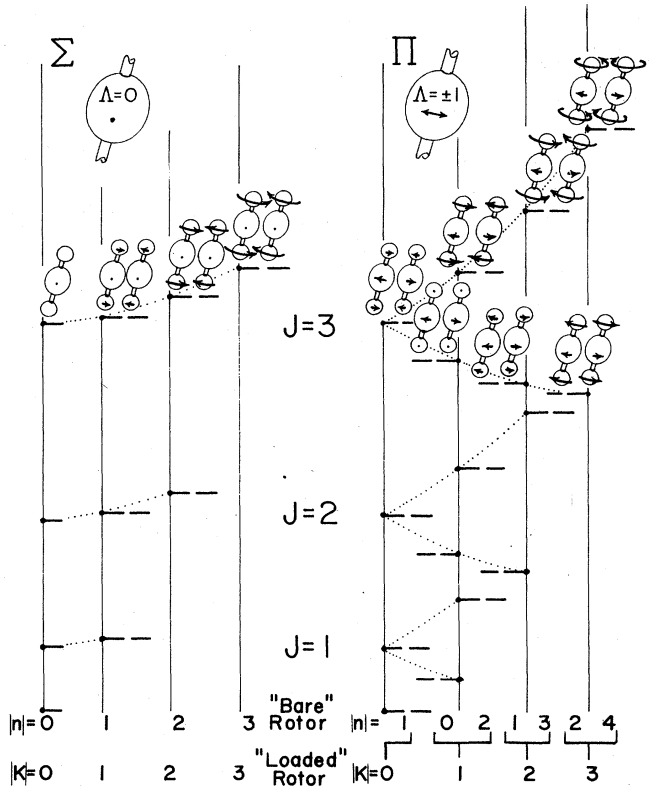

FIG. 18. Σ and Π BOA states for symmetric top molecule. The electronic or vibronic "load" is indicated by an ellipsoid surrounding a "bare" dumb-bell rotor. Arrows indicate the direction of rotation of moving wave states and relative amounts of momentum n or K. Only for the $(n=0,\Pi)$ states will it be necessary to make up standing waves to form the "Λ-doublet" states which are shown in Fig. 19.

undergo a different sort of splitting (so-called "Λ doubling") which is discussed in the next section.

The loaded symmetric rotor can only be an approximate or qualitative model for a molecule, and we give it only to motivate the definition of the general rovibronic species label. This will be denoted $\binom{B}{b}$ in the following section which is a generalization of the rotor momentum (n) in the present example. The general rovibronic labels correspond to "internal" symmetry of the rotor. Together with the external symmetry labels $\binom{J}{M}$ they remain good quantum numbers, during any transformation from the BOA bases to weak-coupling bases or anywhere in between. Furthermore, in Sec. IV we prove that the properly defined rovibronic labels are conserved during optical transitions, while the vibronic label [the vibronic label Λ in Eq. (3.11) will generalize to $\binom{A}{a}$ in the next section] and the loaded rotor label [the loaded rotor label K generalizes to $\binom{C}{c}$] are free to change.

One advantage of the loaded-symmetric rotor model is that we can easily understand why (n) is sacred. The symmetric or cylindrical rotor is "slippery" for the electron. No matter how the electron tries to "grab" the rotor, it will always precess in such a way to keep the (n) constant. The electron can embrace the rotor, become constricted by it, but if the rotor really has $\bar{R}_2$ internal symmetry nothing can change its (n).

Only linear molecules *really* have cylindrical internal symmetry, and for these only $n=0$ is permitted. All other axially symmetric molecules which have off-axis nuclei must posess a less-than-cylindrical finite symmetry. Then wave functions such as Eq. (3.11) should be combined to correspond to IR (A, B, or C) of finite symmetry as explained in the following. Nevertheless, some linear molecules with electronic core momentum Λ_c can be treated approximately as "bare" ($n=\Lambda_c$) rotors. (See Sec. III.E.1.)

B. General rotor and electron

We start again with the weakly coupled states involving an electron and a rotor. We let the electron be in an l orbital, and the rotor in a state described by the wave functions of the form (2.33)

$$\left\langle \left| lN \begin{matrix} B^* & J \\ b & M \end{matrix} \right\rangle = \sum_m C^{l\,NJ}_{M-m\,mM}\, Y^l_{M-m}(\theta\phi)\,\mathcal{Y}^{NB*}_{mb}$$

$$= \sum_n \binom{N}{n}\binom{B}{b}^* \sum_m C^{l\,NJ}_{M-m\,mM}\, Y^l_{M-m}(\theta\phi)\,\mathfrak{D}^{N*}_{mn}\sqrt{[N]}\,.$$

In this section we will suppress the parity designations of O_3 and make notational abbreviations such as

$$\binom{N}{n}\binom{B}{b} \equiv \binom{N^p}{n}\binom{B}{b}, \text{ and } \mathfrak{D}^N_{mn} \equiv \mathfrak{D}^{Np}_{mn}(\mathrm{O}(\alpha\beta\gamma)),$$

but it will be understood that they may be there.

Now we transform the electronic harmonic to the body frame (3.3) and use the coupling relation (3.5) to obtain

$$\left|lN\begin{matrix}B^* & J\\ b & M\end{matrix}\right\rangle = \sum_n \begin{pmatrix} N \\ n \end{pmatrix}\begin{matrix} B \\ b \end{matrix}\Big)^* \sum_\Lambda Y_\Lambda^l(\bar{\Theta}\bar{\phi}) \sum C^{lNJ}_{\Lambda nK}\, \mathfrak{D}^{J*}_{MK}\sqrt{[N]}\,. \tag{3.13}$$

Next we use the inverses of the sphere-to-point-group (crystal field) relations (2.32) as required by (2.36).

$$Y^l_\Lambda = \sum_{Aa}\begin{pmatrix} l \\ \Lambda \end{pmatrix}\begin{matrix} A \\ a \end{matrix}\Big)^* \mathcal{Y}^A_a\,, \tag{3.13a}$$

$$\mathfrak{D}^{J*}_{MK}\sqrt{[J]} = \sum_{Cc}\begin{pmatrix} J \\ K \end{pmatrix}\begin{matrix} C \\ c \end{matrix}\Big) r^{JC*}_{Mc}\,. \tag{3.13b}$$

Inserting these into the preceding expression for $|lN^{B^*\ J}_{b\ M}\rangle$, we find

$$\left|lN\begin{matrix}B^* & J\\ b & M\end{matrix}\right\rangle = \sum_{A,a}\sum_{C,c}\left[\left(\frac{[N]}{[J]}\right)^{1/2}\sum_{\Lambda Kn} C^{lNJ}_{\Lambda nK}\begin{pmatrix} l \\ \Lambda \end{pmatrix}\begin{matrix} A \\ a \end{matrix}\Big)^*\begin{pmatrix} N \\ n \end{pmatrix}\begin{matrix} B \\ b \end{matrix}\Big)^*\begin{pmatrix} J \\ K \end{pmatrix}\begin{matrix} C \\ c \end{matrix}\Big)\right]\mathcal{Y}^A_a(\bar{\Theta}\bar{\phi})r^{JC*}_{Mc}\,. \tag{3.14}$$

In Appendix A we prove that the factor in brackets is proportional to a product of an internal $\bar{\mathcal{G}}$ symmetry coupling coefficient C^{ABC}_{abc} which couples $\bar{\mathcal{G}}$ harmonics A and B to make a C harmonic, i.e.,

$$\sum_{ab} C^{ABC}_{abc}\mathcal{Y}^A_a\mathcal{Y}^B_b = \mathcal{Y}^C_c(AB)\,,$$

and something which we call the molecular isoscalar factor $\langle (l)A, (N)B \,\|\, (J)C\rangle$ [Buch, 1972] which is independent of a, b, or c.

$$\left(\frac{[N]}{[J]}\right)^{1/2}\sum_{\Lambda n} C^{lNJ}_{\Lambda nK}\begin{pmatrix} l \\ \Lambda \end{pmatrix}\begin{matrix} A \\ a \end{matrix}\Big)^*\begin{pmatrix} N \\ n \end{pmatrix}\begin{matrix} B \\ b \end{matrix}\Big)^*\begin{pmatrix} J \\ K \end{pmatrix}\begin{matrix} C \\ c \end{matrix}\Big) = \left(\frac{[B]}{[C]}\right)^{1/2} C^{ABC}_{abc}\langle (l)A, (N)B \,\|\, (J)C\rangle \tag{3.15}$$

[$[D]$ stands for the dimension of $\bar{\mathcal{G}}$ IR $\mathfrak{D}^D$]].

Inserting (3.15) into (3.14) gives the desired general relation between weakly coupled states and BOA constricted states:

$$\left|lN\begin{matrix}B^* & J\\ b & M\end{matrix}\right\rangle = \sum_A\sum_C \langle (l)A, (N)B \,\|\, (J)C\rangle \left|\text{BOA } lA, C\begin{matrix}B^* & J\\ b & M\end{matrix}\right\rangle, \tag{3.16a}$$

where the latter are defined as follows:

$$\left|\text{BOA } lAC\begin{matrix}B^* & J\\ b & M\end{matrix}\right\rangle = \sum_a\sum_c C^{ABC}_{abc}\left(\frac{[B]}{[C]}\right)^{1/2}\mathcal{Y}^A_a(\bar{\Theta}\bar{\phi})r^{JC*}_{Mc}\,. \tag{3.16b}$$

The ordering in the coupling coefficient, namely "A and B gives C", would suggest that the electron in multiplet A is combined with a bare rotor in multiplet B to give a loaded rotor frame belonging to multiplet C. In fact, we shall see this is a very useful way to think of it physically for spectroscopy.

However, the sum in (3.16b) is over a and c, not a and b. Indeed, we may use the finite group factorization lemma

$$\frac{1}{\circ\bar{\mathcal{G}}}\sum_g \mathfrak{D}^A_{aa'}(g)\mathfrak{D}^B_{bb'}(g)\mathfrak{D}^{C*}_{cc'}(g) = \frac{1}{\circ\bar{\mathcal{G}}}\sum_g \mathfrak{D}^A_{aa'}(g)\mathfrak{D}^{C*}_{cc'}(g)(\mathfrak{D}^{B*}_{bb'}(g))^* = \frac{1}{[C]}C^{ABC}_{abc}C^{ABC}_{a'b'c'}\,, \tag{3.17}$$

[this is just another arrangement of fundamental coupling definitions like (3.5)] to prove that

$$C^{ABC}_{abc} = C^{AC*B*}_{ac\ b}\left(\frac{[C]}{[B]}\right)^{1/2} p(ABC)\,. \tag{3.18}$$

Here $p(ABC)$ is an adjustable phase which we will take to be unity (Griffith, 1962). Then the BOA-constricted states may be defined as follows:

$$\left|\text{BOA } lAC\begin{matrix}B^* & J\\ b & M\end{matrix}\right\rangle = \sum_a\sum_c C^{AC*B*}_{ac\ b}\mathcal{Y}^A_a(\bar{\Theta}\bar{\phi})r^{JC*}_{Mc}\,. \tag{3.19}$$

This equation gives the BOA-constricted states of definite rovibronic species (B^*, b). These are obtained by coupling an A electron to a C^* rotor which has the electron "built into it" to get a bare B^* rotor. We will discuss some more physical interpretations of this "subtractive" coupling after we give two examples of frame transformation relations.

1. $D_{\infty h}$ - symmetric rotor and ($l = 1$) electron

We rederive the wave functions used in Fano's MCQD theory of H_2 (Fano, 1970) and show how physical properties and symmetry labels are obtained very easily.

We noted at the end of Sec. II that the only possible labels for a bare diatomic rotor are $B = \Sigma_g^+$ and $B = \Sigma_u^+$. These in turn are the only two allowed rovibronic species labels that a loaded diatomic (X_2) molecule can ever have, no matter how many electrons or vibrations it is carrying or "constricting".

However, for each BOA electronic or vibronic state A, we may get several loaded-frame states C according to (3.16), namely, all those C contained in $A\otimes B$. If we suppose we are dealing with an $l^p = 1^-$ electron, then Table VIII shows that $A = \Sigma_u^+$ and $A = \Pi_u$ states will show up. This gives

$$C = A\otimes B = \Sigma_u^+\otimes\Sigma_g^+ = \Sigma_u^+ \tag{3.20a}$$

$$C = \Pi_u\otimes\Sigma_g^+ = \Pi_u \tag{3.20b}$$

states for species $B = \Sigma_g^+$ and

$$C = A\otimes B = \Sigma_u^+\otimes\Sigma_u^+ = \Sigma_g^+ \tag{3.21a}$$

$$C = \Pi_u\otimes\Sigma_u^+ = \Pi_g \tag{3.21b}$$

states for species $B = \Sigma_u^+$.

Now each B or C corresponds to a column in Table VIII, which gives (up-side-down) the successive levels corresponding to that particular rotor or loaded-frame

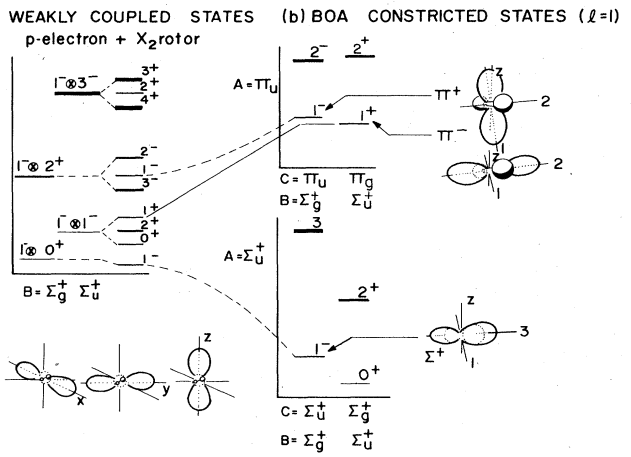

FIG. 19. Correlation diagram for $l=1$ electronic states in the presence of an X_2 rotor. (a) Weakly-coupled states. (N^P, B, and J^P are good labels.) (b) BOA-constricted states. (A, B, C, and J^P are good labels.) States with the same $B=\Sigma_g^+$ and $J^P=1^-$ are connected by dotted lines. The $B=\Sigma_u^+$ and $J^P=1^+$ state (solid line) turns out to be the same for either side as long as $l=1$ is unspoiled. Note that $A=\Pi_u$-doublets are represented by standing waves in the body system. The lower doublet is alternatively + and − parity.

state. Some of the resulting J^p states coming from Eq. (3.20) are shown in the BOA level diagram on the right of Fig. 19, while the N^p states arising from $B=\Sigma_g^+$ and Σ_u^+ of the bare rotor are indicated on the left.

The diagram shows the $n=0$ part of Fig. 17 with labeling that is more detailed but easier to comprehend. It also shows sketches of the BOA-waves ($1^-, A=\Pi_u, B=\Sigma_g^+$) and ($1^-, A=\Sigma_u^+, B=\Sigma_g^+$) which are of interest in the MCQD analysis along with the ($1^+, A=\Pi_u, B=\Sigma_u^+$)"Λ-doubling" partner of the first state. [The first and third states are called Π^+ and Π^- respectively by Fano (Fano, 1970)].

Let us rederive the $A=\Pi_u$ waves and the transformation indicated by the dotted lines in Fig. 19 using (3.15, 16). This will make the physics of the symmetry labeling more clear. To do this we need coupling coefficients

$$C^{\Pi_u \Sigma_g^+ \Pi_u}_{a\ \ c} = \delta_{ac} = C^{\Pi_u \Sigma_u^+ \Pi_g}_{a\ \ c} \tag{3.22}$$

and the angular functions in (2.59, 60) and (2.62). Then we obtain from (3.16b) the following BOA wave functions.

$$\begin{aligned}\langle|\Pi^+\rangle &= \sum_{ac} \sqrt{\tfrac{1}{2}}\, C^{\Pi_u \Sigma_g^+ \Pi_u}_{a\ \ c}\, \mathcal{Y}^{\Pi_u}_a \boldsymbol{\gamma}^{1^-\Pi_u}_{Mc} \\ &= (\mathcal{Y}^{\Pi_u}_x \boldsymbol{\gamma}^{1^-\Pi_u}_{Mx} + \mathcal{Y}^{\Pi_u}_y \boldsymbol{\gamma}^{1^-\Pi_u}_{My})/\sqrt{2} \\ &= (Y^1_1 D^{1^-}_{M1}{}^* + Y^1_{-1} D^{1^-}_{M-1}{}^*)\sqrt{\tfrac{3}{2}} \\ &\sim (-\cos(\phi-\alpha)\sin\Theta\sin\beta\cos\beta + \cos\Theta\sin^2\beta), \\ &\qquad\qquad \text{(for } M=0) \quad (3.23a)\end{aligned}$$

$$\begin{aligned}\langle|\Pi^-\rangle &= \sum_{ac} \sqrt{\tfrac{1}{2}}\, C^{\Pi_u \Sigma_u^+ \Pi_g}_{a\ \ c} \mathcal{Y}^{\Pi_u}_a \boldsymbol{\gamma}^{1^+\Pi_g}_{Mc} \\ &= i(Y^1_1 D^{1^+}_{M1}{}^* - Y^1_{-1} D^{1^+}_{M-1}{}^*)\sqrt{\tfrac{3}{2}} \\ &\sim (\sin(\phi-\alpha)\sin\Theta\sin\beta), \quad (\text{for } M=0) \qquad (3.23b)\end{aligned}$$

Using (3-15) we obtain the isoscalar factors in the matrix

$$\begin{array}{l|ccc} & |N=0^+\rangle & |N=2^+\rangle & |N=1^-\rangle \\ \hline \langle\Sigma^+| = \langle A=\Sigma_u^+ B=\Sigma_g^+| & (1/3)^{1/2} & -(2/3)^{1/2} & 0 \\ \langle\Pi^+| = \langle A=\Pi_u B=\Sigma_g^+| & (2/3)^{1/2} & (1/3)^{1/2} & 0 \\ \langle\Pi^-| = \langle A=\Pi_u B=\Sigma_u^+| & 0 & 0 & 1 \end{array} \tag{3.24}$$

The 2×2 submatrix is precisely the U matrix in Fano's MCQD theory (Fano, 1970).

We may verify that the weak-coupling states become eigenvectors when $\epsilon_\Sigma = \epsilon_\Pi$ in the matrix

$$\langle \mathbf{H}\rangle = \begin{array}{c} \begin{array}{ccc} |\Sigma^+\rangle & |\Pi^+\rangle & |\Pi^-\rangle \end{array} \\ \begin{vmatrix} \epsilon_\Sigma+4 & -2\sqrt{2} & 0 \\ -2\sqrt{2} & \epsilon_\pi+2 & 0 \\ 0 & 0 & \epsilon_\pi+2 \end{vmatrix} \end{array} /2I_{\bar{x}\bar{y}}, \tag{3.25}$$

which is the representation of

$$\mathbf{H} = \mathbf{H}_e + (\mathbf{J}^2 + \mathbf{L}^2 - 2\mathbf{J}_{\bar{x}}\mathbf{L}_{\bar{x}} - 2\mathbf{J}_{\bar{y}}\mathbf{L}_{\bar{y}} - 2\mathbf{J}_{\bar{z}}\mathbf{L}_{\bar{z}})/2I_{\bar{x}\bar{y}},$$

constructed in the BOA basis. Equation (3.25) shows that the two Π become degenerate only if $\epsilon_\pi - \epsilon_\Sigma \to \infty$, which is well known.

It is important to distinguish Coriolis splitting from Λ-doubling. Coriolis splitting occurs with $n\neq 0$ (see Sec. III. A) while Λ-doubling occurs with $n=0$. Coriolis splitting separates two oppositely *moving* wave states and is roughly analogous to the Zeeman effect in atomic physics. Here Λ-doubling forms and separates two *standing* wave states, and one might compare it to "quenching" of atomic orbitals in crystal fields. For the X_2 Λ-doubling in Fig. 19, we have sketched these two standing waves. One state (Π^+) is symmetric to ($z-\bar{z}$) plane reflections, while the other is anti-symmetric. These standing wave states are a direct consequence of the total symmetry analysis. (Π^+) and (Π^-) belong to different B, and are not necessarily degenerate. We discuss the general significance of the total symmetry operators in the following section.

It is interesting to construct the ($l=1$) energy matrix for a range of J and n values, and study the eigenvalue spectrum as a function of ($\epsilon_\pi - \epsilon_\Sigma$). The ($n=0$) matrix for arbitrary J is

$$\langle \mathbf{H}\rangle = \begin{array}{c} \begin{array}{ccc} |\Sigma^+\rangle & |\Pi^+\rangle & |\Pi^-\rangle \end{array} \\ \begin{bmatrix} J(J+1)+2 & -2(J(J+1))^{1/2} & 0 \\ -2(J(J+1))^{1/2} & \epsilon_\pi + J(J+1) & 0 \\ 0 & 0 & \epsilon_\pi + J(J+1) \end{bmatrix} \end{array},$$

where we let $B_v = 1 = 1/I_{\bar{x}\bar{y}}$, and $\epsilon_\Sigma = 0$. The eigenvalues of the (2 by 2) block are

$$h = \frac{\epsilon_\pi + 2(J(J+1)+1) \pm (\epsilon_\pi{}^2 - 4\epsilon_\pi + 4(2J+1)^2)^{1/2}}{2}.$$

Plots of the eigenvalues are given in Fig. 20. The Λ doublets show up in the BOA limit Π spectrum in the upper right-hand side of the figure, while the Σ levels are below. On the left-hand side the results for the weak coupling limit ($\epsilon_\pi \cong 0$) are shown, and it is instructive to study the ordering of levels for low ϵ_π. Each N level splits into three parts: $J=N+1$, $J=N$, and $J=N-1$.

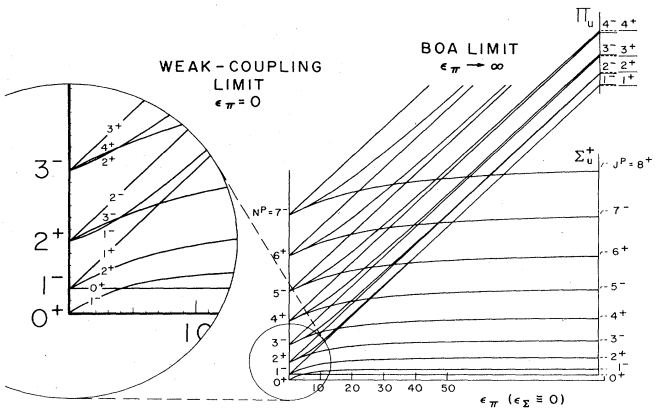

FIG. 20. ($n=0$) J-level plots ($J=0$–8) for ($l=1$: Σ, Π) as functions of electronic energy difference (ϵ_π). The right-hand side of the figure shows the separate Π and Σ manifolds that will arise in the BOA limit as $\epsilon_\pi \to \infty$. (In this figure we set $\epsilon_\Sigma = 0$, and let the rotational constant $B_v = 1/I_{xy}$ be unity.) Splitting or "λ doubling" is seen in the Π manifolds increasing with J. Corresponding downshifts from the pure rotational spectrum ($\sim B_v J(J+1)$ are seen in the Σ manifold. For small values of ϵ_π ($\epsilon_\pi < 5$) there is a near degeneracy between $J = N \pm 1$ levels, particularly for larger values of rotor momentum N. At $\epsilon_\pi = 0$ and $\epsilon_\pi = 4$ the degeneracy is exact, while between these points the $J = N-1$ level lies slightly below the $J = N+1$ level. Pairs of $J = (N \pm 1)$ weak-coupling levels are analogous to the Π pairs seen in the BOA limits, only the former are defined with respect to a *laboratory* axis. The weakly coupled $J = N$ state can be thought of as a lab analog of a Σ state.

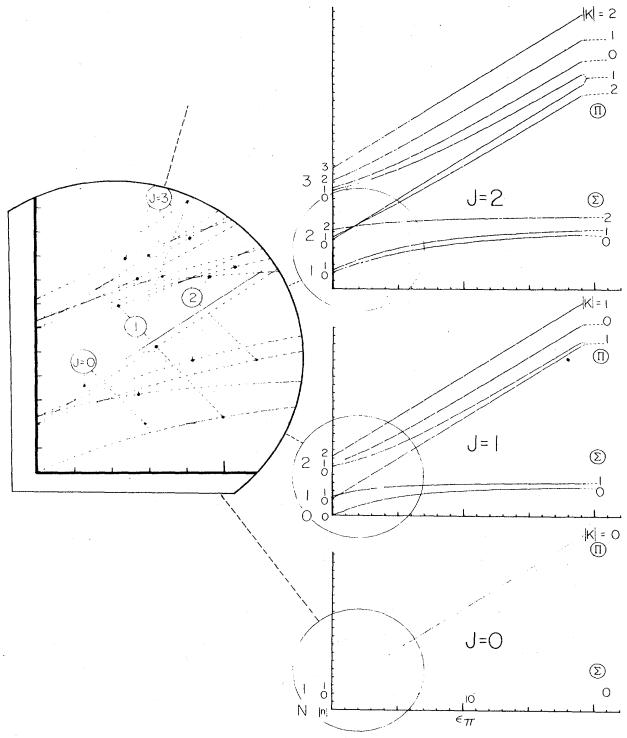

FIG. 21. ($n=0-4$) J-level plots for ($l=1$: Σ, Π) energy levels. (For just the $n=0$ levels, see Fig. 20.)

However, for low ϵ_π, the $N \pm 1$ pair remain nearly degenerate, while the N level splits off by itself. Between $\epsilon_\pi = 0$ and $\epsilon_\pi = 4$ the $J = N-1$ level lies below the $J = N+1$ level, but this splitting diminishes with each increasing N value. One can imagine the rapidly spinning rotor as a pinwheel whose axis more or less establishes a particular direction in lab space which becomes less uncertain as N increases. [Recall the cone picture of angular momentum used in Figs. 10–12.] The ($l=1$) electron tends to orient its orbit with respect to this direction. One may therefore think of the $J = N \pm 1$ pair as the lab analog of Π states, while the $J = N$ level corresponds to a "lab Σ".

The energy matrix for ($l=1$) and arbitrary (n) and (J) is given by

$$H = \begin{bmatrix} n^2 A_v + (J(J+1) - n^2 - 2n) B_v + \epsilon_\pi & -B_v(2(J+n+1)(J-n))^{1/2} & 0 \\ -B_v(2(J+n+1)(J-n))^{1/2} & n^2 A_v + (J(J+1) - n^2 + 2) B_v + \epsilon_\Sigma & -B_v(2(J-n+1)(J+n))^{1/2} \\ 0 & -B_v(2(J-n+1)(J+n))^{1/2} & n^2 A_v + (J(J+1) - n^2 + 2n) B_v + \epsilon_\pi \\ Y_1^1 \mathfrak{D}^{J*}_{Mn+1} & Y_0^1 \mathfrak{D}^{J*}_{Mn} & Y_{-1}^1 \mathfrak{D}^{J*}_{Mn-1} \end{bmatrix}$$

Eigenvalue plots for $A_v = 1/I_z = 1.30$, $B_v = 1/I_{xy} = 1.00$, and $\epsilon_\Sigma = 0$ are given in Fig. 21. The plots are quite confusing when drawn all together as they are on the left-hand side of the figure. However, when the levels are separated according to J as on the right-hand side, then it is easier to see how the correlation pattern goes. One should compare the approximate (Π, K) labeled BOA levels with those in the schematic diagram of Fig. 18. Finally, it is worth noting that the weak coupling levels ($\epsilon_\pi \cong 0$) for ($N=2, n=1$) show the same sort of approximate degeneracy for the $J = N \pm 1$ pair that is seen in the ($n=0$) case. However, this effect disappears for $N = n = 2$; presumably the rotor behaves less like a fixed-axis pinwheel when its internal momentum component is as large as the total.

2. O-symmetric rotor and ($l=2$) electron

We will derive the 2×2 matrix which connects the two $(^{B=T_1}_{b}\ ^{J=1}_{M})$ states in the octahedral molecule consisting of a cubic symmetry frame and an excited $d(l=2)$ electron. The pair of states are indicated by connecting dotted lines in Fig. 22 where the $J = 0, 1, 2, \ldots$ BOA

levels are sketched on the left, while the $N=0,1,2,3$ weak coupled levels are on the right.

The weakly coupled $N=1$ state in which we are interested is

$$|l=2 \quad N=1 \begin{matrix} B=T_1 & J=1 \\ b=2 & M \end{matrix}\rangle$$

$$= \sum_{\substack{AC \\ ac}} \langle (2)A(1)T_1 \| (1)C\rangle \, C_{a\,2\,c}^{A\,B=T_1\,C}\, \mathcal{Y}_a^A \, r_{M\,c}^{J=1\,C}$$

$$= \sum_{\substack{A \\ ac}} \langle (2)A(1)T_1 \| (1)T_1\rangle \, C_{a\,2\,c}^{A\,T_1\,T_1}\, \mathcal{Y}_a^A \, r_{M\,c}^{1\,T_1}$$

according to (3.16) or (3.19), where we use only real IR of cubic (0) symmetry, and note that $J=1$ contains only $C=T_1$.

To evaluate the isoscalar factors we need the sum in (3.15),

$$\sum_{\Lambda n} C_{\Lambda\,n\,K}^{2\;1\;1} \begin{pmatrix} 2 & A \\ \Lambda & a \end{pmatrix}^* \begin{pmatrix} 1 & T_1 \\ n & 2 \end{pmatrix}^* \begin{pmatrix} 1 & T_1 \\ K & c \end{pmatrix}$$

$$= \langle (2)A(1)T_1 \| (1)T_1\rangle \, C_{a\,2\,c}^{A\,T_1\,T_1} . \quad (3.26)$$

For each possible A we choose one non-zero coupling coefficient (Dimmock *et al.*, 1963). For $A=E$ we have

$$C_{1\,2\,2}^{E\,T_1\,T_1} = -1/2 , \quad (3.27)$$

so the sum on the left gives

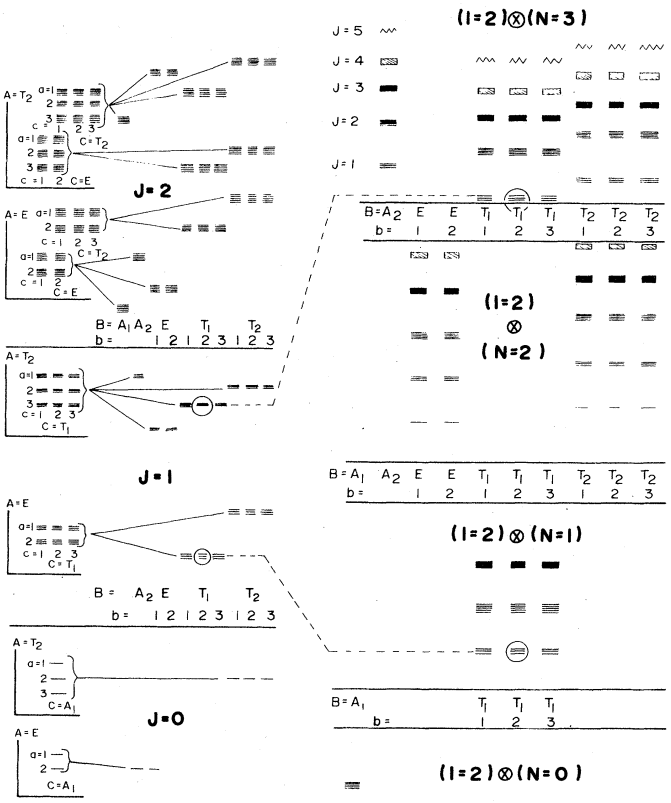

FIG. 22. Correlation diagram for $l=2$ electronic levels in the presence of an octahedral rotor. BOA-constricted states are indicated on the left. There A and C are good quantum labels. Weakly coupled states are indicated on the right. There N is good. On either side the labels (J, B) are good and the dotted lines connect those for which $J=1$ and $B=T_1$ as discussed in the text.

$$\sum_{\Lambda n} C_{\Lambda\,n\,K}^{2\;1\;1} \begin{pmatrix} 2 & E \\ \Lambda & 1 \end{pmatrix}^* \begin{pmatrix} 1 & T_1 \\ n & 2 \end{pmatrix}^* \begin{pmatrix} 1 & T_1 \\ K & c \end{pmatrix} = C_{011}^{211} \begin{pmatrix} 1 & T_1 \\ 1 & 2 \end{pmatrix}^* \begin{pmatrix} 1 & T_1 \\ 1 & 2 \end{pmatrix} + C_{0\,-1\,-1}^{211} \begin{pmatrix} 1 & T_1 \\ -1 & 2 \end{pmatrix}^* \begin{pmatrix} 1 & T_1 \\ -1 & 2 \end{pmatrix} ,$$

$$= (1/\sqrt{10})(i/\sqrt{2})(-i/\sqrt{2}) + (1/\sqrt{10})(i/\sqrt{2})(-i/\sqrt{2}) ,$$

$$= 1/\sqrt{10} . \quad (3.28)$$

The desired isoscalar factor follows from dividing (3.28) by (3.27). We find

$$\langle (2)E(1)T_1 \| (1)T_1\rangle = -2/\sqrt{10} .$$

The final frame transformation matrix analogous to 3.8 is given by

$$\begin{array}{cc|c} |N=1 \;\; B=T_1 \;\; J=1\rangle & |N=3 \;\; B=T_1 \;\; J=1\rangle & \\ \hline -2/\sqrt{10} & (3/5)^{1/2} & |\text{BOA}\; A=E \quad B=T_1 \quad J=1\rangle \\ (3/5)^{1/2} & 2/\sqrt{10} & |\text{BOA}\; A=T_2 \quad B=T_1 \quad J=1\rangle \end{array} \quad (3.29)$$

C. Symmetry interpretations of vibronic species

In ordinary symmetry coupling theory one considers a system in state A coupled weakly to a system in state B. One starts by imagining the coupling is turned off so states $\{|{}^A_1\rangle|{}^B_1\rangle, |{}^A_1\rangle|{}^B_2\rangle, \ldots\}$ are all degenerate. Then these states are a basis for the IR $\mathfrak{D}^A \otimes \mathfrak{D}^B$ of the group $\mathcal{G}_A \times \mathcal{G}_B$ of independent rotations of the two systems.

$$\left\langle \begin{matrix} A & B \\ a' & b' \end{matrix} \middle| (\mathbf{R}_A \mathbf{S}_B) \middle| \begin{matrix} A & B \\ a & b \end{matrix} \right\rangle = (\mathfrak{D}^A \otimes \mathfrak{D}^B)_{a'a;b'b} .$$

Then with the coupling turned on we reduce the symmetry to the group $\mathcal{G}_{AB} = (\mathbf{R}_A, \mathbf{R}_B)\ldots(\mathbf{S}_A, \mathbf{S}_B)\ldots$ of "rigid" rotations. Only the operators which move the two systems around together will commute with the coupling interaction. Finally, we reduce $\mathfrak{D}^A \otimes \mathfrak{D}^B$ to IR $\mathfrak{D}^C$ of $\mathcal{G}_{AB}$ using coupling coefficients which give (1st order) coupling eigenstates

$$|AB^C_c\rangle = \sum_{ab} C^{ABC}_{abc} \left|\begin{matrix} A \\ a \end{matrix}\right\rangle \left|\begin{matrix} B \\ b \end{matrix}\right\rangle .$$

Now "constriction theory" is quite different in most ways yet there are enough similarities to make the comparison interesting. Let us discuss the symmetry properties of a general BOA state

$$\left|\text{BOA}\, AC \begin{matrix} B & J \\ b & M \end{matrix}\right\rangle = \sum_{ac} C^{AC\,B}_{acb}\, \mathcal{Y}^A_a(\bar{x}\bar{q})\, r^{JC}_{Mc} \tag{3.30}$$

which has the same form as (3.19) except now we let $\mathcal{Y}^A_a$ represent a general *vibronic* state involving any number of electrons and vibrational excitations, all referred of course, to the body frame.

Now let internal vibronic operators $\bar{R}_{ev}$ exist for each element R in the internal symmetry group $\bar{\mathcal{G}}$. These may include improper operations but let us consider a proper $R = 120°$ rotation for a three-fold symmetric molecule. The effect of this $\bar{R}_{ev}$ is shown in Fig. 23(a). It moves all the electrons and all the vibrational disturbances around counter-clockwise by 120° *with respect to the body frame.* The effect on the vibronic function is the following:

$$\bar{\mathbf{R}}_{ev}\mathcal{Y}^A_a = \sum_{a'} \mathfrak{D}^A_{a'a}(R)\, \mathcal{Y}^A_{a'} . \tag{3.31}$$

Now let internal frame operators $\bar{\mathbf{R}}_J$ be defined as they were in Sec. II. Here $\bar{\mathbf{R}}$ takes the whole universe, excluding our molecule, and rotates it counter-clockwise by 120°. However this is the same thing as rotating the molecule rigidly by −120°, i.e., *clockwise*, as shown in Fig. 23(b). The effect on the frame function is the following:

$$\bar{\mathbf{R}}_J r^{JC}_{Mc} = \sum_{c'} \mathfrak{D}^C_{c'c}(R)\, r^{JC}_{Mc'} . \tag{3.32}$$

We now see what these two operators do when performed simultaneously on BOA state (3.30):

$$\begin{aligned}
(\bar{\mathbf{R}}_{ev}, \bar{\mathbf{R}}_J)\left|\text{BOA}\, AC \begin{matrix} B & J \\ b & M \end{matrix}\right\rangle &= \sum_{ac} C^{ACB}_{acb}\, \bar{\mathbf{R}}_{ev}\mathcal{Y}^A_a \bar{\mathbf{R}}_J r^{JC}_{Mc} \\
&= \sum_{ac,\,a'c'} D^A_{a'a}(R) D^C_{c'c}(R) \\
&\qquad \times C^{ACB}_{acb}\, \mathcal{Y}^A_{a'}\, r^{JC}_{Mc'} , \\
&= \sum_{a'c'b'} C^{A\,C\,B}_{a'c'b'} D^B_{b'b}(R)\, \mathcal{Y}^A_{a'}\, r^{JC}_{Mc'} , \\
&= \sum_{b'} D^B_{b'b}(R) \left|\text{BOA}\, AC \begin{matrix} B & J \\ b' & M \end{matrix}\right\rangle .
\end{aligned}$$

Geometrically, we see in Fig. 23 that the *electrons and vibrations are left unmoved* with respect to the laboratory, while the *nuclei are permuted.* The group $\mathcal{G}_{VS} = \ldots(\bar{\mathbf{R}}_{ev}, \bar{\mathbf{R}}_J)\ldots$ of combined rotations which defines the

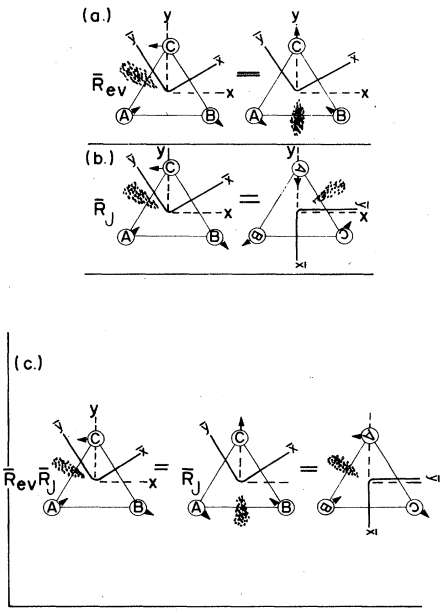

FIG. 23. Effect of 120° rotation on X_3 molecule. (a) R_{ev} rotates all vibronic disturbances with respect to the body frame. Anything referred to the lab frame in the outside world is left alone. (b) $\bar{R}_J$ rotates the lab and the whole outside world with respect to the body frame as in Fig. 2(b). The effect (shown) is the same as rotating the molecule and everything referred to the body frame rigidly in the *opposite* direction with respect to the lab frame. (c) Combining $\bar{\mathbf{R}}_{ev}$ and $\bar{\mathbf{R}}_J$ gives a permutation of the three nuclei which is the "under-all" rovibronic symmetry.

rovibronic species, corresponds directly with the *nuclear permutation symmetry,* one of the "best" symmetries in nature. This is why the rovibronic species B must be conserved. It is as though we were labeling the "soul" of a molecule.

One may want to know why $\bar{\mathbf{R}}_{ev}$ is not a symmetry operator by itself, i.e., why we cannot move the electrons and vibrational distortions from one equivalent nucleus to another. The answer is that it would be one if we had only potentials to consider, but *the kinetic part of the Hamiltonian rules* $\bar{\mathbf{R}}_{ev}$ *out.* Note that $\bar{\mathbf{R}}_{ev}(00\gamma)$ (for $\gamma = 90°$) would convert one "Λ double" into the other in Fig. 19.

The preceding analyses apply to all orthogonal operations, be they proper or improper. For example, an improper reflection operation $\bar{\sigma}$ is depicted in Fig. 24. We see that the "under-all" operation $(\bar{\sigma}_{ev}, \sigma_J)$ has the effect of transposing nuclei A and B.

The description of "underall" symmetry operations is similar to that given in previous works (Louget-Higgins, 1963; Hougen, 1975; Bunker, 1975; Louck and Galbraith, 1976) as far as proper rotations are concerned. Louck and Galbraith take particular care to develop an operational formalism which preserves the Eckart frame.

However, the standard treatment of improper operations (cf., Hougen, 1962; 1963; and 1975) formally deletes the "unfeasible" inversion **I** of the rotor. The effect is the same as reinverting the frame and content of the lower right-hand triangle in Fig. 24. In other words

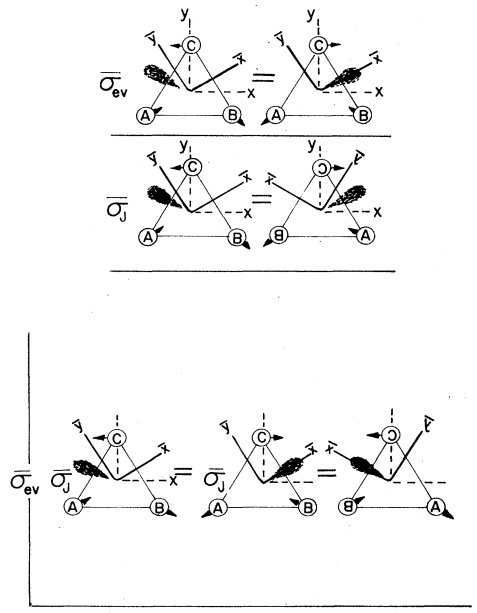

FIG. 24. Effect of (improper) vertical plane reflection on X_3 molecule. The "under-all" rovibronic symmetry operation is the permutation of nucleus A with B.

the standard reflection puts nuclei at points in the lab space that previously were unoccupied. Clearly, this is a valid symmetry operation, but it is a confusing mixture of our internal and external operations. We will compare the physical labelings that result from using the two approaches in Sec. V.

An important point about the commutation properties of symmetry operators should be made. Coupling coefficients are designed to reduce representations $\mathfrak{D}^A \otimes \mathfrak{D}^B$ restricted to subgroup $\mathcal{G}$ of $\mathcal{G} \times \mathcal{G}$. It is tacitly assumed that operators belonging to the left $\mathcal{G}$ factor group in $\mathcal{G} \times \mathcal{G}$ commute with those in the right factor, according to the definition of the outer product ($\times$). This presents no problem in ordinary coupling theory since the two factors are usually assumed to act on independent systems. However, it is necessary to prove that each internal vibronic operator like $\bar{\mathbf{R}}_{ev}$ generated by $\bar{\mathbf{L}}$ commutes with the internal operators $\bar{\mathbf{R}}_J$ generated by total momentum operator $\bar{\mathbf{J}}$, even though they are not acting on independent systems. This may be done geometrically with the aid of diagrams like Fig. 23 and 24. Note that an operator $\bar{\mathbf{R}}_N$ generated by $\bar{\mathbf{N}}$, which acts on just the nuclear rotor but not the vibronic parts, would not commute with $\bar{\mathbf{R}}_{ev}$. On the other hand *external* operators like $\mathbf{R}_{ev}$ generated by $\mathbf{L}$ and $\mathbf{R}_N$ generated by $\mathbf{N}$ will commute, while $\mathbf{R}_{ev}$ and $\mathbf{R}_J$ do not.

Finally, one might be concerned that a given nuclear permutation might not be uniquely represented if it could be performed using two or more different orthogonal operations. For example, the permutation (12) of the diatomic nuclei may be done by any of the operations in the third, fourth, or fifth classes of the group O_{2i} shown in Fig. 15.

However, the exclusion of all but the two IR $B = \Sigma_g^+$ and $B = \Sigma_u^+$ has automatically made the definition of the (12) permutation unique. For Σ_g^+ the signs are all positive for the (12) operations so this labels the even (s) symmetry species, while Σ_u^+ stands for odd or antisymmetry (a) species, since the (12) signs are all negative.

D. Tableaus and statistical weights

The symmetry classification of even or odd for a nuclear wave function of a homonuclear diatomic molecule is easy enough to understand. However, homonuclear polyatomic molecular symmetry definition is in general more difficult since the number ($n!$) of permutations can be large. Fortunately, some powerful and almost magical formulas and algorithms based upon Young tableaus are available for application and development. We will introduce the use of tableaus by first labeling the diatomic symmetry species. A tableau is an arrangement of n boxes which is used to denote permutational symmetry of an n-particle wave function. For example $n = 2$ boxes in a row [see Fig. 25(a)] denotes symmetry i.e., (s) or $B = \Sigma_g^+$, while a column denotes *anti*-symmetry i.e., (a) or $B = \Sigma_u^+$. [See Fig. 25(b).]

However, most of the theory and application of the tableaus concerns so called *para*symmetric n-box tableaus ($n \geq 3$) which belong to neither the symmetric (i.e., one row) nor the antisymmetric (i.e., one column) IR of the permutation group S_n. Furthermore, for n identical nuclei, there will be one or more *orbital tableau* corresponding to each B label of the spatial point group as we will show. Then for each orbital tableau there will be just one *spin tableau*, which describes, among other things, the permutational properties of the nuclear spin wave. According to the general Pauli Principle the spin tableau of a Bose nuclear state (i.e., integral spin nuclei: $I = 0, 1, 2, \ldots$) is identical to the orbital tableau [see Fig. 26(a)], while the spin tableau of a Fermi nuclear state (i.e., half-intergral spin nuclei: $I = \frac{1}{2}, \frac{3}{2}, \frac{5}{2}, \frac{5}{2}, \ldots$) is *conjugate* ($\{\tilde{\mu}\}$) to orbital tableau, [see Fig. 26(b)] that is, the columns are interchanged with the rows.

The association of an IR (B) of a point group $\bar{\mathcal{G}}$ with the right tableau IR of a permutation group S_n is usually easy to do if $\bar{\mathcal{G}}$ is "greater than or equal" to S_n. For example, a quick comparison of character tables of C_{3v} (Table X) and S_3 (see Hamermesh, 1960, or Appendix C) gives the spin tableaus belonging with IR A_1, A_2, and E, respectively (see righthand side of Table X). Here we find (recall Figs. 23 and 24) that the point group C_{3v} is equal or isomorphic to S_3. A similar relationship exists between the tetrahedral point group T_d and the permutation group S_4 (see Table XIII).

However, if the permutation group is greater than the point group in question, then a detailed character calculation may be needed. Fortunately, some convenient and powerful formulas make this job easy. For example, the permutation group S_6 of XY_6 molecule is much larger than its highest spatial point symmetry group O_h.

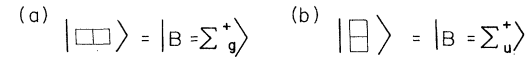

FIG. 25. Orbital tableau labeling of a homonuclear diatomic rotor.

(That is, O_h is a subgroup of S_6.) We use the tableau formulas described in Appendix D to make the correlation table shown in Fig. 27. Note that each IR (B) of O_h is correlated with several spin tableaus in its column of the table.

Now, to compute the spin statistical weights we use the powerful Robinson formula (Robinson, 1960) given in Fig. 28 (see Galbraith, 1978 for similar treatment). This formula gives directly the number $l^{\mu s}$ of nuclear spin states associated with each tableau $\{\mu_s\}$. The sum of these numbers taken over each tableau associated with "soul" label B will be the desired statistical weight W_B

$$W_B = \sum_{\mu} l^{\mu s} f_B^{\mu s} . \tag{3.33}$$

Here $f_B^{\mu s}$ is the correlation frequency from a correlation table like the one for O_h in Fig. 28, i.e., the number of times that IR (B) appears in the $[\mu]$th IR of the permutation group.

For example, let us compute $W_{A_{2g}}$, $W_{A_{2u}}$, $W_{T_{1g}}$, and $W_{T_{1u}}$ for SF_6 in which the spin of F is $I=\frac{1}{2}$

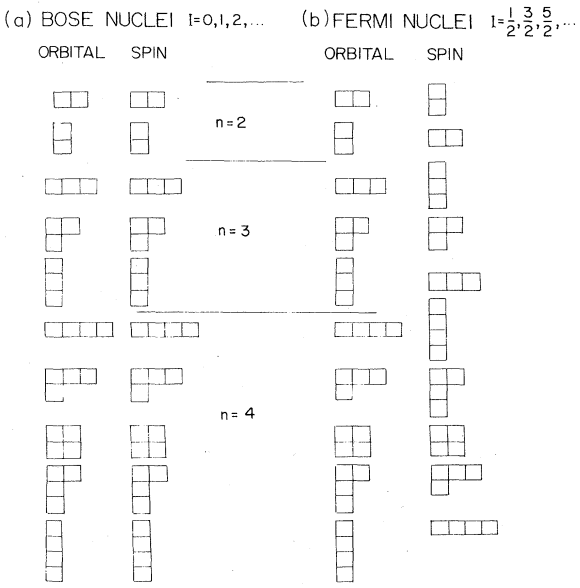

FIG. 26. Orbital and spin tableaus used to label homonuclear n-atomic molecules $(n=2,3,4,\ldots)$.

$W_{A_{2g}} = 0$

$W_{A_{2u}} =$ [2345 / 12 ; 5421 / 21] + [234567 ; 654321] $= 3 + 7 = 10$

$W_{T_{1g}} =$ [2345 / 12 ; 5421 / 21] $= 3 = W_{T_{1u}}$.

The individual weights do not agree with those obtained by standard methods (Cantrell and Galbraith, 1976). However, the ratio of sums over (u) and (g) agree, i.e., $W_{A_2} : W_{T_1} = 5:3$ using either method. As long as inversions do not play a dynamic role, either method gives the same weights. We will discuss this point more fully when we treat methane (CH_4) in Sec. V.B (example 3).

As a final example, let us calculate the weights for a fictitious molecule XY_6 in which each Y nucleus has spin $I=\frac{5}{2}$.

$W_{A_{2g}} =$ [678 / 5 / 4 / 3 / 621 / 3 / 2 / 1] + [67 / 56 / 45 / 43 / 32 / 21]

$= 280 + 175 = 445$

$W_{T_{1g}} =$ [678 / 5 / 4 / 3 / 621 / 3 / 2 / 1] + [678 / 56 / 4 / 531 / 3 / 1] + [6789 / 5 / 4 / 6321 / 2 / 1] + [6789 / 56 / 5421 / 21]

$= 280 + 896 + 840 + 1134 = 3150$

$W_{A_{2u}} =$ [67 / 56 / 45 / 43 / 32 / 21] + [6789 / 56 / 5421 / 21] + [67891011 / 654321]

$= 175 + 1134 + 462 = 1771$

$W_{T_{1u}} =$ [67 / 5 / 4 / 3 / 2 / 61 / 4 / 3 / 2 / 1] + [678 / 5 / 4 / 3 / 621 / 3 / 2 / 1] + [67 / 56 / 45 / 43 / 32 / 21] + [678 / 56 / 4 / 531 / 3 / 1] + [6789 / 56 / 5421 / 21]

$= 35 + 280 + 175 + 896 + 1134 = 2520$.

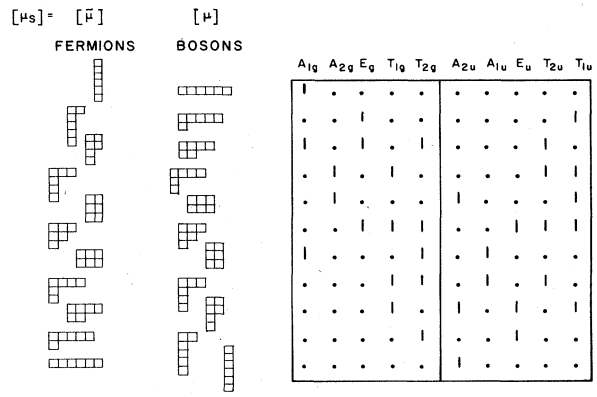

FIG. 27. Spin tableau-(B) correlation for octahedral XY_6 molecule (see Appendix D).

Finally, it is possible to enumerate and compute all the properties of the nuclear spin states using tableau algorithms. The procedure is virtually the same as the one used to derive the ^{2S+1}L terms in a complex atomic l^n configuration (Harter, 1973; Drake, 1975; Harter and Patterson, 1976a). Here we replace the single electron momentum l with the internal momentum I of each nucleus. Then we compute the total nuclear spins I_T that are possible for that molecular species in the same way that we find the allowed total L for the atomic multiplet. For $I=\frac{1}{2}$ nuclei the procedure is quite simple. Each spin tableau must have at most two rows that define just one total nuclear spin I_T, where $2I_T$ equals the number of unpaired tableau boxes.

It is possible to use the tableaus to help one determine the form of the nuclear dipole and quadrupole hyperfine structure, as we will mention in the following section.

E. Possibilities for (J^p) or (B) failure

We briefly discuss some situations in which the "sacred" (J^p,B-tableau$\{\mu\}$) labels might "fail". "Failure" or nonconservation of trusted quantum variables or labels generally occurs when some new mechanism which was previously ignored turns out to play a crucial role in a more accurate experiment. For example, the orbital momentum label L for certain atoms failed when electron spin and orbit coupling was observed in atomic fine structure. Then it became necessary to add spin

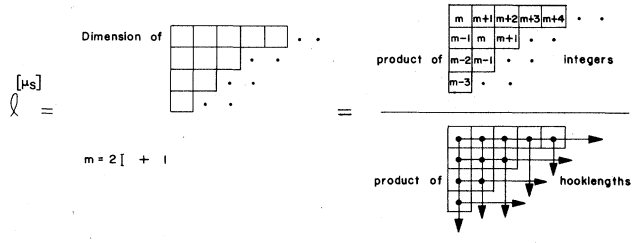

FIG. 28. Robinson formula for statistical weights. The "hooklength" of a box in the tableau is the number of boxes in a "hook" which includes that box and all boxes in the line to the right and in the column below it.

momentum S to orbital momentum in order to construct a new labeling operator: $J=L+S$. This worked well until nuclear hyperfine structure showed that an even better labeling operator would be the eigenvalues of $F=L+S+I$, where I is the operator of nuclear spin.

One must generally introduce new operators and a more complete basis of states when old quantum labels fail. The new eigenstates then turn out to be combinations of states with different values of the old "failed" label. Of course, if it turns out that the amplitude of one old state dominates in each new eigenstate, then the old label may still serve as an approximate label for the new states, too. For example, many light atom electronic states are given a Russell-Saunders labeling such as $|^{2S+1}L_J\rangle = |^3D_1\rangle$, even though the eigenstates have small amounts of other L and S, i.e., $|^3S_1\rangle$, $|^1P_1\rangle$, $|^1D_1\rangle, \ldots$

We consider two possible sources of trouble for the "soul" (J^p,B-$\{\mu\}$) labeling of molecular species: core excitation, and nuclear moment interaction.

1. Core excitation

The model "bare rotor" imagined in Secs. II.3 and III.1 to 3 consists of some arrangement of identical "bare" nuclei, i.e., a configuration of identical geometrical points. However, most molecular cores or rotors also have electrons orbiting between them. Therefore, the bare rotor model will be useful only if we can ignore the core electrons and treat them all as a single charge "blob" having the assumed rotor symmetry.

Core electrons cannot be ignored if they are easily excited to other states, if they carry observable orbital or spin momentum, or if they overlap appreciably with the electron or electrons orbiting or scattering "outside" of the core. Whenever there are two or more core states $|A_c\rangle, |A_c'\rangle, \ldots$, we must write them as factors in the total vibronic states $|A_cA\ldots\rangle, |A_c'A\ldots\rangle, \ldots$ which will be used finally to describe all vibronic activity.

General vibronic eigenstates may include large exchange correlations between core and "outside" electrons. Each eigenstate may finally be labeled by permutation tableaus and a total vibronic activity label A_T. Modern methods for treating multi-electron multiconfiguration electronic states are rapidly being developed, (Goddard, 1967; Harter, 1973; Paldus, 1976; Patterson and Harter, 1976 b, c) and they are closely related to the methods we are using to define the multi-nuclear label B-$\{\mu\}$. Nevertheless, a number of applications will have to be worked out successfully before it is clear how to use all these new techniques effectively in problems of complex molecular-electron scattering, excitation, and ionization.

In any case, it is clear that all observable vibronic activity must be treated as such and included under the (A) label. It must not be confused with that which belongs to the nuclear permutation symmetry label (B-$\{\mu\}$) of the bare rotor.

2. Nuclear spin or multipole effects

The (B-$\{\mu\}$) label and the underlying nuclear permutation symmetry can be broken if each nucleus comes equipped with a magnetic dipole, electric quadrupole, or any multi-

pole moment large enough to be observed. Nonzero moments imply the existence of nonzero nuclear internal momentum (this is generally called nuclear "spin" outside of nuclear physics) and the internal spin states could in principle be used to "tag" or distinguish one nucleus from another. The breakdown is similar to that which occurs when a spin–orbit interaction is introduced to an LS coupled basis in atomic theory. If the interaction is strong the J eigenstates will be combinations of states belonging to different total spin S, i.e., to different tableaus.

However, for most molecules the nuclear spin rotation or quadrupole interactions are extremely small. Therefore the $(B\text{-}\{\mu\})$ soul label may be used in the manner we have been describing. By using the ultra-high resolution of the recent saturation spectroscopy (Hanes, 1969; Hansch, 1971; Hall, 1974, and 1976) it has become possible to observe high J hyperfine splitting of $(B\text{-}\{\mu\})$ levels, but mixing of different $(B\text{-}\{\mu\})$ has not been noted. (However, it should occur for very nearly degenerate high-J cluster states.)

Furthermore, analysis of nuclear hyperfine splitting for high J can be made quite simple, even for nuclei of spin $\frac{5}{2}$ or $\frac{7}{2}$. It has been shown by Levenson (Levenson and Schalow, 1972) how to obtain very accurate formulas for diatomic iodine I_2 levels in terms of nuclear spin components M_1 and M_2 defined on an axis in the direction of the total momentum. Two developments permit the application of these simple methods to symmetric polyatomic molecules. First, we know that even the spherical top molecular rotation states of a given level are very nearly quantized with respect to just one internal axis (see Sec. II.A.). Secondly, we have clearly defined the nuclear spin tableau states associated with any $(B\text{-}\{\mu\})$ species. (It will be particularly interesting to examine this for high spin XY_4 and XY_6 molecules since different states can choose different axes.)

We give a brief description of how the approximate form of a hyperfine splitting pattern might be derived and displayed for a symmetric polyatomic molecule. Consider a symmetric XY_3 molecule for which the X spin is zero, but the three Y nuclei each have spin $I=1$, and consider the $(B=E, \{\mu\}=\{2,1\})$ species. This species belongs to the $2+1$ box spin tableau, and Fig. 29 shows the tableaus filled with all the allowed nuclear spin quantum numbers M_1, M_2, and $M_3=1$, 0, or -1. The permutational symmetry rules demand that numbers must decrease as we read down any column (roughly speaking, this is because columns are antisymmetrized), but that numbers may be equal or decreasing as we read to the right in the rows (roughly speaking, the rows represent a symmetrization). We end up with the eight independent states shown in Fig. 29, just as Fig. 28 predicts we should.

Now, the first terms in Levenson's formulas for hyperfine spin or dipole-rotation energy (E_D) and quadrupole energy (E_Q) are

$$E_D \cong d\sum_{i=1}^{n} M_i \qquad E_Q \cong q\sum_{i=1}^{n} (M_i)^2 ,$$

where he needed the diatomic case ($n=2$) only. In Fig. 29 we have plotted E_D vs E_Q for the eight spin tableau states in the $(n=3)$ case in question. This diagram is

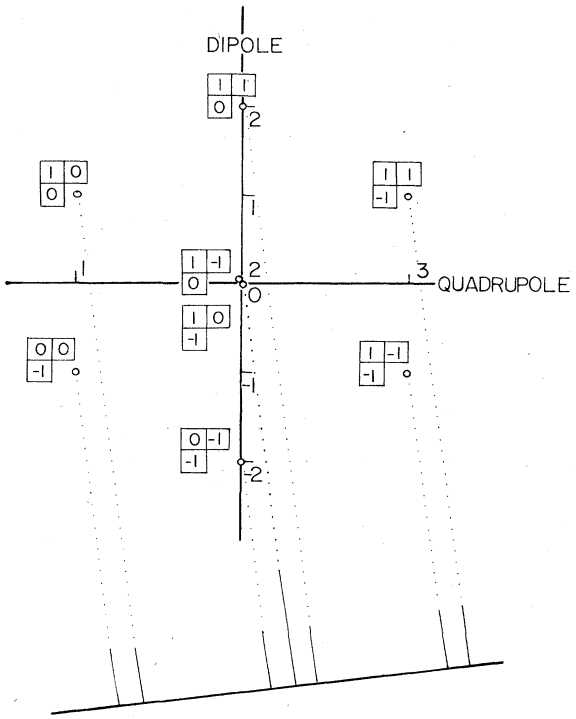

FIG. 29. Unitary spin weight diagram and possible hyperfine pattern.

called a unitary *Weight* diagram, and in fact is the one used to display the famous "eight-fold way" of Gell-Mann and Zweig in high energy physics.

The diagram is useful for understanding the XY_3 spectra, because it serves as a nomogram for obtaining possible hyperfine level and spectral patterns. Any projection of the points in the hexagonal diagram is a possible approximate level pattern. The projection drawn in Fig. 29 corresponds to a ratio of about 8 : 1 for the parameters q and d.

IV. ROVIBRONIC MULTIPOLE MATRIX ELEMENTS AND TRANSITIONS (BOA BASES)

We now derive and interpret selection rules for multipole operators which are used to describe optical transitions or external field perturbations. We treat the BOA states first, and discuss the weak coupling states in Sec. V.

As in Sec. III, we begin by treating the symmetric rotor first since it is simple enough to allow easy visualization of the results. In the process we rederive the Honl-London formulas (Honl and London, 1925). After that we treat the general BOA constricted rotor.

A. Symmetric top molecular transitions

We consider matrix elements involving the elementary BOA states in Eq. 3.11 and multipole operators

$$\mathbf{T}^k_q = \mathbf{T}^k_q(\ldots x_e \ldots q_v \ldots) \tag{4.1}$$

which are functions only of lab-defined electronic or nu-

clear coordinates. A simple example of $\mathbf{T}^k_q$ is the electric dipole operator

$$d_z = \sum_e \rho_e \mathbf{z}_e + \sum_N \rho_N \mathbf{Z}_N \equiv \mathbf{T}^1_0 \tag{4.2}$$

in the perturbation operator

$$\mathbf{V} = -\mathbf{E}\cdot\mathbf{d} = -E_z d_z . \tag{4.3}$$

This describes the effect of a static uniform E field (Stark effect) or, in the limit of long wavelength, the effect of z-polarized radiation. [Electric dipole ($E1$) transitions.]

The matrix elements of $\mathbf{T}^k_q$ in the BOA basis will be

$$\begin{aligned} M_{\substack{J'M' \; J\,M \\ \Lambda' n' \; \Lambda n}}(v' \leftarrow v) &= \left\langle V'_{\Lambda'} n' \begin{matrix} J' \\ M' \end{matrix} \middle| \mathbf{T}^k_q(x_e\, q_v) \middle| V_\Lambda n \begin{matrix} J \\ M \end{matrix} \right\rangle \\ &= \left\langle \; \middle| \sum_{r=-k}^{k} \mathfrak{D}^{k*}_{qr}\, \mathbf{T}^k_r(\bar{x}_e\, \bar{q}_v) \middle| \; \right\rangle \\ &= \sum_{r=-k}^{k} \int d(\alpha\beta\gamma) \mathfrak{D}^{J'}_{M'\Lambda'+n'} \mathfrak{D}^{k*}_{qr} \mathfrak{D}^{J*}_{M\Lambda+n} ([J'][J])^{1/2} \int d(\bar{x}_e\, \bar{q}_v) V'^{*}_{\Lambda'} \mathbf{T}^k_r V_\Lambda \\ &= \sum_{r=-k}^{k} ([J]/[J'])^{1/2} C^{kJJ'}_{qMM'} C^{kJJ'}_{r\Lambda+n\Lambda'+n'} \langle V'_{\Lambda'} | \mathbf{T}^k_r | V_\Lambda \rangle , \end{aligned} \tag{4.4}$$

where the $\mathbf{T}^k_q$ is transformed to the body system in the second line, and the fundamental (factorization lemma) definition of coupling coefficients $C^{kJJ'}_{qMM'}$ is used in the last line. In addition, the vibronic integral defined by

$$\langle V'_\Lambda | \mathbf{T}^k_r | V_\Lambda \rangle \equiv \int d(\bar{x}_e\, \bar{q}_v) V'^{*}_{\Lambda'}\, \mathbf{T}^k_r\, V_\Lambda \tag{4.5}$$

could be expanded by the Wigner-Eckart theorem to give

$$\langle V'_{\Lambda'} | \mathbf{T}^k_r | V_\Lambda \rangle = C^{kll'}_{r\Lambda\Lambda'} \langle V' \| \mathbf{T}^k \| V \rangle \tag{4.6}$$

if we were to assume that each vibronic function $V_\Lambda = V^l_\Lambda$ belonged to a definite l. However, we shall not make this assumption since general vibronic states are made of more than one l.

Nevertheless, the internal cylindrical symmetry of the rotor requires that the body axis components in the vibronic integral add up as follows: $r+\Lambda=\Lambda'$. The same applies to the components in the second coupling coefficient in Eq. (4.4) i.e., $r+\Lambda+n=\Lambda'+n'$. Combining these, we have the first rovibronic selection rule

$$n' = n , \tag{4.7}$$

i.e., "internal" n is conserved no matter which "external" perturbations are applied.

To compute the kth transition probability t^k we need to compute the square of the T^k matrix, sum over the final state M' and average over the initial M, as follows:

$$\begin{aligned} t^k_{\substack{J' \; J \\ \Lambda' \; \Lambda}}(v' \leftarrow v)_n &= \frac{1}{[J]} \sum_{M=-J}^{J} \sum_{M'=-J'}^{J'} |M_{\substack{J'M' \; J\,M \\ \Lambda' n \; \Lambda\, n}}|^2 \\ &= \frac{1}{[k]} (C^k_{r=\Lambda'-\Lambda \; \Lambda+n \; \Lambda'+n})^2 |\langle V'_{\Lambda'} | \mathbf{T}^k_r | V_\Lambda \rangle|^2 . \end{aligned} \tag{4.8}$$

The external coupling coefficient $C^{kJJ}_{qMM'}$ disappears because of the symmetry relation

$$(C^{kJJ'}_{qMM'})^2 = [J']/[k] (C^{J\;J'\;k}_{M-M'-q})^2 \tag{4.9}$$

and the orthonormality relation

$$\sum_{MM'} C^{J\;J'\;k}_{M-M'-q} C^{J\;J'\;k'}_{M-M'-q'} = \delta^{kk'}_{qq'}$$

of coupling coefficients. Finally the transition line strength $L(k)$ is proportional to the product

$$L(k) \sim t^k_{\substack{J' \; J \\ \Lambda' \; \Lambda}} W_{J\Lambda}(n, \text{temperature}) \tag{4.10}$$

of t^k and the relative population $W_{J\Lambda}$ of the initial state. $W_{J\Lambda}$ in turn is a product of a Boltzman factor which depends on initial state energy and temperature, and the statistical weight factor discussed in the preceding section. (The statistical weight depends on the rovibronic label B which is (n) for the symmetric rotor.)

We discuss briefly the important $k=1$ or dipole case of Eq. (4.8). The coefficient of the vibronic integral is given by the formulas in Table IX, and follows from the

TABLE IX. Dipole ($k=1$) coefficients of vibronic integral in Eq. (4.8).

$K=\Lambda+n$	P Branch $J'=J-1$	Q Branch $J'=J$	R Branch $J'=J+1$
p sub-band ($\perp$ band) $r=-1, K'=K-1, \Lambda'=\Lambda-1$	$\frac{(J+K-1)(J+K)}{6J(2J+1)}$	$\frac{(J-K+1)(J+K)}{6J(J+1)}$	$\frac{(J-K+2)(J-K+1)}{6(J+1)(2J+1)}$
q sub-band ($\parallel$ band) $r=0, K'=K, \Lambda'=\Lambda$	$\frac{(J+K)(J-K)}{3J(2J+1)}$	$\frac{K^2}{3J(J+1)}$	$\frac{(J-K+1)(J+K+1)}{3(J+1)(2J+1)}$
r sub-band ($\perp$ band) $r=1, K'=K+1, \Lambda'=\Lambda+1$	$\frac{(J-K-1)(J-K)}{6J(2J+1)}$	$\frac{(J+K+1)(J-K)}{6J(J+1)}$	$\frac{(J+K+2)(J+K+1)}{6(J+1)(2J+1)}$

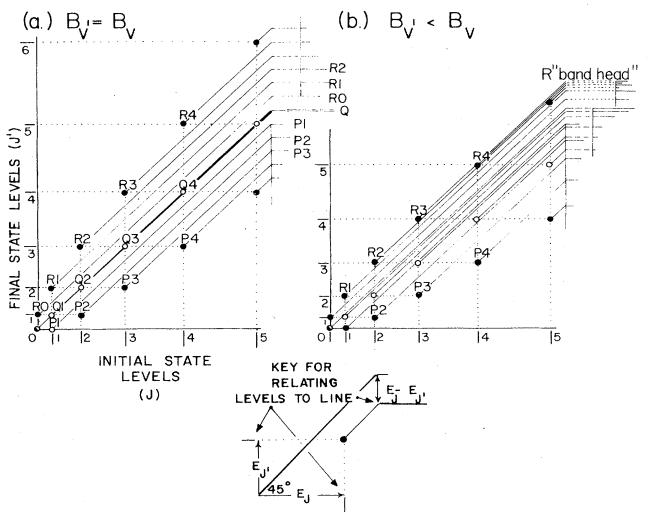

FIG. 30. Demonstrating the use of a rovibronic nomogram for the model $\Sigma \rightarrow \Sigma$ transitions by dipole excitation in a symmetric-top molecule.

general coupling coefficient formulas. These are related to the well known Honl–London formulas.

In order to visualize the transitions that occur in molecules it may be helpful to construct a nomogram which converts level diagrams directly into spectra. In Fig. 30a we show the simplest examples of the $\Sigma \rightarrow \Sigma$ dipole transition ($\Lambda' = 0 = \Lambda$) between two sets of J levels with the same rotational constants $B_{v'} = B_v$. The idea is to plot the initial and final levels on the x and y axes and put a dot at ($x = E_J$ $y = E_{J'}$) for each allowed transition $J \rightarrow J'$. Then lines drawn at 45° from each of these points give immediately a scale model of the expected line spectra as shown in the key of the figure.

The diagram is useful to show the form of the spectra for different rotational constants $B_{v'} < B_v$. For $B_{v'} = B_v$ the transition dots form a parabola inclined at 45°, while for $B_{v'} < B_v$, the parabola tips more. This results in the formation of a band head on the high side or R-branch as shown in Fig. 30(b).

The strength of the lines in Fig. 30 would depend upon the entries in Table IX, the vibronic matrix $\langle V'_{\Lambda'=0} | \mathbf{T}^1_{r=0} | V_{\Lambda=0} \rangle$ and the initial populations. From the table we see that the Q_q branch is ruled out for $r = 0 = k$, so the $Q(J)$ lines should be missing in Fig. 30. For pure rotational transitions (microwave spectra) we need a nonzero $\langle V_0 | \mathbf{T}^1_0 | V_0 \rangle$ i.e., a permanent $\bar{z}$ dipole moment. For vibrational or vibronic transitions (infrared and optical spectra) we need a nonzero *induced* dipole moment $\langle V'_0 | \mathbf{T}^1_0 | V_0 \rangle$ parallel to $\bar{z}$. We will show in the following sections how more detailed symmetry analysis provides selection rules for general types of moments very easily.

B. General matrix formula and selection rules

We consider now the matrix elements between BOA wave functions

$$\left\langle \left| AC \begin{matrix} B & J^p \\ b & M \end{matrix} \right\rangle = \sum_{ac} C^{ACB}_{acb}\, \mathcal{Y}^A_a(\bar{x}_e \bar{q}_v) r^{J^p C}_{M c} \tag{4.11a}$$

of the multipole operator $\mathbf{T}^{kq}_r$ that would arise in the treatment of external (lab-fixed) perturbations or externally induced transitions. The rotor functions

$$r^{J^p C}_{M c} = \sum_{M''} \begin{pmatrix} J^p \\ M'' \end{pmatrix} \begin{matrix} | \\ | \end{matrix} \begin{matrix} C^* \\ c \end{matrix} \Big)^* \mathfrak{D}^{J^p *}_{MM''}(\mathbf{O}(\phi\theta\chi)) \sqrt{[J]} \tag{4.11b}$$

have external (O_3) and internal $\bar{\mathcal{G}}$ symmetry definitions as we have described.

The general matrix element for an $A \rightarrow A'$ vibronic transition is

$$M^{kq}_{\substack{J'J \\ M'M}}(A'_{c'} \leftarrow A_c) = \left\langle A'C' \begin{matrix} B' & J'^{p'} \\ b' & M' \end{matrix} \middle| \mathbf{T}^{kq}_r(\text{lab}) \middle| AC \begin{matrix} B & J^p \\ b & M \end{matrix} \right\rangle$$

$$= \left\langle \left| \sum_s \mathbf{T}^{kq}_s(\text{body}) \mathfrak{D}^{kq*}_{rs} \right| \right\rangle , \tag{4.12}$$

where we have expressed abstractly the usual transformation from lab to body frame. Expanding (4.12) using (4.11b) gives

$$M^{kq}_{\substack{J'J \\ M'M}}(A'_{c'} \leftarrow A_c) = \sum \int (O_3) \mathfrak{D}^{J',p'}_{M'M'''} \mathfrak{D}^{kq*}_{rs} \mathfrak{D}^{J^p*}_{MM''} \begin{pmatrix} J'^{p'} \\ M''' \end{pmatrix} \begin{matrix} | \\ | \end{matrix} \begin{matrix} C'^* \\ c' \end{matrix} \Big) \begin{pmatrix} J^p \\ M'' \end{pmatrix} \begin{matrix} | \\ | \end{matrix} \begin{matrix} C^* \\ c \end{matrix} \Big)^*$$

$$\times C^{ACB}_{acb} C^{*A'C'B'}_{a'c'b'} \int d(\bar{x}\,\bar{q})\, \mathcal{Y}^{A'*}_{a'} \mathbf{T}^{kq}_s \mathcal{Y}^A_a ([J][J'])^{1/2} \tag{4.13}$$

The first factor is an integral and sum over O_3 which is

$$\int (O_3) \mathfrak{D}^{J',p'}_{M'M'''} \mathfrak{D}^{kq*}_{rs} \mathfrak{D}^{J^p*}_{MM''} = C^{kqJ^pJ',p'}_{rMM'} C^{kqJ^pJ',p'}_{sM''M'''} / [J'] \tag{4.14}$$

according to the "factorization lemma". This immediately gives an external parity selection rule

$$p' = pq \tag{4.15}$$

among others. Meanwhile, internal or body-frame selection rules for $\mathbf{T}^{kq}_s$(body) between two vibronic states depend on an integral over vibronic coordinates.

$$\int d(x'q') \mathcal{Y}^{A'}_{a'} \mathbf{T}^{kq}_s \mathcal{Y}^A_a \equiv \left\langle \begin{matrix} A' \\ a' \end{matrix} \middle| \mathbf{T}^{kq}_s \middle| \begin{matrix} A \\ a \end{matrix} \right\rangle$$

$$= \sum_{Dd} \begin{pmatrix} k^q \\ s \end{pmatrix} \begin{matrix} | \\ | \end{matrix} \begin{matrix} D^* \\ d \end{matrix} \Big) \left\langle \begin{matrix} A' \\ a' \end{matrix} \middle| \mathcal{T}^D_d \middle| \begin{matrix} A \\ a \end{matrix} \right\rangle$$

$$= \sum_{Dd} \begin{pmatrix} k^q \\ s \end{pmatrix} \begin{matrix} | \\ | \end{matrix} \begin{matrix} D \\ d \end{matrix} \Big)^* C^{DAA'}_{daa'} \langle A' \| D \| A \rangle \tag{4.16}$$

In (4.16) we have decomposed the O_3 tensor operator into $\mathcal{T}^D_d$ operators of $\bar{\mathcal{G}}$ and then used the $\bar{\mathcal{G}}$ Wigner-Eckart

theorem. This factor is zero unless $\mathfrak{D}^{k^q}\otimes\mathfrak{D}^{A}$ contains $\mathfrak{D}^{A'}$ i.e., unless $C^{DAA'}_{daa'}$ is nonzero for some D in k^q.

Combining (4.16) and (4.14) gives the usual form for the external (O_3) Wigner-Eckart theorem.

$$M^{k^q}_{\substack{J'J\\M'M}}(A'_{c'}\leftarrow A_c)=C^{k^qJ^pJ'^{p'}}_{rMM'}\langle A'B'C'J'^{p'}\|\mathbf{T}^{k^q}\|ABCJ^p\rangle \tag{4.17}$$

It is the "internal" information which interests us inside the reduced matrix element of (4.17). (Generally the sum over final and average over initial M states eliminates the coupling coefficient $C^{k^qJ^pJ'^{p'}}$ entirely, as shown in the preceeding section.) We have

$$R\equiv\langle A'B'C'J'^{p'}\|\mathbf{T}^{k^q}\|ABCJ^p\rangle$$
$$=\sum_D\langle A'\|D\|A\rangle\sum_{\substack{aa'\\cc'\\d}}C^{ACB}_{acb}C^{A'C'B'}_{a'c'b'}C^{DAA'}_{daa'}\sum_{\substack{M''M'''\\s}}C^{k^qJ^pJ'^{p'}}_{sM''M'''}\begin{pmatrix}k^q & D\\ s & d\end{pmatrix}^*\begin{pmatrix}J^p & C^*\\ M'' & c\end{pmatrix}^*\begin{pmatrix}J'^{p'} & C'^*\\ M''' & c'\end{pmatrix}([J]/[J'])^{1/2}\,. \tag{4.18}$$

Now we recognize the latter part of (4.18) to be a product of the molecular isoscalar factor (3.15) and another $\mathcal{G}$ coupling coefficient, (3.18)

$$R=\sum_D\langle A'\|D\|A\rangle\sum C^{ACB}_{acb}C^{A'C'B'}_{a'c'b'}C^{DAA'}_{daa'}C^{DC'C}_{dc'c}$$
$$\times\langle(k^q)D(J^p)C^*\|(J'^{p'})C'^*\rangle\,. \tag{4.19}$$

Finally the sum over the coupling coefficient is a $\overline{\mathcal{G}}$ Racah coefficient which is discussed in Appendix B where we have the well known definition

$$\sum_{\substack{acd\\a'c'}}C^{ACB}_{acb}C^{A'C'B'}_{a'c'b'}C^{DAA'}_{daa'}C^{DC'C}_{dc'c}\equiv\begin{bmatrix}A & D & A'\\ C' & B & C\end{bmatrix}\delta^{B'B}\delta_{b'b}\,.$$

The matrix element is then

$$M^{k^q}_{\substack{J'J\\M'M}}(A'_{c'}\leftarrow A_c)_B=C^{k^qJ^pJ'^{p'}}_{rMM'}\sum_{\substack{Din\\k^q}}\langle A'\|D\|A\rangle\begin{bmatrix}A & D & A'\\ C' & B & C\end{bmatrix}\langle(k^q)D(J^p)C^*\|(J'^{p'})C'^*\rangle\ \text{if } B'=B$$
$$=0\ \text{if } B'\neq B\ \text{ or } b'\neq b\,. \tag{4.20}$$

We see that the "internal" label (B,b) of rovibronic species can never be changed by an "external" $\mathbf{T}^{k^q}_r$(lab). This is an important difference between the selection rules implied here and corresponding ones in the literature as we will explain in examples which follow.

Internal and external selection rules are obtained without even evaluating the coefficients in (4.20). We see that in this framework the external rules will have the same form as the well known atomic physics rules for k^q moment transition of J^p to $J'^{p'}$, while the internal rules for a D transition of A to A' will be identical to the rules used for years in crystal-field or elementary molecular spectroscopy.

However (4.20) will also provide (when squared and summed over degenerate initial and final states) a formula for the relative transition probabilities for the whole band of the $A\rightarrow A'$ transition in terms of a few vibronic integrals $\langle A'\|D\|A\rangle$, in the same way as was done to get Eqs. (4.4) in the preceeding section. The difficulty of numerically evaluating expressions like Eq. (4.20) will depend on the assumed nature of the molecule. For low symmetry molecules, the Racah coefficients are simpler, often just 1 or 0; but the components of the molecular isoscalar factor may have to be obtained from diagonalization of an assumed Hamiltonian. For higher symmetry molecules, the Racah coefficients are needed, but the molecular isoscalar factors may be approximated without any diagonalization (cf., Sec. II.A.2–4, or Patterson and Harter, 1977a). If the initial state A is a scalar ground state, the Racah coefficient reduces to 1 or 0 in any case. For high symmetry molecules the statistical weight is the most important factor since the angular coefficients do not usually vary that much from line to line of an allowed band.

1. O_{2i} symmetric molecules X_2, XYX, $XYYX$, . . .

The form of the section rules, and in particular the conservation of (B), suggests a convenient graphical visualization for rovibronic transition spectra. We consider here only the electric dipole transitions for BOA states of symmetric (O_{2i}) linear molecules. However, we describe simple procedures which are generally applicable.

The electric dipole ($E1$) transition operator belongs to the 1^- IR of O_3 and therefore, by Table VIII, to $D=\Sigma^+_u$ and $D=\Pi_u$ IR of cylindrical symmetry O_{2i}. Let us consider the $(A=\Sigma^+_g\rightarrow A'=\Sigma^+_u)$ and the $(A=\Sigma^-_u\rightarrow A'=\Pi_g)$ transitions which are internally allowed. [Because $(A=\Sigma^+_g)\otimes(D=\Sigma^+_u)=(A'=\Sigma^+_u)$ the first is allowed, and because $(A=\Sigma^-_u)\otimes(D=\Pi_u)=(A'=\Pi_g)$ the second is allowed by Eq. (4.16).] The latter is interesting because Σ^-_u is dipole forbidden to go back to ground state Σ^+_g. These lines show up in the electron spectra of certain X, XYX, and $XYYX$ molecules.

The $\Sigma^+_g\rightarrow\Sigma^+_u$ transitions are shown in Fig. 31(a). We place the initial levels along the abscissa grouped into rows according to their B labels. Along the ordinate, we

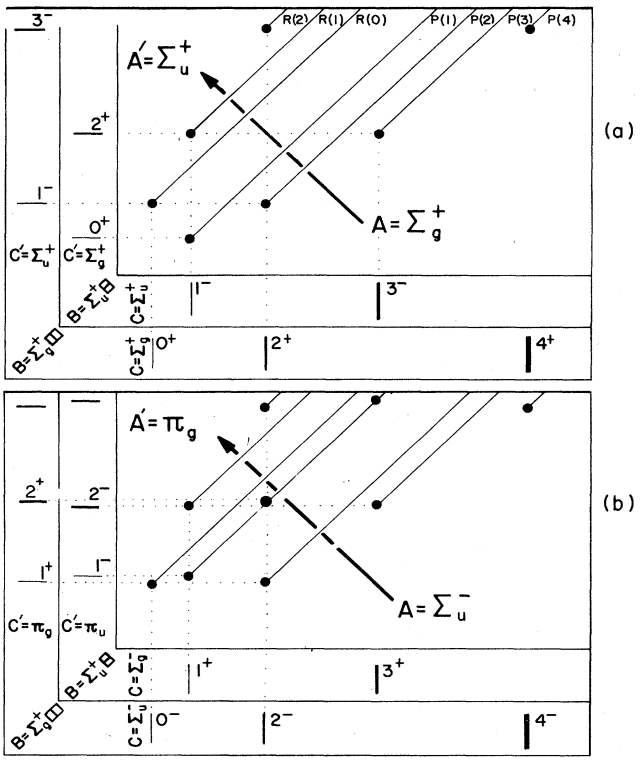

FIG. 31. Electric dipole transitions in linear symmetric (O_{2i}) molecules $X_2, XYX, \ldots$ (a) $\Sigma_g^+ \rightarrow \Sigma_u^+$. (b) $\Sigma_u^- \rightarrow \Pi_g$. Transitions are only allowed between levels lying in the same B corridor. Note that the ($\Sigma_u^- \rightarrow \Pi_g$) Q branch is not Λ doubled since the upper Π doublet is always involved in a $J \rightarrow J$ transition.

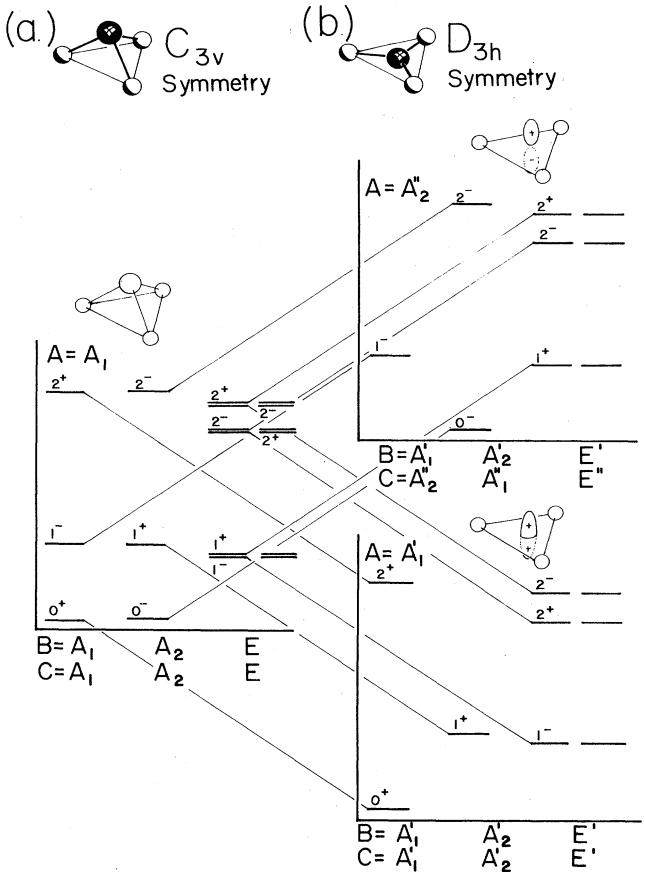

FIG. 32. Correlation of (a) NH_3-like (C_{3v}) molecular ground state (A_1) levels with (b) ground (A_1') and excited (A_2'') levels of CH_3-like (D_{3h}) molecules.

put the final levels, matching the rovibronic B label of the final levels with those of the initial levels, since we have shown that B is conserved. In order to find the levels in each B column, we write down in each B row all the C contained in $A \otimes B$, and in each B column all the C' contained in $A' \otimes B$. Then we look up the J^p levels that go with each C from Table VIII, and place them according to whatever model energy formula we have. [For the Σ^+ levels we just space them according to $J(J+1)$.]

Now for each B we find the transitions allowed by the external selection rules i.e., the P branch: $J^{\pm} \rightarrow J^{\mp} - 1$, Q branch: $J^{\pm} \rightarrow J^{\mp}$, or R branch: $J^{\pm} \rightarrow J^{\mp} + 1$ by placing a dot at the co-ordinates determined by each allowed pair of levels. The actual spectra are then obtained by extending lines at 45° from all the allowed points as shown in Fig. 30.

Note how the $\Sigma_g^+ \rightarrow \Sigma_u^+$ transition does not allow a Q branch, and how the P and R branches form two sides of a parabola tipped by 45°. If the rotational constant for Σ_u^+ was less than for Σ_g^+ then this parabola would tip over more and a "band head" would form on the R side. In the $\Sigma_u^- \rightarrow \Pi_g$ transition we have a clipped parabola with one Q line running up the center. (Λ-doubling is not evident in the Q line because just the upper doublets participate.) Each B column and row will be associated with one or more Young Tableau. This immediately tells us the nuclear spins and species population ratios if we use the convenient formulas discussed in Sec. III.D.

2. C_{3v} and D_{3h} symmetric molecules XY_3

We discuss now some states and transitions of XY_3 molecules having C_{3v} symmetry and D_{3h} symmetry (Fig. 32(a) and (b), respectively). The molecules CH_3 and CD_3 are generally considered to be D_{3h} symmetric, while NH_3 is said to have the lower C_{3v} symmetry. These examples are interesting because NH_3 has the well known tendency to "invert".

We begin by recalling the C_{3v} and D_{3h} character tables (Tables Xa and Xb). We indicate the correspondence between the IR and tableau assignments for the bare rotor statistics. Note that only IR A_1', A_2', and E' of D_{3h} can be bare rotor (B) labels since we require that horizontal reflection operator σ_h be a unit operator.

From the character tables we may construct the necessary O_3 frequency or correlation tables (Tables XI) for the reduction of angular momentum states to subgroups C_{3v} and D_{3h}.

In order to compare the symmetry D_{3h} with its subgroup C_{3v} we will need the correlation Table XII.

In Fig. 32 we show the scalar $A = A_1$ vibronic manifold of a pyramidal (C_{3v}) molecule, and correlate the levels with those of a planar (D_{3h}) molecule. On the left (C_{3v}) side of the figure we imagine a molecule like NH_3 which can invert the central atom only relatively infrequently,

TABLE X. Character tables of (A) C_{3v} and (B) D_{3h}.

A. C_{3v}

	1	z rotations $\bar{R}\left(\frac{2\pi}{3}00\right)$	Vertical reflections σ_v $I\cdot\bar{R}(0\pi0)$	Boson $\{\mu_s\}$	Fermions $\{\mu_s\}$
$(z)A_1$	1	1	1	$\{3\}$	$\{1\}\{1\}\{1\}$
A_2	1	1	−1	$\{1\}\{1\}\{1\}$	$\{3\}$
$(x,y)E$	2	−1	0	$\{2\}\{1\}$	$\{2\}\{1\}$

B. D_{3h}

	1	$\bar{z}$ rotations $\bar{R}\left(\frac{2\pi}{3}00\right)$	$(\bar{x}\bar{y})$ rotations $\bar{R}(0\pi0)$	Horizontal reflection $\bar{\sigma}_h$ $I\bar{R}(\pi00)$	Rotation inversions $I\bar{R}\left(\frac{\pi}{3}00\right)$	Vertical reflections $\bar{\sigma}_v$ $I\bar{R}(0\pi0)$	Boson $\{\mu_s\}$	Fermions $\{\mu_s\}$
A_1'	1	1	1	1	1	1	$\{3\}$	$\{1\}\{1\}\{1\}$
$(J_z)A_2'$	1	1	−1	1	1	−1	$\{1\}\{1\}\{1\}$	$\{3\}$
$(x,y)E'$	2	−1	0	2	−1	0	$\{2\}\{1\}$	$\{2\}\{1\}$
A_1''	1	1	1	−1	−1	−1	Excluded	
$(z)A_2''$	1	1	−1	−1	−1	1		
$(J_xJ_y)E''$	2	−1	0	−2	1	0		

if at all. On the right (D_{3h}) side we envision a molecule in which the central atom oscillates quite freely through the molecular plane. In fact we picture the first z rovibrations with $A=A_2''$ to have much higher energies than the unexcited $A=A_1'$ states.

Now each (A) rovibrational manifold is made according to the usual "(ABC) method" outlined in preceding sections. We first write down all C in $A\otimes B$ for allowed bare rotor B. Then we draw the appropriate J^p levels from the Cth column of Table XI above each C in Fig. 32. The new trick here is to correlate nearly degenerate states (J^+,J^-) in the A_1 manifold of the C_{3v} structure with those D_{3h} vibronic states A_1' and A_2'' in the A_1 column of Table XII. These pairs are inversion doublets in NH_3, but correspond to well separated vibronic states in CH_3 or CD_3.

Now an electric dipole component parallel to $\bar{z}$ belongs to IR $D=A_2''$ of D_{3h}, or IR $D=A_1$ of C_{3v} (see Tables X). This will permit a transition $A=A_1'\to A_2''$ in the D_{3h} vibronic label, and $A_1\to A_1$ in the C_{3v} label. ($A_1'\to A_2''$) transitions are indicated in the nomogram in Fig. 33 for CH_3 and CD_3. The levels which are drawn on the axes of the nomogram are plotted using Eq. 3.12 for the symmetric top. The symmetric top quantum numbers K or n are only approximately valid, but good enough to be very useful. In this example we would have $K=n$ since A_1' and A_2'' correspond to $\Lambda=0$. It is interesting to note that n is conserved for all the transitions in Fig. 33 which are allowed by the (ABC) rules.

The statistical weight factors are indicated by line segments at the top of Fig. 33 (D is a spin-1 boson, and H is a spin-$\frac{1}{2}$ fermion). These are computed as follows using Fig. 28.

TABLE XI. Correlation tables. (A) $O_3\downarrow C_{3v}$ and (B) $O_3\downarrow D_{3h}$.

A. $O_3\downarrow C_{3v}$

	A_1	A_2	E
$J^p=0^+$	1	⋯	⋯
0^-	⋯	1	⋯
1^+	⋯	1	1
1^-	1	⋯	1
2^+	1	⋯	2
2^-	⋯	1	2
⋯	⋯	⋯	⋯
⋯	⋯	⋯	⋯

B. $O_3\downarrow D_{3h}$

	A_1'	A_2'	E'	A_1''	A_2''	E''
$J^p=0^+$	1	⋯	⋯	⋯	⋯	⋯
0^-	⋯	⋯	⋯	1	⋯	⋯
1^+	⋯	1	⋯	⋯	⋯	1
1^-	⋯	⋯	1	⋯	1	⋯
2^+	1	⋯	1	⋯	⋯	1
2^-	⋯	⋯	1	1	⋯	1
3^+	⋯	1	1	1	1	1
3^-	1	1	1	⋯	1	1

TABLE XII. $D_{3h}\downarrow C_{3v}$ correlation.

	A_1	A_2	E
A_1'	1	⋯	⋯
A_2'	⋯	1	⋯
E'	⋯	⋯	1
A_1''	⋯	1	⋯
A_2''	1	⋯	⋯
E''	⋯	⋯	1

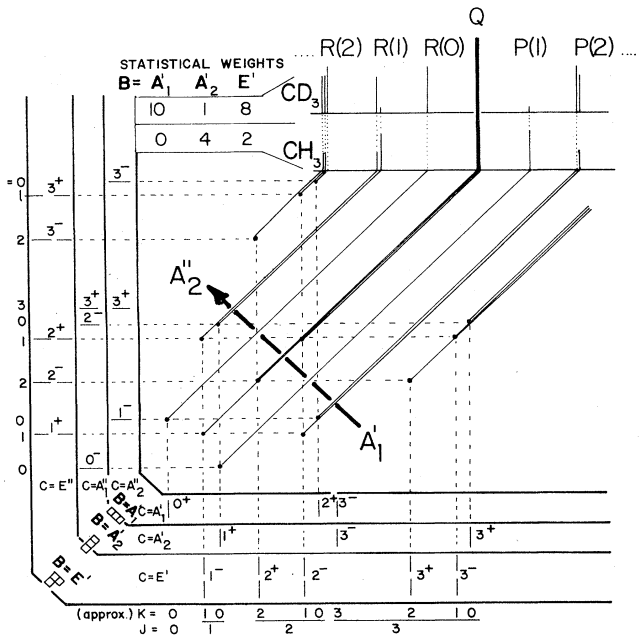

FIG. 33. Electric dipole allowed ($A_1' \rightarrow A_2''$) transitions of CH_3 and CD_3. Transitions may occur between those levels which belong to the same B corridor, but then only between those levels for which the external rules $J^{\pm} \rightarrow J^{\mp}+1, J^{\mp}$, or $J^{\mp}-1$ are satisfied.

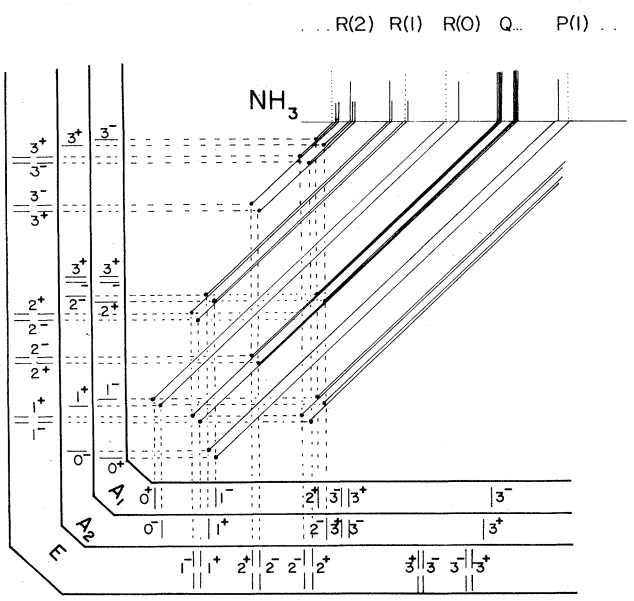

FIG. 34. Electric dipole ($A_1 \rightarrow A_1$) transitions in NH_3. Level ordering was deduced from the two preceding figures. The results clearly show the origin of the observed alteration of intensities in the inversion doubled spectra.

For CD_3 $W_{A_1'} = \dfrac{345}{321} = 10$, $W_{A_2'} = \dfrac{1}{3} = 1$, $W_E = \dfrac{2}{31} = 8$

For CH_3 $W_{A_1'} = \dfrac{0}{3} = 0$, $W_{A_2'} = \dfrac{234}{321} = 4$, $W_{E'} = \dfrac{1}{31} = 2$

Finally, Fig. 34 shows a schematic of the spectral lines which show up in an NH_3 ($A_1 \rightarrow A_1$) transition.

V. ROVIBRONIC MATRIX ELEMENTS AND TRANSITIONS (WEAKLY COUPLED BASES)

A. Spherical top vibrational transitions

Some of the most interesting spectral results in recent years have involved transitions in the "spherical-top" molecules such as SF_6, UF_6, SiF_4, CF_4, and methane (CH_4). Of these, CH_4 has been studied the longest since it has the least rotational inertia and therefore the most easily resolvable rotational structure (Plyler, *et al.* 1960; Hecht, 1960 a and b). Before discussing the fine rotational structure, it is worthwhile to review briefly the angular momentum theory of the spherical top rovibrational states which has been developed for some time (Jahn, 1938; Hecht, 1960a). It is instructive to discuss the structure of the angular momentum bases in the light of the frame transformation relations.

One may couple a lab-defined vibronic wave function $\phi_m^l(\text{lab})$ and a spherical top rotor wave function $\mathfrak{D}_{mn}^N(\alpha\beta\gamma)$ to construct the wave function of a total momentum (J) state as follows:

$$\langle\,|[lN](n)_M^J\rangle = \sum_m C_{M-mmM}^{lNJ}\phi_{M-m}^l(\text{lab})\mathfrak{D}_{mn}^{N*}(\alpha\beta\gamma)\sqrt{[N]}\ . \quad (5.1)$$

This was called a weakly coupled wave function in Sec. III. It is simple to use the procedures given in Sec. III to relate the preceding to BOA wave functions, or internally coupled states.

$$\langle\,|[lN](n)_M^J\rangle = \sum_K C_{\Lambda nK}^{lNJ}\phi_{\Lambda}^l(\text{body})\mathfrak{D}_{MK=n+\Lambda}^{J*}(\alpha\beta\gamma)\sqrt{[N]}$$

The preceeding differs only by a phase $(-1)^{N-J}$ from the wave function

$$\langle\,|[lJ](M)_n^N\rangle = \sum_K C_{\Lambda Kn}^{lJN}(-1)^{\Lambda}\phi_{-\Lambda}^l(\text{body})\mathfrak{D}_{MK=n-\Lambda}^{J*}(\alpha\beta\gamma)\sqrt{[J]} \quad (5.2)$$

If the rotor really had R_3 symmetry then one could choose

the internal (ABC) quantum labels to be $A = l^*$, $B = N$, and $C = J$. Then the preceding wave function would have practically the same form as the general BOA-constricted state given in Eq. 3.19. In other words, *for a rigid spherical top the weakly-coupled and BOA-constricted states are the same*, except for an overall phase.

However, a CH_4 molecule is not a rigid ball, but a deformable tetrahedral configuration. BOA-constricted states will be labeled by A, B, and C equal to T_d IR, not those of R_3. In general BOA-constricted states will be quite different from weakly coupled states for which N is still a good quantum number. (This was demonstrated in Sec. III.B.2. where it was shown that for either set of states we can still count on J^p and B to be good labels.) So the question remains, which will be a more convenient basis for starting CH_4 rovibronic problems?

In order to analyze the fundamental dipole allowed vibrations ($l = 1, F_2$), Hecht chose wave functions which are virtually identical to the ones given in Eq. 5.2. He used these as a basis for a very thorough analysis of the CH_4 rovibrational lines observed by Plyler. The same sort of analysis has been carried out recently for SF_6 (Fox *et al.*, 1976). Among other things these analyses show that generally states with different N are mixed only slightly. Apparently then the weakly-coupled states are a better starting point for spherical top vector ($l = 1$) vibration analysis than BOA-constricted ones.

It may be that the $l = 2, 3, \ldots$ rotonic or rovibronic lines of CH_4 will be analyzed better starting from the BOA-constricted bases. (We are assuming that such lines can be resolved somehow.) For now we shall restrict our attention to the weakly coupled bases only.

One advantage of the weakly coupled bases is that the powerful Wigner–Racah algebra (Fano and Racah, 1959) can be used to express the matrix elements in terms of angular momentum $3nj$ coefficients or R_3 Racah coefficients. Formulas and tables exist for these coefficients and so they are easier to evaluate than the corresponding point symmetry Racah coefficients which turned up in the BOA basis calculations. Another advantage is that one may use either of two forms $|[lN]J\rangle$ (Eq. 5.1) or $|[lJ]N\rangle$ (Eq. 5.2) for the base states. The first is more convenient for treating lab-defined "external" operators, while the second form is convenient for treating body-defined "internal" operators.

The analysis by Hecht (1960 a) of the internal vibration–rotation operators uses the second form. From the Wigner-Eckart theorem he obtains

$$\langle [l'J']^{N'}_{n'} \| [\bar{\mathbf{V}}^{k_1}(\text{vib}) \times \bar{\mathbf{V}}^{k_2}(\text{rot})]^{k}_{r} \| [lJ]^{N}_{n} \rangle = C^{kNN'}_{rnn'} \langle |l'J'] N' \| [k_1 k_2]k \| [lJ]N \rangle . \tag{5.3a}$$

The reduced matrix element is obtained by applying Racah algebra to the internally coupled states

$$\langle [l'J']N' \| [k_1k_2]k \| [lJ]N \rangle = ([l'][J'][N][k])^{1/2} \begin{Bmatrix} k_1 & k_2 & k \\ l & J & N \\ l' & J' & N' \end{Bmatrix} \langle l' \| \bar{\mathbf{V}}^{k_1}(\text{vib}) \| l \rangle \langle J' \| \bar{\mathbf{V}}^{k_2}(\text{rot}) \| J \rangle . \tag{5.3b}$$

Some examples of these operators will be discussed in Sec. III.V.C.

For external operators such as lab-fixed radiation fields, it is more convenient to use the states $|[lN]J\rangle$ which are coupled in terms of the external quantum numbers. Then standard Racah algebra gives the following matrix element:

$$\langle [l'N']^{J'}_{M'} | [\bar{\mathbf{V}}^{k_1}(\text{vib}) \times \bar{\mathbf{V}}^{k_2}(\text{rot})]^{k}_{r} | [lN]^{J}_{M} \rangle = C^{kJJ'}_{rMM'} \langle [l'N']J' \| [k_1k_2]k \| [lN]J \rangle ,$$

where

$$\langle [l'N']J' \| [k_1k_2]k \| [lN]J \rangle = ([l'][N'][J][k])^{1/2} \begin{Bmatrix} k_1 & k_2 & k \\ l & N & J \\ l' & N' & J' \end{Bmatrix} \langle l' \| v^{k_1}(\text{vib}) \| l \rangle \langle N' \| v^{k_2}(\text{rot}) \| N \rangle . \tag{5.4}$$

For an example of this formula consider the vibrational dipole transition operator $[v^1(\text{vib}) \times v^0(\text{rot})]^{k=1}_{r}$ acting between vibrationally unexcited states $|[l = 0N]J = N\rangle$, and singly excited states $|[l = 1N]J\rangle$. The 9-j coefficient in the resulting reduced matrix element

$$\langle [1N']J' \| [10]1 \| [0N]J = N \rangle = 3([N][J])^{1/2} \begin{Bmatrix} 1 & 0 & 1 \\ 0 & N & N \\ 1 & N' & J' \end{Bmatrix} \langle 1 \| \bar{\mathbf{V}}^1(\text{vib}) \| 0 \rangle \langle N' \| \bar{\mathbf{V}}^0(\text{rot}) \| N \rangle$$

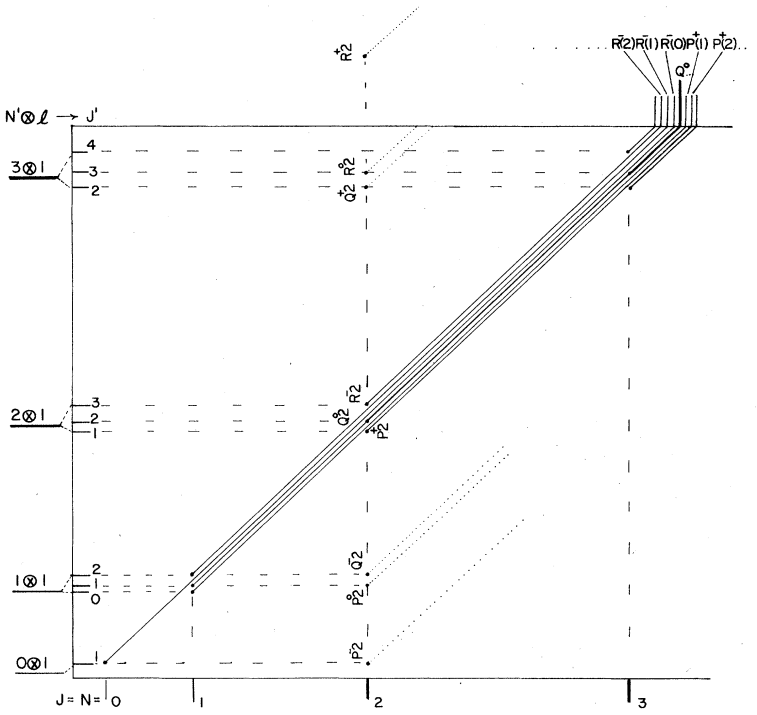

FIG. 35. Rough sketch of ($l=0\rightarrow1$) rovibrational dipole transitions in spherical-top molecules. "Allowed" transitions which do not change rotor momentum N are indicated by slanted solid lines. The "forbidden" transitions starting from $N=2$ are indicated by slanted dotted lines.

can be evaluated immediately to give

$$\begin{Bmatrix} 1 & 0 & 1 \\ 0 & N & N \\ 1 & N' & J' \end{Bmatrix} = \delta_{N,N'}\{NJ'1\}/3[N]. \tag{5.5}$$

where

$$\{NJ'1\} = \begin{cases} 1 \text{ if } J' = N-1, N, \text{ or } N+1 \\ 0 \text{ otherwise.} \end{cases}$$

This gives the simplest spherical top dipole selection rule: N remains unchanged while J may change by one unit at the most. If N eigenstates are energy eigenstates, too, then spectral analysis is much simpler.

First to gain a rough picture of the spectra, we show along the y-axis of Fig. 35 the weakly-coupled rovibrational levels. These are plotted using the diagonal components of the first perturbation term $H_1' = -2B\xi\,\bar{\mathrm{J}}\cdot\bar{\mathrm{L}}$ in Hecht's Hamiltonian. These components are given by

$$-B\xi\bar{\mathbf{J}}\cdot\bar{\mathbf{L}} = -B\xi[J'(J'+1) - N'(N'+1) + l(l+1)]$$

$$= \begin{cases} -2B\xi[N'+2] \text{ for } J = N'+1 \\ -2B\xi \text{ for } J = N' \\ -2B\xi[-N'+1] \text{ for } J = N'-1\,, \end{cases} \tag{5.6}$$

where the vibrational momentum l is assumed to be unity ($l=1$) for the dipole-active fundamentals. The x axis of Fig. 35 shows the pure rotational levels of the ground state according to the symmetric top energy formula

$$E_N = BN(N+1).$$

The levels in the figure are drawn in units of B. We take $\xi = -0.1$ which is more or less the value of the Coriolis constant found in the experiments.

If we only consider those transitions for which the rotor momentum N is conserved, we obtain a spectrum of the simple form shown on the top of Fig. 35 which is quite like that of the diatomic rotor (recall Fig. 30). Apparently the transitions which change N are quite weak in CH_4, and have not been found in SF_6.

Now an interesting part of the spectrum for either of these molecules comes in the form of the fine structure of each of the lines $P(N)$, $R(N)$ and even $Q(N)$ which can be resolved. We shall review the structure of the $P(7)$ lines of CH_4 as an example in the following section.

B. Labeling fine structure of XY_4 molecules

The internal symmetry of the CH_4 rotor is known to be tetrahedral (T_d). The character table of T_d shown in Table XIII is exactly the same as that of the cubic octahedral group O, since the last two classes $\mathbf{I}\cdot\mathbf{R}(\frac{\pi}{2}00)$ $\mathbf{I}\cdot\mathbf{R}(\frac{\pi}{2}\frac{\pi}{2}\frac{\pi}{2})$ of T_d are just the same operators in O multiplied by inversion $\mathbf{I}$.

The correlation of T_d IR with O_3 IR may be computed using character theory. Table XIV gives the results for $J \leq 7$. Let us first determine the pure rotational levels with $N=7$. The levels listed in Fig. 36 according to T_d bare rotor labels (B) are consistent with 7^+ entries in Table XIV. However, the ordering and qualitative spacing may be determined using the cubic "wheels" in Fig. 8 as we will explain shortly. The thing to notice first is that for each 7^+ level there is drawn a degenerate partner with 7^-. This is analogous to the NH_3 levels when the inversion frequency goes to zero as shown on the left of Fig. 32.

TABLE XIII. T_d characters and symmetry.

T_d	1	$R(\frac{2\pi}{3})$	$R(\pi 00)$	$IR(\frac{\pi}{2}00)$	$IR(\frac{\pi}{2}\frac{\pi}{2}\frac{\pi}{2})$	Boson $\{\mu_s\}$	Fermion $\{\mu_s\}$
A_1	1	1	1	1	1	{4}	{1}{1}{1}{1}
A_2	1	1	1	−1	−1	{1}{1}{1}{1}	{4}
E	2	−1	2	0	0	{2}{2}	{2}{2}
$(L_xL_yL_z)F_1$	3	0	−1	1	−1	{2}{1}{1}	{3}{1}
$(xyz)F_2$	3	0	−1	−1	1	{3}{1}	{2}{1}{1}{1}

The IR B^I of an inversion partner for a given state B will be that IR which gives the opposite sign for all operations that contain the inversion I. (Remember that I commutes with all rotations.) Glancing at the T_d character table we see that the partner of an A_1 is an A_2, the partner of an F_1 is an F_2, and the partner of an E is another E.

If any *single* pair of H atoms in CH_4 were to trade places with some frequency ν_I then there would be a splitting of these inversion partners by an energy proportional to $h\nu_I$. Note however, that only one type of CH_4 pair in Fig. 36 has both partners with non-zero statistical weight, namely the E pair. For CD_4 the F_1 and F_2 pair could show up, too, but if they did, F_2 would "outweigh" F_1 by a factor of five.

The fact that "extra" lines have not shown up for the lowest transitions of CH_4 indicates that the operations in T_d with inversion attached do not happen very often to the molecule. There have been some experimental results which have been conjectured to be inversion doubling. However, Hougen explained these without needing inversion (Hougen, 1971).

Now it is interesting to compare the labeling of Fig. 36 with that of Hougen (1975). In the latter "nonfeasible" operations which include inversion are treated differently when applied to the bare rotor. The rotational part of the operation is done, but the inversion is left undone. In other words, T_d operations become O operations as far as the rotor is concerned.

Furthermore, Hougen only considers the T_d IR that correlate with J^+. For $J^+=7^+$ there will be the following T_d IR from Table XIV.

$$7^+ \rightarrow A_2+E+F_1+F_1+F_2+F_2. \tag{5.7}$$

Hougen's assignment of CH_4 statistical weights is 5 for both A_1 and A_2, 3 for both F_1 and F_2, and 2 for E. (For CD_4: 15 for $A_{1,2}$, 18 for $F_{1,2}$, and 12 for E.)

Now we can see how to convert back and forth between labeling of Fig. 36 and that of Hougen. They both give exactly the same thing *if the XY_4 structure does not "invert"*. For $(7^+, B=A_2)$ and $(7^-, B=A_1)$ read A_2 in Eq. (5.7) with total weight of $5+0=5$ in CH_4, and $0+15=15$ for CD_4. For $(7^+, B=F_1)$ and $(7^-, B=F_2)$ read F_1 in Eq. (5.7) with a total weight of $3+0=3$ for CH_4, and $3+15=18$ for CD_4. For $(7^+, E)$ and $(7^-, E)$ read E in Eq. (5.7) with a total weight of $1+1=2$ in CH_4 and $6+6=12$ in CD_4.

One advantage of standard T_d labeling is that we can use the cubic "wheel" in Fig. 8 immediately to order the fine structure levels. This is because one is really labeling (O) operations. Looking up at $J=7$ we have

$$J=7 \rightarrow \underbrace{(T_1+E+T_2)}+A_2+\underbrace{(T_2+T_1)} \tag{5.8}$$

Cluster: $K_3=7\rightarrow(1_3)$ $K_4=7\rightarrow(3_4)$

This is the observed ordering in CH_4. The three-fold axes of the tetrahedron are "hardest" so the (1_3) cluster is the highest in the CH_4 vibrational ground states. (The

TABLE XIV. $O_3 \downarrow T_d$ correlation.

	A_1	A_2	E	F_1	F_2		A_2	A_1	E	F_2	F_1
$J^p=0^+$	1	···	···	···	···	0^-	1	···	···	···	···
1^+	···	···	···	1	···	1^-	···	···	···	1	···
2^+	···	···	1	···	1	2^-	···	···	1	···	1
3^+	···	1	···	1	1	3^-	···	1	···	1	1
4^+	1	···	1	1	1	4^-	1	···	1	1	1
5^+	···	···	1	2	1	5^-	···	···	1	2	1
6^+	1	1	1	1	2	6^-	1	1	1	1	2
7^+	···	1	1	2	2	7^-	···	1	1	2	2

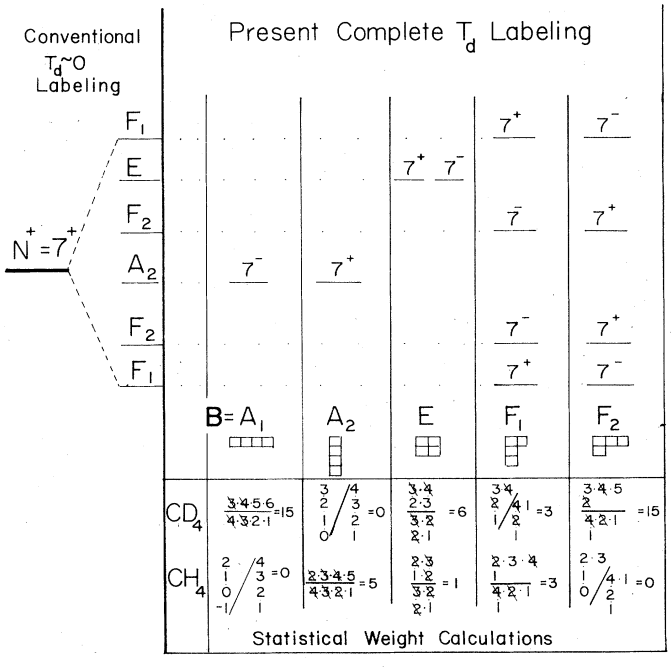

FIG. 36. Comparison of conventional CH_4 labeling with present labeling. The latter shows clearly the "hidden" structure of inversion doublets which has a structure very much like that of NH_3. For CH_4, however, only the E levels are actually double according to the statistical weight calculations.

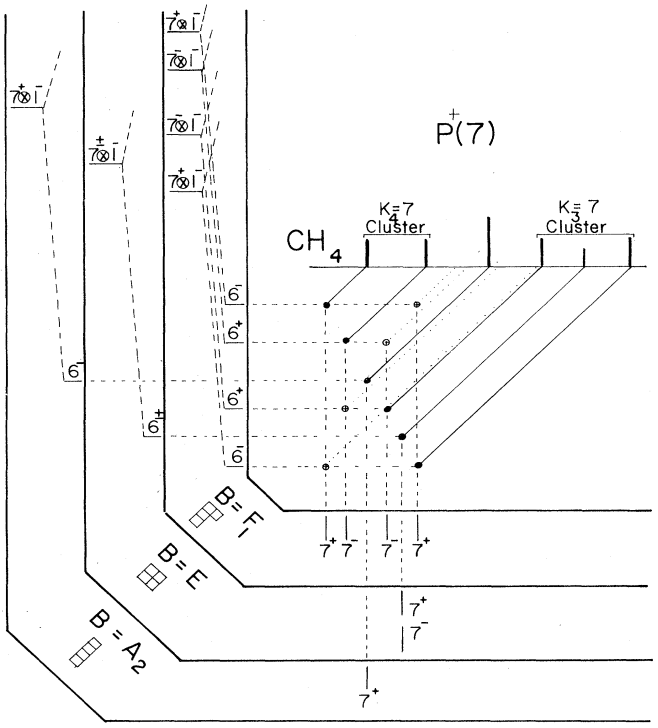

FIG. 37. The $P^+(7)$ fine structure for CH_4. The transitions allowed by internal ($B \rightarrow B$) and external ($7^{\pm} \rightarrow 6^{\mp}$) selection rules are indicated by small circles. However, the open circles belong to very weak or unobserved lines. They represent transitions between different clusters or axes of the rotor.

splitting of the ground levels is exaggerated in Fig. 37).

It has been stated that the main advantage of the older labeling is that it gives less information, i.e. it ignores inversions which do not happen. The problem is, however, that this "advantage" brings with it more work and less elegance. It is better to use a well developed mathematics like O_3 representation theory without adding artificial constraints.

This is particularly clear when it comes to deriving selection rules. Fig. 37 shows a nomogram of the strongest $P(7)$ lines of CH_4 for which N is conserved. [These are called $P^+(7)$. The $P^0(7)(N'=6)$ and $P^-(7)(N'=5)$ lines may be treated similarly.] Now, we have proved that the B labels at the vertex or origin of the nomogram must be strictly conserved. However, Hougen's rovibronic labels are generally changed during optical transitions.

We consider the electric dipole transitions in Fig. 37. The dipole is labeled $k^q = 1^-$ so the external selection rules are $J^p = 7^{\pm} \rightarrow J'^{p'} = 6^{\mp}$, $7^{\mp}$, or $8^{\mp}$. We draw only $7^{\pm} \rightarrow 6^{\mp}$ transitions ($P(7)$) which conserve B. Comparison of the possible lines with experimental spectra shows that there is an additional conservation or selection rule in effect. This rule is approximate but nevertheless extremely important. It states that transitions between *different clusters* like $(B = F_1, N^p = J^p = 7^+(1_3)) \rightarrow (B = F_1, N^p = 7^+(3_4), l = 1^-, J^p = 6^-)$ are forbidden or at least very weak. The fine structure spectra that one observes finally in CH_4 and SF_6 ends up looking like the level diagram of the ground state manifolds even for small J.

It is probably possible to put the cluster selection rule in a quantitative form now that analytic expressions for cluster eigenvalues and eigenvectors exist. Each cluster is labeled by an internal angular momentum component $K = n$. In this respect the labeling situation is like that of CH_3 or CD_3 treated in the preceding example. There each A_1, A_2, or E state was still made mostly from a single K state of the fictitious symmetric top. However the spherical top K states differ from those of the symmetric top. Spherical top K_n may be defined with respect to first one, then another symmetry axis. (The symmetric top K is always the $\bar{z}$ component.) It would be interesting to predict the breaking of the cluster "selection rules" in regions where threefold clusters are melting into fourfold ones, or in transitions for which N changes.

Additional qualitative problems remain which might be understood using simple physical and symmetry arguments. One would hope that it would be possible to derive the sign and order of magnitude of some of the Coriolis and centrifugal parameters outside of an exhaustive numerical calculation. It is difficult to visualize why ξ comes out small and negative in the CH_4 analyses given so far, and why the fine structure patterns invert in the excited vibrational states.

C. Further applications of cluster bases

Calculations of vibronic structure of spherical tops can become laborious even for fundamental ($l = 1$) vibrations. Since one is starting with a $(6J+3) \times (6J+3)$ Hamiltonian matrix the problem at higher and higher J gets worse quickly. However, it is likely that most of the high J spectral analysis can be done more easily using the cluster bases introduced in Sec. II.2, 3, and 4. If so, then the matrix that needs to be solved for ($l = 1$) is only 3×3. Furthermore, the results would be given analytically and be understood physically.

Let us assume the extreme case of degenerate cluster states, i.e., let the splitting or tunneling factors in Sec. II.A.3 vanish. Then states $|^N_{n=K_3}\rangle$ or $|^N_{n=K_4}\rangle$ are rotor eigenstates. The rotor is stuck rotating, on one axis; either a threefold or a fourfold axis, with high total momentum N and high axis component $n = (K_3 \text{ or } K_4) = N, N-1, N-2, \ldots$ One may forget the spherical or cubic symmetry of the rotor and assume it has cylindrical or axial symmetry due to the dominant centrifugal distortion. Clearly, vibronic states of the "not-so-spherical-top" assume the same form as those for the symmetric molecule in Sec. III.A. The weakly coupled wave functions will have the form

$$\left\langle \left| lN(n=K_{3,4})^J_M \right\rangle = \sum_m C^{l\,N\,J}_{M-m\,m\,M} Y^l_{M-m}(\theta\phi) \mathfrak{D}^N_{mn=K_{3,4}}(\alpha\beta\gamma)\,, \right. \tag{5.9}$$

and be related to the BOA functions

$$\left\langle \left| \mathrm{BOA}^{\,l}_{\Lambda}(n=K_{3,4})^J_M \right\rangle = Y^l_{\Lambda}(\bar{\theta}\bar{\phi})\, \mathfrak{D}^{\,J}_{MK=\Lambda+n}(\alpha\beta\gamma)\,, \right. \tag{5.10}$$

by the relation derived in Sec. III.A

$$\left| lN(n)^J_M \right\rangle = \sum_{\Lambda} \left(\frac{[N]}{[J]}\right)^{1/2} C^{lNJ}_{\Lambda n K=\Lambda+n} \left| \mathrm{BOA}^{\,l}_{\Lambda}(n)^J_M \right\rangle . \tag{5.11}$$

The tranformation for the $l=1$ case is given by the following orthogonal matrix

$$\langle \text{BOA}|\text{weak coupling}\rangle = \begin{array}{c} \\ \langle\Pi_{(\Lambda=1)}| \\ \langle\Sigma_{(\Lambda=0)}| \\ \langle\Pi_{(\Lambda=-1)}| \end{array} \begin{array}{c} \begin{array}{ccc} |N=J-1\rangle & |N=J\rangle & |N=J+1\rangle \end{array} \\ \begin{bmatrix} \left(\frac{(J+n)(J+n+1)}{2J(2J+1)}\right)^{1/2} & \left(\frac{(J-n)(J+n+1)}{2J(J+1)}\right)^{1/2} & \left(\frac{(J-n)(J-n+1)}{(2J+2)(2J+1)}\right)^{1/2} \\ \left(\frac{(J+n)(J-n)}{J(2J+1)}\right)^{1/2} & \frac{-n}{[J(J+1)]^{1/2}} & -\left(\frac{(J+n+1)(J-n+1)}{(J+1)(2J+1)}\right)^{1/2} \\ \left(\frac{(J-n)(J-n+1)}{2J(2J+1)}\right)^{1/2} & -\left(\frac{(J+n)(J-n+1)}{2J(J+1)}\right)^{1/2} & \left(\frac{(J+n)(J+n+1)}{(2J+2)(2J+1)}\right)^{1/2} \end{bmatrix} \end{array} . \tag{5.12}$$

Note that as J and n become larger, the difference between BOA and weakly coupled states diminishes. For example consider $J=30$. For $n=31$ there is no difference since only one state is possible

$$\langle \text{BOA}|\text{weak coupling}\rangle_{(J=30,\,n=31)} = \begin{array}{c} \\ \langle\Pi_{(\Lambda=-1)}| \end{array} \begin{array}{c} |N=31\rangle \\ \begin{bmatrix} 0 & 0 & 0 \\ 0 & 0 & 0 \\ 0 & 0 & 1 \end{bmatrix} \end{array} .$$

For $n=30$ there are two states but off-diagonal components are small.

$$\langle \text{BOA}|\text{weak coupling}\rangle_{(J=30,\,n=30)} \begin{array}{c} \\ \langle\Sigma_{(\Lambda=0)}| \\ \langle\Pi_{(\Lambda=-1)}| \end{array} \begin{array}{c} \begin{array}{ccc} |N=30\rangle & |N=31\rangle \end{array} \\ \begin{bmatrix} 0 & 0 & 0 \\ 0 & -0.984 & -0.180 \\ 0 & -0.180 & -0.984 \end{bmatrix} \end{array} .$$

For $n=29$ or less three states are present

$$\langle \text{BOA}|\text{weak coupling}\rangle_{(J=30,\,n=29)} = \begin{array}{c} \\ \langle\Pi_{(\Lambda=1)}| \\ \langle\Sigma_{(\Lambda=0)}| \\ \langle\Pi_{(\Lambda=-1)}| \end{array} \begin{array}{c} \begin{array}{ccc} |N=29\rangle & |N=30\rangle & |N=31\rangle \end{array} \\ \begin{bmatrix} 0.992 & 0.180 & 0.023 \\ 0.180 & -0.951 & -0.252 \\ 0.023 & -0.252 & 0.967 \end{bmatrix} \end{array} .$$

The off-diagonal components increase as n decreases for a given J.

The $(l=1)$ vibrational problem in the degenerate cluster approximation reduces to finding for given J and n what combinations of $|N=J-1\rangle$, $|N=J\rangle$, and $|N=J+1\rangle$, or else $|\Pi_{(\Lambda=1)}\rangle$, $|\Sigma_{(\Lambda=0)}\rangle$, and $|\Pi_{(\Lambda=-1)}\rangle$ are eigenvectors of the centrifugal-coriolis Hamiltonian. In this way we may learn to what extent the vibration has "settled into" the internal rotation axis, i.e., to what extent the BOA label Λ is a good quantum number. It has been conventional to set up the Hamiltonian in the weak coupling (good N) basis, We shall briefly sketch the procedure given by Hecht (1960) for obtaining the matrix elements needed here.

Hecht considers several cubically symmetric combinations of tensors $[\overline{V}^{k_1}(\text{vib})\times V^{k_2}(\text{rot})]^k$ of order $k=4$ or less. The most important $(k=4)$ operator for the vibrationally excited state involves $[\overline{V}^2\times\overline{V}^2]^4$ and is roughly equivalent to $L_y^2J_x^2+L_x^2J_z^2+L_z^2J_y^2$. This is responsible for most of the cluster splitting that is observed in the excited $(l=1)$ states. Contributions from operators of the form $[\overline{V}^0\times V^4]^4$, i.e., $J_x^4+J_y^4+J_z^4$ are initially less important but grow more rapidly with increase of J.

The evaluation of these operators in the weak coupling basis begins with Eq. 5.3 where the $k=4$ coupling coefficients have been given already by Eqs. 2.48, 49, and 50. The reduced matrix elements are

$$\langle [lJ]N'\,\|[k_1k_2]4\,\|[lJ]N\rangle = 3([l][J][N])^{1/2}\begin{Bmatrix} k_1 & k_2 & 4 \\ l & J & N \\ l & J & N' \end{Bmatrix}\langle l\,\|\overline{V}^{k_1}(\text{vib})\,\|l\rangle\langle J\,\|\overline{V}^{k_2}(\text{rot})\,\|J\rangle . \tag{5.13}$$

The reduced matrix factors can be evaluated further using Racah algebra. For example, given that $\langle J\,\|\mathbf{J}^1\,\|J\rangle = (j(j+1))^{1/2}$ and assuming that $\overline{\mathbf{V}}^2(\text{rot})=[\mathbf{J}^1\times\mathbf{J}^1]^2$, $\overline{V}^3(\text{rot})=[\overline{\mathbf{V}}^2(\text{rot})\times\mathbf{J}^1]^3$, etc. we may use the formula

$$\langle J\,\|[k_1k_2]^k\,\|J'\rangle = (-1)^{k_1+k_2}\sum_{J''}([k][J''])^{1/2}\begin{Bmatrix} k_1 & k_2 & k \\ J' & J & J'' \end{Bmatrix} \times\langle J\,\|k_1\,\|J''\rangle\langle J''\,\|k_2\,\|J'\rangle$$

(Rotenberg *et al.*, 1959) recursively. For example we have

$$\langle J\,\|[J^1\times J^1]^2\,\|J\rangle = ([2][J])^{1/2}\begin{Bmatrix} J & J & 2 \\ 1 & 1 & J \end{Bmatrix}(\langle J\,\|J^1\,\|J\rangle)^2 = [(2J+3)(2J+2)2J(2J-1)/24]^{1/2} .$$

The 9-j symbols can be reduced for most of the cases

to 6-j symbols and expressed as polynomials. For $l=1$, $k_1=0$, and $k_2=k=4$ the 9j coefficient in Eq. 5.13 is

$$\begin{Bmatrix} 0 & 4 & 4 \\ 1 & J & N \\ 1 & J & N' \end{Bmatrix} = (-1)^{J+N+1} \begin{Bmatrix} 4 & N' & N \\ 1 & J & J \end{Bmatrix} \Big/ (3[k])^{1/2},$$

while $l=1$, $k_1=2=k_2$, and $k=4$ one has

$$\begin{Bmatrix} 2 & 2 & 4 \\ 1 & J & N \\ 1 & J & N' \end{Bmatrix} = \left(\frac{7}{5}\right)^{1/2} \begin{Bmatrix} N' & J & 3 \\ 1 & 4 & N \end{Bmatrix} \begin{Bmatrix} J & J & 2 \\ 1 & 3 & N' \end{Bmatrix}.$$

Each of these 6-j coefficients is a different rational root of polynomials in J [see for example Rotenberg (1959, pp. 18–19) for different values of $(N', N) = J-1$, J, and $J+1$.]

For 3×3 Hamiltonian in the degenerate cluster basis we need only the matrix elements

$$\langle N' \left| [\bar{\nabla}^{k_1} \times \bar{\nabla}^{k_2}] \right|^k_0 | N \rangle = C^{kNN'}_{0nn} \langle N' \| [k_1 k_2] k \| N \rangle$$

if we ignore mixing of different clusters, i.e., different n. In this case there is considerable cancellation between the $(k=4)$ coupling coefficient and reduced matrix elements, and so these Hamiltonian components are much simpler than the factors that produce them. Additional scalar terms evaluated by Hecht including the term $-2B\xi \bar{J}\cdot\bar{L}$ which gives the zeroth order diagonal values (recall Fig. 35) must be included in the Hamiltonian matrix.

Approximate Hamiltonians constructed according to the degenerate cluster approximation are being tested for a wide range of spherical tops and (J, n) cluster lines. First the mathematical accuracy of the approximation must be checked using results obtained by *tour de force* diagonalization. The behavior of the spectrum as various terms are increased or decreased must be understood. We speculate that whenever an approximate model plot shows two clusters crossing, the true spectrum will exhibit "super level crossing" the shared (B) components mix with each other. Several interesting effects will probably be found when cluster bases are examined in detail.

VI. CONCLUSION AND POSSIBLE FUTURE DEVELOPMENTS

One logical extension of the theory given in the preceeding will be the development of a whole network of transformations between all the various Hund's cases and sub-cases for molecular electronic coupling. The generalization of the Fano-Chang transformation which we developed takes us from Hund's case (a) to case (d), if we choose to ignore electron spin.

Indeed, we have not said much about electron spin, or about any half-integral representations of rotation or their relation to molecular symmetry species. In the past this topic has generally meant having to deal with double group representations. This often meant double trouble both for computing and for visualizing the physical problem.

However, a new approach to group representations in general can be made which is based upon some old ideas found by Hamilton (Harter and dos Santos, 1978). One advantage of this approach is that integral spin and half-integral spin representations are treated on a nearly equal footing. If anything, the mathematics of the latter actually becomes simpler than ordinary representation theory was before. We show some results of this approach by giving in Fig. 38 the half-integral equivalents to the symmetry reduction wheels of Figs. 6 and 8.

This type of wheel and the theory behind it will be useful whenever a constricted rotor (C) label or vibronic activity (A) label is to be related to a half-integral angular momentum. It is hard to see exactly where this will come up in the theory of symmetric polyatomic molecules. It is possible that electron spin orbit interaction may be strong in an odd electron radical or ion, or in some disassociation process. Nevertheless, our procedures for separating the internal molecular excitations into well defined (A), (B), and (C) parts will be directly applicable whenever it becomes necessary to relate any of them to any externally defined angular momentum states.

Finally, we mention the interesting problem of what happens to the "soul" (B, $\{u\}$) of a molecule when it "dies" i.e., when it disassociates in some way. We conjecture that it stays around long enough to be useful in predicting the distribution of "sub souls" amongst any of the symmetric daughter molecules or radicals. The problem is quite analogous to that of fast disassociation, or more correctly, ionization of atoms in x-ray photoelectron spectroscopy (XPS or ESCA). There, if an atom is not given time to readjust from one electronic tableau state to another, then the tableau algorithms can be used directly to predict the distribution of states amongst the stripped or ionized atoms. The tableau label $\{u\}$ describes the permutational symmetry of the identical particle wavefunction of the rotor, and this will be conserved as long as the spin rotation interaction is small. Using tableau algorithms (Harter, 1973, Harter and Patterson, 1976a and b), it is a simple matter to express n-particle tableau states in terms of $(n-1)$-

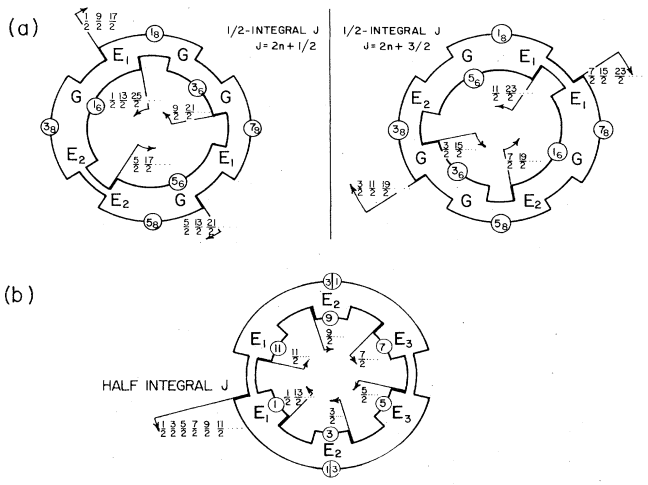

FIG. 38. Progressions of symmetry species in J-angular momentum levels. (Half-integral J). (a) cubic-octahedral symmetry. (b) Hexagonal symmetry.

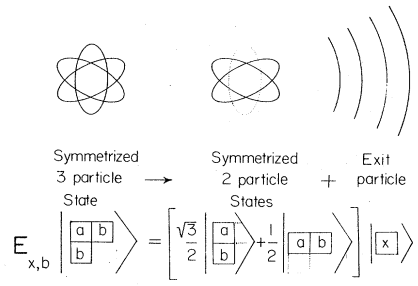

FIG. 39. Unitary tableau representation of fast-ionization or dissociation. Unitary "destruction-creation" operator $E_{x,b} \sim a_x^\dagger a_b$ converts an n-particle tableau state into a combination of $(n-1)$-particle tableau states with the nth particle removed. Combination coefficients give the relative amplitudes for the states left behind.

particle tableau states as indicated in Fig. 39, for an $(n=3)$ example.

For symmetric molecules we have indicated that the tableau "soul" label is much better than its atomic equivalent since nuclear spin-rotation interactions are much smaller than the analogous atomic spin-orbit coupling. In short, this label promises at least as many applications and developments as its religious namesake.

ACKNOWLEDGMENTS

We thank Drs. Paul Engelking, James Berquist, and Ken Evenson for suggesting pedagogical improvements of the manuscript. We thank Dr. Ch. Jungen for several interesting suggestions concerning the interpretation of symmetric top level structure. We thank Dr. Phil Bunker for carefully reading the manuscript and correcting some errors in the text and references. Finally we thank Dr. R. S. McDowell and coworkers for making their recent results available to us.

APPENDIX A. MOLECULAR ISOSCALAR FACTORS

Coupling the electron and rotor angular momentum states, we find

$$\sum_{m'n} C^{lNJ}_{m'nM'} \left|\begin{matrix} l \\ m' \end{matrix}\right\rangle \left|\begin{matrix} N \\ n \end{matrix}\right\rangle = \left|\begin{matrix} J \\ M' \end{matrix}\right\rangle . \tag{A1}$$

We now use the crystal field transformation coefficients to expand each angular momentum state as a linear combination of internal finite symmetry states of group $\bar{\mathcal{G}}$. For example, we have

$$\left|\begin{matrix} l \\ m' \end{matrix}\right\rangle = \sum_{Aa} \begin{pmatrix} A \\ a \end{pmatrix} \begin{matrix} l \\ m' \end{matrix} \left|{}^{A}_{a}(l)\right\rangle , \tag{A2}$$

where the parentage of the finite symmetry states are noted in parentheses. From these two expressions we find

$$\sum_{\substack{AB \\ ab}} \sum_{m'n} C^{lNJ}_{m'nM'} \begin{pmatrix} A \\ a \end{pmatrix} \begin{matrix} l \\ m' \end{matrix} \begin{pmatrix} B \\ b \end{pmatrix} \begin{matrix} N \\ n \end{matrix} \left|{}^{A}_{a}(l)\right\rangle \left|{}^{B}_{b}(N)\right\rangle = \sum_{Cc} \begin{pmatrix} C \\ c \end{pmatrix} \begin{matrix} J \\ M \end{matrix} \left|{}^{C}_{c}(J)\right\rangle . \tag{A3}$$

Writing $\left|{}^{A}_{a}(l)\right\rangle \left|{}^{B}_{b}(N)\right\rangle$ as $\left|{}^{A}_{a}(l){}^{B}_{b}(N)\right\rangle$ and using Eq. (2.36b), we find

$$\sum_{m'nM'} C^{lNJ}_{m'nM'} \begin{pmatrix} A \\ a \end{pmatrix} \begin{matrix} l \\ m' \end{matrix} \begin{pmatrix} B \\ b \end{pmatrix} \begin{matrix} N \\ n \end{matrix} \begin{pmatrix} J \\ M' \end{pmatrix} \begin{matrix} C \\ c \end{matrix} = \left\langle {}^{A}_{a}(l){}^{B}_{b}(N) \middle| {}^{C}_{c}(J) \right\rangle . \tag{A4}$$

The scalar product on the right of Eq. (A3) can be analyzed using group elements $\bar{g}$ of $\bar{\mathcal{G}}$. Thus,

$$\left\langle {}^{A}_{a}(l){}^{B}_{b}(N) \middle| {}^{C}_{c}(J) \right\rangle = \left\langle {}^{A}_{a}(l){}^{B}_{b}(N) \middle| \bar{g}^\dagger \bar{g} \middle| {}^{C}_{c}(J) \right\rangle = \sum_{a'b'c'} \mathfrak{D}^{A}_{a'a}{}^{*}(g) \mathfrak{D}^{B}_{b'b}{}^{*}(g) \mathfrak{D}^{C}_{c'c}(g) \times \left\langle {}^{A}_{a'}(l){}^{B}_{b'}(N) \middle| {}^{C}_{c'}(N) \right\rangle$$

Since Eq. (A5) is independent of $\bar{g}$, we may sum over all group elements $\bar{g}$ and divide by the order of the group ${}^{\circ}\mathcal{G}$.

$$\left\langle {}^{A}_{a}(l){}^{B}_{b}(N) \middle| {}^{C}_{c}(J) \right\rangle = \sum_{a'b'c'} \frac{1}{{}^{\circ}\mathcal{G}} \sum_{\bar{g}} \mathfrak{D}^{A}_{a'a}{}^{*}(g) \mathfrak{D}^{B}_{b'b}{}^{*}(g) \mathfrak{D}^{C}_{c'c}(g) \times \left\langle {}^{A}_{a'}(l){}^{B}_{b'}(N) \middle| {}^{C}_{c'}(J) \right\rangle . \tag{A5}$$

Using the finite group factorization lemma (3.17), we find

$$\left\langle {}^{A}_{a}(l){}^{B}_{b}(N) \middle| {}^{C}_{c}(J) \right\rangle = \frac{1}{[C]} C^{ABC}_{abc} \sum_{a'b'c'} C^{ABC}_{a'b'c'} \left\langle {}^{A}_{a'}(l){}^{B}_{b'}(N) \middle| {}^{C}_{c'}(J) \right\rangle \tag{A6}$$

From Eqs. (A4) and (A6) it follows that

$$\left(\frac{[N]}{[J]}\right)^{1/2} \sum_{m'nM'} C^{lNJ}_{m'nM'} \begin{pmatrix} A \\ a \end{pmatrix} \begin{matrix} l \\ m' \end{matrix} \begin{pmatrix} B \\ b \end{pmatrix} \begin{matrix} N \\ n \end{matrix} \begin{pmatrix} J \\ M' \end{pmatrix} \begin{matrix} C \\ c \end{matrix} = \left(\frac{[B]}{[C]}\right)^{1/2} C^{ABC}_{abc} \langle (l) A(N) B \| (J) C \rangle \tag{A7}$$

where

$$\langle (l) A(N) B \| (J) C \rangle = \left(\frac{[N]}{[J][B][C]}\right)^{1/2} \times \sum_{a'b'c'} C^{ABC}_{a'b'c'} \left\langle {}^{A}_{a'}(l){}^{B}_{b'}(N) \middle| {}^{C}_{c'}(J) \right\rangle \tag{A8}$$

is a molecular isoscalar factor which is independent of indices a', b', and c'.

APPENDIX B. RACAH COEFFICIENTS FOR FINITE GROUPS

We shall couple the product states $\left|{}^{A}_{a}\right\rangle \left|{}^{D}_{d}\right\rangle \left|{}^{C'}_{c'}\right\rangle$ of the finite symmetry group $\bar{\mathcal{G}}$ in two different ways. Coupling the states $\left|{}^{A}_{a}\right\rangle$ and $\left|{}^{D}_{d}\right\rangle$ first, we find

$$\left| (AD) C' {}^{B'}_{b'} \right\rangle = \sum_{\substack{ad \\ a'c'}} C^{ADA'}_{ada'} C^{A'C'B'}_{a'c'b'} \left|{}^{A}_{a}\right\rangle \left|{}^{D}_{d}\right\rangle \left|{}^{C'}_{c'}\right\rangle . \tag{B1}$$

Coupling the states $\left|{}^{D}_{d}\right\rangle$ and $\left|{}^{C'}_{c'}\right\rangle$ first, we find

$$\left| A (DC')^{B}_{b} \right\rangle = \sum_{\substack{ac \\ dc'}} C^{ACB}_{acb} C^{DC'C}_{dc'c} \left|{}^{A}_{a}\right\rangle \left|{}^{D}_{d}\right\rangle \left|{}^{C'}_{c'}\right\rangle . \tag{B2}$$

The scalar product of the states in Eqs. (B1) and (B2) gives

$$\left\langle (AD)C'^{B'}_{b'} \middle| A(DC')^{B}_{b} \right\rangle = \sum_{\substack{acd \\ a'c'}} C^{ACB}_{acb} C^{A'C'B'}_{a'c'b'} C^{DAA'}_{daa'} C^{DC'C}_{dc'c} , \tag{B3}$$

where we assume a sign convention such that

$$C^{ADA'}_{ada'} = C^{DAA'}_{daa'} .$$

Analyzing this scalar product, we find for elements $\bar{g}$ of $\bar{\mathcal{G}}$, that

$$\begin{aligned} \left\langle {B' \atop b'} \middle| {B \atop b} \right\rangle &= \frac{1}{{}^{\circ}\mathcal{G}} \sum_{\bar{g}} \left\langle {B' \atop b'} \middle| \bar{g}^{\dagger} \bar{g} \middle| {B \atop b} \right\rangle \\ &= \frac{1}{{}^{\circ}\mathcal{G}} \sum_{\bar{g} b'' b'''} \mathfrak{D}^{B}_{b''b}(g) \mathfrak{D}^{B'*}_{b'''b'}(g) \left\langle {B' \atop b'''} \middle| {B \atop b''} \right\rangle \\ &= \delta_{BB'} \delta_{bb'} \frac{1}{[B]} \sum_{b''} \left\langle {B \atop b''} \middle| {B \atop b''} \right\rangle \\ &= \delta_{B'B} \delta_{b'b} \langle B | B \rangle \end{aligned} \tag{B4}$$

Thus $\langle {B \atop b} | {B \atop b} \rangle$ is independent of b.

Defining the Racah coefficient in terms of this scalar product,

$$\langle (AD)C'B' | A(BC')B \rangle = \begin{bmatrix} A & D & A' \\ C' & B & C \end{bmatrix} , \tag{B5}$$

and using Eqs. (B3) and (B4), we have the result given in Sec. III.

$$\sum_{\substack{acd \\ a'c'}} C^{ACB}_{acb} C^{A'C'B'}_{a'c'b'} C^{DAA'}_{daa'} C^{DC'C}_{dc'c} = \begin{bmatrix} A & D & A' \\ C' & B & C \end{bmatrix} \delta_{B'B} \delta_{b'b} .$$

APPENDIX C. S_n CHARACTER FORMULA

We give a formula (Coleman, 1966) for S_n characters $\chi^{[\mu_1 \cdots \mu_p]}_{1^{\alpha}2^{\beta}3^{\gamma}\cdots}$. Here the S_n IR is labeled by a tableau symbol $[\mu_1 \cdots \mu_p]$ wherein μ_j means that row j has μ_j boxes. The S_n classes are labeled by the notation $1^{\alpha}2^{\beta}3^{\gamma}\cdots n$ wherein α, β, γ, ... are the number of permutation 1-cycles, 2-cycles, 3-cycles, ... respectively. For example, the permutation (1)(3)(2, 5)(4, 7, 6, 8) would be in the class $1^2 2^1 3^0 4^1 5^0 6^0 7^0 8^0$ of S_8. The character then is given by the following formula and definitions. Note that the formula starts with a column of numbers that are the hooklengths of the first column of the tableau. Then the definitions are used to whittle it down to a sum of sequentially numbered columns which each contribute unity according to Def. 2.

$$\chi^{[\mu_1 \cdots \mu_p]}_{1^{\alpha}2^{\beta}3^{\gamma}\cdots} = \partial_1^{\alpha} \partial_2^{\beta} \partial_3^{\gamma} \cdots \begin{vmatrix} \mu_1 + p - 1 \\ \cdot \\ \cdot \\ \cdot \\ \mu_{p-2} + 2 \\ \mu_{p-1} + 1 \\ \mu_p \end{vmatrix} ;$$

Def. 1:

$$\partial_m \begin{vmatrix} a \\ b \\ c \\ \cdot \\ \cdot \\ \cdot \end{vmatrix} = \begin{vmatrix} a-m \\ b \\ c \\ \cdot \\ \cdot \\ \cdot \end{vmatrix} + \begin{vmatrix} a \\ b-m \\ c \\ \cdot \\ \cdot \\ \cdot \end{vmatrix} + \begin{vmatrix} a \\ b \\ c-m \\ \cdot \\ \cdot \\ \cdot \end{vmatrix} + \cdots ;$$

Def. 2:

$$\begin{vmatrix} p-1 \\ \cdot \\ \cdot \\ \cdot \\ 2 \\ 1 \\ 0 \end{vmatrix} = 1 ;$$

Def. 3:

$$\begin{vmatrix} a \\ b \\ c \\ \cdot \\ \cdot \\ \cdot \end{vmatrix} = 0$$ if any two numbers in the column are equal, or if any number is less than zero;

Def. 4:

$$\begin{vmatrix} a \\ b \\ c \\ \cdot \\ \cdot \\ \cdot \end{vmatrix} = - \begin{vmatrix} b \\ a \\ c \\ \cdot \\ \cdot \\ \cdot \end{vmatrix}$$ interchanging any two numbers gives a change of sign.

For example, here is the character of the [56, 13] IR of class 2, 11, 56 of S_{69}:

$$\chi^{[56,13]}_{2,11,56} = \partial_2 \partial_{11} \partial_{56} \begin{vmatrix} 57 \\ 13 \end{vmatrix} = \partial_2 \partial_{11} \begin{vmatrix} 1 \\ 13 \end{vmatrix}$$

$$= \partial_2 \begin{vmatrix} 1 \\ 2 \end{vmatrix} = \begin{vmatrix} 1 \\ 0 \end{vmatrix} = 1 .$$

APPENDIX D. THE O_h-S_6 TABLEAU CORRELATION

To obtain the octahedral (O_h) to permutations (S_6) correlation for the XY_6 molecule we need only those S_6 classes which correspond to O_h operations when the Y atoms are numbered 1–6. The necessary S_6 characters are found using the formula from Appendix C, and are recorded in the upper part of Table XV. The well known O_h char-

TABLE XV. Characters of permutation group (S_6) and octahedral (O_h) subgroup.

	1^6	3^2	2^2	4^1	2^3	2^3	6^1	2^1	2^14^1	$2^2=S_6$ Class
$\{\mu\}=\{6\}$	1	1	1	1	1	1	1	1	1	1
$\{5,1\}$	5	−1	1	1	−1	−1	−1	3	−1	1
$\{4,2\}$	9	0	1	−1	3	3	0	3	1	1
$\{4,1,1\}$	10	1	−2	0	−2	−2	1	2	0	−2
$\{3,3\}$	5	2	1	−1	−3	−3	0	1	−1	1
$\{3,2,1\}$	16	−2	0	0	0	0	0	0	0	0
$\{2,2,2\}$	5	2	1	1	3	3	0	−1	−1	1
$\{3,1,1,1\}$	10	1	−2	0	2	2	−1	−2	0	−2
$\{2,2,1,1\}$	9	0	1	1	−3	−3	0	−3	1	1
$\{2,1,1,1,1\}$	5	−1	1	−1	1	1	1	−3	−1	1
$\{1,1,1,1,1,1\}$	1	1	1	−1	−1	−1	−1	−1	1	1
A_{1g}	1	1	1	1	1	1	1	1	1	1
A_{2g}	1	1	1	−1	−1	1	1	1	−1	−1
E_g	2	−1	2	0	0	2	−1	2	0	0
T_{1g}	3	0	−1	1	−1	3	0	−1	1	−1
T_{2g}	3	0	−1	−1	1	3	0	−1	−1	1
A_{1u}	1	1	1	1	1	−1	−1	−1	−1	−1
A_{2u}	1	1	1	−1	−1	−1	−1	−1	1	1
E_u	2	−1	2	0	0	−2	1	−2	0	0
T_{1u}	3	0	−1	1	−1	−3	0	1	−1	1
T_{2u}	3	0	−1	−1	1	−3	0	1	1	−1
	1	120° Class	180° Class	90° Class	180° Class	I				

acters are given in the lower part of the same table. Finally, standard character matching gives the desired correlation table of Fig. 27.

SYNOPSIS OF TERMINOLOGY

(ABC) Rules for labeling BOA states

(A) Label internal ($\overline{\mathcal{G}}$) symmetry A of electronic, vibrational, or vibronic activity or excitation. When relating BOA states to weakly coupled or scattering state of momentum (l), the labels considered will be those A correlated with l: $\mathfrak{D}^l \downarrow \overline{\mathcal{G}} = .. \oplus A \oplus ..$

(B) Label internal ($\overline{\mathcal{G}}$) symmetry B of bare rotor. There must be one or more Young tableau $\{\mu\}$ labels correlated with each IR(B) of $\mathcal{G}$ in order that it be used (Section III.C, D). [Any (B) without unique correlation is excluded (Sec. II.C).] Nuclear spin "statistical" weights (Sec. III.D) and hyperfine states (Sec. III.E.2) are determined by spin tableau

$$\{\mu_s\} = \begin{cases} \{\mu\} \text{ for Bose nuclei.} \\ \{\tilde{\mu}\} \text{ for Fermi nuclei.} \end{cases}$$

(C) Label internal ($\overline{\mathcal{G}}$) symmetry C of constricted rotor by writing all IR contained in tensor product $A \otimes B = \ldots \oplus C \oplus \ldots$ Then the total rotational angular momentum levels J^p belonging to each (ABC) triad are just those correlated with C: $\mathfrak{D}^{J^p} \downarrow \overline{\mathcal{G}} = \ldots \oplus C \oplus \ldots$

(ABC) Rules for multipole (T^{k_q}(lab)) selection rules for BOA states

(D) Determine internal ($\overline{\mathcal{G}}$) symmetry labels D correlated with the multipolarity-parity k_q: $\mathfrak{D}^{k_q} \downarrow \overline{\mathcal{G}} = \ldots \oplus D \oplus \ldots$ Then transition $[ABC, J^p] \rightarrow [A'B'C', J'^{p'}]$ is allowed if

(a) A' is contained in an $A \otimes D$ product

(b) $B' = B$

(c) C' is contained in a $C' \otimes D$ product

(d) $\mathfrak{D}^{J'p'}$ is contained in a $\mathfrak{D}^{k_q} \otimes \mathfrak{D}^{Jp}$ product.

Bare rotor

A rotating configuration of (nuclear) points imagined to be held in an equilibrium position for the molecule being considered. In principle no electronic or vibronic states or excitations are supposed to be present in a bare rotor but in practice the bare rotor may usually be less than totally bare. Generally one has a reasonable approximation of the bare rotor by simply removing the most easily activated electrons or vibrations from the molecule being considered. The wave function of the bare rotor is [Eq. (2.33)]

$$\gamma_{mb}^{NB}(\phi\theta\chi) = \sum_n \begin{pmatrix} N & B^* \\ n & b \end{pmatrix}^* \mathfrak{D}_{mn}^{N*}(\phi\theta\chi)\sqrt{[N]}\,,$$

where the coefficients $\left(\begin{smallmatrix} N & B^* \\ n & b \end{smallmatrix}\right)$ are determined by considerations of internal $\overline{\mathcal{G}}$ symmetry and the inertial and centrifugal distortion Hamiltonian.

BOA Born-Oppenheimer approximation

BOA constriction

Coupling process using a sum over internal angular momentum or symmetry variables to make a state in which the vibronic wave is attached to the rotor and rides with it. Process is intended to produce Born–Oppenheimer approximate states.

Clusters (of levels)

Degeneracy of near-degeneracy beyond that expected by standard symmetry analysis (Secs. II.A).

Constricted rotor

A rotating configuration of points with (BOA) vibronic excitations locked into the assumed symmetry of the rotor so they ride around with it. The wave function of the BOA molecular state is [Eq. (3.16b)]

$$\left\langle \text{vibronic}, \phi\theta\chi \middle| (\text{BOA}) A C_{b\ M}^{B^*\ J} \right\rangle = \sum_{a,c} C_{abc}^{ABC} \left(\frac{[B]}{[C]}\right)^{1/2} \mathcal{Y}_a^A(\text{vibronic}) r_{Mc}^{JC*}(\phi\theta\chi),$$

where the rotor part r_{Mc}^{JC*} has the same form of definition as the bare rotor wave function.

Correlation (of symmetry representations)

The process by which IR $\mathfrak{D}^\alpha$ of a group $\mathcal{G}$ are related to those D^A of a subgroup $\mathcal{H}$. Generally, an IR of $\mathcal{G}$ is a reducible representation (RR) of $\mathcal{H}$, and each IR D^A is repeated some number $f_A^\alpha (= 0, 1, 2, \ldots)$ of times in the *RR* $\mathfrak{D}^\alpha$ of $\mathcal{G}$

$$\mathfrak{D}^\alpha \downarrow \mathcal{H} = (D^A \oplus D^A \oplus \ldots) \oplus (D^B \oplus \ldots) = f_A^\alpha D^A \oplus f_B^\alpha D^B \ldots$$

f_A^α is the correlation frequency. $f_A^\alpha f_B^\alpha \ldots$ define the row (α) of a *Correlation Table*. The columns of a correlation table give the decomposition of induced representations

$$D^A \uparrow \mathcal{H} = f_A^\alpha \mathfrak{D}^\alpha \oplus f_A^\beta \mathfrak{D}^\beta \oplus \ldots$$

according to the Frobenius Reciprocity Theorem.

Coupling or weak coupling

Standard coupling process using a sum over external momentum variables to make a state of definite total rotational momentum. (See also Sec. III-C.)

Induced representations $D^A \uparrow g$

Suppose a symmetry analysis problem in which the base states $\{|1\rangle, |2\rangle = \mathrm{R}(2)|1\rangle, |3\rangle = \mathrm{R}(3)|1\rangle, \ldots\}$ are obtained by select symmetry operators $\{1, \mathrm{R}(2), \mathrm{R}(3), \ldots\}$ in $\mathcal{G}$ (viz. examples treated in Fig. 9). Suppose further that the operations in a subgroup $\mathcal{H} = \{1, h, \ldots\}$ of $\mathcal{G}$ leave $|1\rangle$ unchanged except to multiply it by a constant, i.e.,

$$\mathrm{h}|1\rangle = D^A(\mathrm{h})|1\rangle$$

where the constant $D^A(\mathrm{h})$ is an IR component of $\mathcal{H}$. Suppose further that all elements outside of $\mathcal{H}$ do change $|1\rangle$. Then the basis $\{|1\rangle, |2\rangle, \ldots\}$ is a basis of the induced representation $D^A \uparrow \mathcal{G}$ of $\mathcal{G}$.

Rovibronic species

Molecular states characterized by internal nuclear spin-permutation symmetry properties. Here we use the notation B (Bare rotor symmetry) and Young tableau $\{\mu\}$ when applicable.

Rovibronic nomogram

Graphical procedure for visualizing spectra given initial and final levels. Initial and final levels are plotted on x and y axes, respectively. Allowed transitions are located by dots at the right coordinates and lines of unit slope through these coordinates represent spectra (see Fig. 30). Different species or (B) states are kept separate (see Fig. 31).

Spherical top

Rotor with spherical symmetry.

Symmetric top

Rotor with cylindrical symmetry.

Tableaus or Young tableaus

An array of n boxes in a pattern $\{\mu\} = \{\mu_1 \mu_2 \ldots \mu_r\}$ of r rows with μ_i ($\geq \mu_{i+1}$) boxes in the ith row. The Young pattern is a powerful labeling device for permutation and unitary representations, and is recently been shown to serve as a source of convenient digital algorithms (viz. Fig. 28).

REFERENCES

Aldridge, J. P., H. Filip, H. Flicker, R. F. Holland, R. S. McDowell, N. G. Nereson, and K. Fox, 1975, J. Mol. Spec. **58**, 165.

Berry, R. S., 1960, J. Chem. Phys. **32**, 933.

Bethe, H., 1929, Ann. Physik (Leipzig) **3**, 133.

Buch, T., 1972, J. Math. Phys. **13**, 1892.

Bunker, P. R., 1975, *Vibrational Spectra and Structure*, edited by J. Dung (Dekker, N.Y.), p. 1.

Bunker, P. R., and D. Papousek, 1969, J. Mol. Spec. **32**, 419.

Cantrell, C. D., and H. W. Galbraith, 1975, J. Mol. Spec. **58**, 158.

Chang, E. S., and U. Fano, 1972, Phys. Rev. A **6**, 173.

Coleman, A. J., 1966, *Induced Representations and Applications* (Queens University Press, Kingston, Ontario).

Dalton, B. J., 1971, J. Chem. Phys. **54**, 11, 4745.

Dimmock, J. O., G. F. Koster, H. Statz, and R. G. Wheeler, 1963, *Properties of the Thirty-Two Point Groups* (MIT Press, Cambridge).

Dorney, A. J., and J. K. G. Watson, 1972, J. Mol. Spec. **42**, 1.

Drake, J., G. W. F. Drake, and M. Schlesinger, 1975, J. Phys. B **8**, 7.

Fano, U., 1970, Phys. Rev. A **2**, 353.

Fano, U., and G. Racah, 1959, *Irreducible Tensorial Sets* (Academic, N. Y.).

Fately, W. G. *et al.*, 1972, *Infrared and Raman Selection Rules: The Correlation Method* (Wiley Interscience, N. Y.)

Feynman, R. P. *et al.*, 1963, *Lectures in Physics* (Addison-Wesley, Reading, Mass.), Vol. III.

Fox, K., H. W. Galbraith, B. J. Krohn, and J. D. Louck, 1976, Abs. RM 13, 31st Symposium on Molecular Spectroscopy, Columbus.

Fox, K., H. W. Galbraith, B. J. Krohn, and J. D. Louck, 1977, Phys. Rev. A **15**, 4, 1363.

Galbraith, H. W., 1978, J. Chem. Phys. (in press).

Goddard, W., 1967, Phys. Rev. **157**, 1, 73.

Griffith, J. S., 1962, *Tensor Methods for Molecular Symmetry Groups* (Prentice Hall, Englewood Cliffs, N. J.).

Hall, J. L., 1974, in *Methodes de Spectroscopie sans Largeur Doppler de Niveaux Excites de Systemes Moleculaires Simples*, edited by J. C. Lehman *et al.* (CNRS Press, Paris), p. 105–125.

Hall, J. L., and J. A. Magyar, 1976, *Topics in Applied Physics* (Springer Verlag), Vol. 13, No. 5, p. 173.

Hamermesh, M., 1960, *Group Theory and Its Application to Physical Problems* (Addison Wesley, Reading, Mass.).

Hanes, G. R., and C. E. Dahlstrom, 1969, Appl. Phys. Lett. **14**, 362.

Hansch, T. W., M. D. Levenson, and A. L. Schawlow, 1971, Phys. Rev. Lett. **26**, 946.

Harter, W. G., 1971, Phys. Rev. A **3**, 1891.
Harter, W. G., 1973, Phys. Rev. A **8**, 2819.
Harter, W. G., and C. W. Patterson, 1976a, Phys. Rev. A **13**, 1067.
Harter, W. G., and C. W. Patterson, 1976b, *A Unitary Calculus for Electronic Orbitals*, Lecture Notes in Physics No. 49 (Springer Verlag).
Harter, W. G., and C. W. Patterson, 1977a, Phys. Rev. Lett. **38**, 5, 224.
Harter, W. G., and C. W. Patterson, 1977b, J. Chem. Phys. **66**, 11, 4872.
Harter, W. G., and C. W. Patterson, 1977c, Intern. J. Quantum Chem. **11**, 479.
Harter, W. G., and N. dos Santos, 1978, Am. J. Phys. **46**, 2 (in press).
Hecht, K. T., 1960, J. Mol. Spec. **5**, 355.
Hecht, K. T., 1960a, J. Mol. Spec. **5**, 390.
Heine, V., 1960, *Group Theory in Quantum Mechanics* (Pergamon Press, New York).
Herzberg, G., 1945, *Infrared and Raman Spectra of Polyatomic Molecules* (Van Nostrand, New York).
Herzberg, G., 1966, *Electronic Structure of Polyatomic Molecules* (McGraw Hill, New York).
Herzberg, G., and Ch. Jungen, 1972, J. Mol. Spec. **41**, 3.
Hinkley, E. D., T. C. Harman, and C. Freed, 1968, Appl. Phys. Lett. **13**, 49.
Hinkley, E. D., and C. Freed, 1969, Phys. Rev. Lett. **23**, 277.
Hinkley, E. D., and P. L. Kelley, 1971, Science **171**, 635.
Hönl, H., and F. London, 1925, Z. Physik **33**, 803.
Hougen, J. T., 1962, J. Chem. Phys. **37**, 1433.
Hougen, J. T., 1963, J. Chem. Phys. **39**, 358.
Hougen, J. T., 1971, J. Chem. Phys. **55**, 1122.
Hougen, J. T., 1976, *MTP International Review of Science*, Physical Chemistry, edited by D. A. Ramsay (Butterworths, London), Vol. 3, No. 2.
Jahn, H. A., 1938, Proc. R. Soc. A **6**, 168, 469, and 495.
Judd, B. R., 1975, *Angular Momentum Theory for Diatomic Molecules* (Academic Press, New York).
Krohn, B. J., 1976, Los Alamos Report LA–6554–MS, Los Alamos, N. M.
Lea, K. R., M. J. M. Leask, and W. P. Wolf, 1962, J. Phys. Chem. Solids **23**, 1381.
Levenson, M. D., and A. L. Schawlow, 1972, Phys. Rev. A **6**, 1, 10.
Lougett-Higgins, H. C., 1963, Mol. Phys. **6**, 445.
Louck, J. D., and H. W. Galbraith, 1976, Rev. Mod. Phys. **48**, 69.
Lowdin, P. O., 1967, Rev. Mod. Phys., **39**, 259.
Mackey, G. W., 1968, *Induced Representations of Groups and Quantum Mechanics* (Benjamin, New York).
McDowell, R. S., H. W. Galbraith, B. J. Krohn, and C. D. Cantrell, 1976, Opt. Comm. 17–2.
Moret-Bailly, J., 1965, J. Mol. Spec. **15**, 355.
Oka, T., 1976, *Molecular Spectroscopy: Modern Research Vol. II* (Academic Press, New York).
Paldus, J., 1975, Intern. J. Quant. Chem. **59**, 165.
Patterson, C. W., and W. G. Harter, 1977a, J. Chem. Phys. **66**, 11, 4886.
Patterson, C. W., and W. G. Harter, 1977b, Phys. Rev. A **15**, 6, 2372.
Patterson, C. W., and W. G. Harter, 1977c, Int. J. Quant. Chem. Symp. **11**, 445.
Pine, A. S., 1976, J. Opt. Soc. Am. **66**, 2, 97.
Plyler, E. K., E. D. Tidwell, and L. R. Blaine, 1960, J. Res. Natl. Bureau Stds. **64A**, 201.
Ponzano, G., and T. Regge, 1968, *Spectroscopic and Group Theoretical Methods in Physics: Racah Memorial Volume* (North Holland Publ. Co), p. 1.
Robinson, G. de B., 1960, *Representations of the Symmetric Group* (Toronto U. P., Toronto).
Rotenburg, M. *et al.*, 1959, *The 3-j and 6-j Coefficients* (MIT Press, Cambridge).
Schulten, K., and R. G. Gordon, 1975, J. Math. Phys. **16**, 10, 1961.
Steinfeld, J. L., 1974, *Molecules and Radiation* (Harper and Row, New York).
Tinkham, M., 1964, *Group Theory and Quantum Mechanics* (McGraw Hill, New York).
Van Vleck, J. H., 1951, Rev. Mod. Phys. **23**, 213.
Watson, J. K. G., 1965, Can. J. Phys. **43**, 1996.